A STUDY ON
DAMAGE POTENTIAL OF GROUND MOTIONS
AND
STRENGTH DEMAND SPECTRA IN LIFETIME OF STRUCTURE

September, 2001

YOSHIO SUNASAKA

A STUDY ON
DAMAGE POTENTIAL OF GROUND MOTIONS
AND
STRENGTH DEMAND SPECTRA IN LIFETIME OF STRUCTURE

September, 2001

YOSHIO SUNASAKA

ABSTRACT

Earthquake-resistant design is a procedure used to assure that strength and deformation capacities of structures exceed the demands imposed by earthquakes with an adequate safety margin. Although the design philosophy is generally accepted, its quantification in the form of design specifications is not enough. One of the most difficult aspects in currying out proper design is to select an earthquake ground motion for seismic design. For this purpose, a good understanding and quantification of ground motion parameters that characterize the severity and damage potential of the earthquake ground motion are needed.

In this dissertation, damage spectrum is defined as damage indices of single-degree-of-freedom systems with natural periods ranging from 0.05 to 5.0 sec. The damage index proposed by Park and Ang and the bilinear model are used to calculate the damage spectrum. The damage index describes the state of the concrete structure from slight damage to severe damage or collapse.

The damage potential of ground motions during recent great earthquakes such as the 1995 Hyogoken-Nanbu earthquake, the 1999 Kocaeli earthquake in Turkey, and the 1999 Chi-Chi earthquake in Taiwan is studied by using the damage spectra. It is shown that damage to structures may be greatly affected by the location of the fault, the geological profile of the site and the fault rupture mechanism. Also, damage spectra of some earthquake ground motions that have been used for design purpose are studied and the required yield strengths of them in view of damage indices of structures are described.

A method of evaluating damage potential of ground motions in a large area during a great earthquake is proposed. The methodology is applied to Kawasaki City and the damage potential of ground motions are studied.

Damage spectra of recorded ground motions during aftershocks are calculated and the damage potential is studied. Then a simulation model for mainshock-aftershock earthquake sequences and a method for estimating the damage potential of the ground motions during the mainshock-aftershock earthquake sequences at a site are proposed. This procedure consists of 3 main steps: (1) simulation of the mainshock-aftershock earthquake sequences at a site in a lifetime of a strusture, (2) calculation of ground motions of the mainshock-aftershock sequences and (3) calculation of damage spectra of the ground motions of the mainshock-aftershock sequences and estimation of damage potential of the earthquake ground motions at the site. Then, a method for evaluating the strength demand spectra with uniform damage level in the lifetime of a structure considering mainshock-aftershock earthquake sequences is proposed. The proposed method is applied to estimation of damage potential of ground motions and strength demand spectra in a lifetime of a structure considering mainshock-aftershock earthquake sequences in Eureka, California.

TABLE OF CONTENTS

CHAPTER 1

INTRODUCTION

1.1 BACKGROUND AND OBJECTIVES

In recent years, many large earthquakes occurred very close to modern cities and caused severe damage to buildings and infrastructure. During the 1971 San Fernando earthquake, the 1987 Wittier Narrows earthquake and the 1989 Loma Prieta earthquake in California, bridges designed to pre-1971 force levels specified by Caltrans or AASHTO were damaged severely. The 1994 Northridge, California earthquake caused severe damage to buildings and infrastructure in the epicentral regions.

The 1995 Hyougoken-Nanbu earthquake affected one of the most modernized areas in Japan with violent ground shaking. Damage to modern engineering structures was beyond engineers' expectations, because it was thought that the structures were designed according to proper earthquake-resistant design standards.

The 1999 Kocaeli earthquake in Turkey and the 1999 Chi-Chi earthquake in Taiwan caused severe damage to buildings and infrastructure. Furthermore, great aftershocks of these earthquakes induced collapse or more severe damage to the structures that had been already damaged by the mainshocks.

The damage to modern engineering structures described above has been forcing engineers and researchers to revise the earthquake-resistant standards and to reevaluate ground motion potential during great earthquakes.

Earthquake-resistant design is a procedure used to assure that strength and deformation capacities of structures exceed the demands imposed by earthquakes with an adequate safety margin. Although the design philosophy is generally accepted, its quantification in the form of design specifications is not enough.

The equivalent lateral force method has been used widely for earthquake-resistant design. This method prescribes that every structure shall be designed and constructed to resist a minimum lateral seismic force, applied statically and independently in the direction of each of the two main axes of the structure. The equivalent lateral force of the structure is determined by the dead weight of the structure and some coefficients, for example, the seismic zone factor, the importance coefficient, the cite coefficient, and the structural factor. For underground structures, the response displacement method has been used widely for earthquake-resistant design. This method prescribes that every underground structure shall be designed and constructed to resist a minimum lateral ground displacement, applied statically. The lateral ground displacement is induced by response to ground

shaking during an earthquake.

These static methods are very simple and easy to use and thus are widely applied to earthquake-resistant design of structures. Severe damage to buildings and infrastructure in modern cities during recent great earthquakes has suggested that these static methods are insufficient for earthquake-resistant design, however. Dynamic methods have been recommended to check the safety of a structure that has been designed by static methods.

In dynamic methods, the stresses and the deflections of the structure are analyzed when the structure is subjected to an arbitrary dynamic loading. For the analysis, adequate material parameters, modeling of the structure, and ground motions are needed. The selection of appropriate ground motions is the most difficult.

The most important aspect of ground motions during earthquakes is the effect the ground motions will have on structures, i.e., the stresses, deformations, or the amount of damage they will produce. In order to select appropriate ground motions for the dynamic analysis, the damage potential of ground motions during recent great earthquakes and aftershocks should be studied and the characteristics should be identified.

1.2 SCOPE

Earthquake ground motions are highly unpredictable and uncertain. Since different earthquake ground motions cause different degrees of damage to structures, it is necessary for engineers to quantify the severity and damage potential of ground motions.

One of the measures of the intensity of a ground motion can be obtained by evaluating the response of a simple structure, such as the single-degree-of-freedom system (SDOF), to the ground motion. When the response of the SDOF, characterized by the structural parameters such as its natural period and damping ratio, to the ground motion is taken as the measure of the earthquake intensity, this response expressed as a function of its natural period is called a response spectrum.

In this dissertation, damage spectrum is defined as damage indices of SDOF systems with natural periods ranging from 0.05 to 5.0 sec. The damage index proposed by Park and Ang (1985) and a bilinear force-displacement relationship are used to calculate the damage spectrum. The damage index describes the state of the concrete structure from slight damage to severe damage or collapse. The damage index can be calculated by inelastic analysis of structural response during earthquakes. Damage to engineering structures caused by recent great earthquakes is summarized, and the damage potential of ground motions during the earthquakes is studied. Damage potential of some earthquake ground motions that have been used for design purpose is studied. A method of evaluating damage potential of ground motions in large areas is described. Furthermore, the damage potential of ground motions during aftershocks is studied, and a method of evaluating damage

potential of ground motions considering mainshock-aftershock earthquake sequences in a design period of a structure is proposed. Then, a method for evaluating the strength demand spectra with uniform damage level in the lifetime of a structure considering mainshock-aftershock earthquake sequences is proposed. The proposed method is applied to estimation of damage potential of ground motions and strength demand spectra in a lifetime of a structure considering mainshock-aftershock earthquake sequences in Eureka, California.

1.3 ORGANIZATION OF THE DISSERTATION

Chapter 2 provides a review of current studies on structural damage indicators and damage potential of ground motions. Damage to engineering structures caused by recent great earthquakes including the 1995 Hyogoken-Nanbu earthquake, the 1999 Kocaeli earthquake in Turkey, and the 1999 Chi-Chi earthquake in Taiwan is also summarized in this chapter.

In Chapter 3, damage spectrum of ground motions is defined and characteristics of damage spectra are described.

Chapter 4 describes damage potential of ground motions during recent great earthquakes including the 1995 Hyogoken-Nanbu earthquake, the 1999 Kocaeli earthquake in Turkey, and the 1999 Chi-Chi earthquake in Taiwan. Damage spectra of some earthquake ground motions that have been used for design purpose are studied and the required yield strengths for the ground motions in view of damage indices of structures are described.

In Chapter 5, a method of evaluating damage potential of ground motions in large areas during earthquakes is proposed, and its application is presented. Damage potential of ground motions in large areas is also described.

In Chapter 6, damage potential of ground motions during aftershocks is studied. A method to evaluate damage potential of ground motions considering mainshock-aftershock sequences in a design period of a structure is proposed. Then, a method for evaluating the strength demand spectra with uniform damage level in the lifetime of a structure considering mainshock-aftershock earthquake sequences is proposed. The proposed method is applied to estimation of damage potential of ground motions and strength demand spectra in a lifetime of a structure considering mainshock-aftershock earthquake sequences in Eureka, California.

Finally, Chapter 7 presents the conclusions on damage potential of ground motions during great earthquakes and aftershocks and the strength demand spectra with uniform damage level in the lifetime of a structure considering mainshock-aftershock earthquake sequences.

CHAPTER 2

REVIEW OF CURRENT STUDIES ON DAMAGE POTENTIAL OF GROUND MOTIONS AND STRUCTURAL DAMAGE

2.1 INTRODUCTION

In recent years, many large earthquakes occurred very close to modern cities and caused severe damage to buildings and infrastructure. In the United States, the 1989 Loma Prieta earthquake in California caused severe damage to engineering structures such as bridges, and the 1994 Northridge earthquake caused severe damage to buildings and infrastructure. The 1995 Hyougoken-Nanbu earthquake affected one of the most modernized areas in Japan with violent ground shaking. Damage to modern engineering structures was beyond engineers' expectations, because it was thought that they were designed according to proper earthquake-resistant design standards. The 1999 Kocaeli earthquake in Turkey and the 1999 Chi-Chi earthquake in Taiwan caused severe damage to buildings and infrastructure. In this chapter, the ground motion parameters that characterize the severity and damage potential of the earthquake ground motions, and structural damage by recent great earthquakes are summarized.

2.2 CURRENT STUDIES ON DAMAGE POTENTIAL OF GROUND MOTIONS

The most important features of ground motions during an earthquake, from the standpoint of its effectiveness in producing structural response, are the amplitude, the frequency content, and the duration. The amplitude is generally characterized by the peak ground acceleration (PGA) or the peak ground velocity (PGV). The frequency content can be represented by the number of zero crossings in the acceleration time history of the ground motion, or Fourier spectrum of the acceleration time history of the ground motion. The duration can be represented roughly by the length of time between the first and the last peaks exceeding a given threshold level. It is evident, however, that these quantitative features provide only a very limited description of the ground motions and do not quantify the damage potential adequately.

A more precise measure of the intensity of a ground motion can be obtained by evaluating the response of a simple structure, such as a SDOF system, to the ground motion. When the maximum value of the response of the SDOF characterized by the structural parameters such as, its natural period and damping ratio, to the ground motion is taken as the measure of the earthquake intensity, this maximum expressed as a function of its natural period is called the response spectrum.

It is evident that a response spectrum provides a more effective measure of damage potential

of the ground motion during earthquake than any single quantity, e.g. PGA. The response spectrum shows directly to what extent any given SDOF would respond to the ground motion. The response spectrum depends on not only the ground motions, but also the structural parameters. This is reasonable, because structural damage during an earthquake depends on not only characteristics of the ground motion but also the structural characteristics.

Response spectra are very effective even if the structural response is assumed to be linear elastic. The amount of expected elastic response is a very significant indication of a ground motion intensity. Moreover, the integral of the response spectrum taken over an appropriate natural period range is very good overall measure of the ground motion intensity. Housner (1952) has defined a quantity as the integral of the velocity response spectrum taken over the range of natural periods from 0.1 to 2.5 sec, and has called this quantity the response-spectrum intensity.

Structural damage during earthquakes involves inelastic deformation. Therefore, the inelastic response spectrum provides a much more effective measure of damage potential of the ground motion during an earthquake.

Iemura, Igarashi and Takahashi (1998) calculated several response spectra including inelastic response spectra for the ground motion record at Kobe during the 1995 Hyogoken-Nanbu earthquake, together with the ground motion record at Sylmar during the 1994 Northridge earthquake. Comparing these response spectra with those for previously obtained historical earthquake ground motion records, they revealed extremely high damage potential for near field earthquake ground motions.

The soil-structure interaction has a strong effect on the response of the superstructures. Toki et al. (1998) considered simple 3-degree-of-freedom model, foundation (sway, rocking) and superstructure, for the soil-structure interaction system. Assuming the three types of restoring forces for foundation, liner, bilinear and Hardin-Drnevich model, they calculated strength demand spectra for the interaction systems. They showed that the demanded strength for the 3-degree-of-freedom system could be reduced by incorporation of the effect of hysteresis characteristics of the foundation.

Krawinkler et al. (1983) proposed the following cumulative damage model to describe component performance for specific failure modes in steel structures:

$$D = C\sum_{i=1}^{N}(\Delta\delta pi)^{c} \quad (2.1)$$

where D is the cumulative damage, N is the number of damaging excursions, $\Delta\,\delta\,p$ is the plastic deformation range of an individual excursion i, and C, c are structural performance parameters.

Park and Ang (1985) proposed a cumulative damage indicator based on the liner combination of plastic displacement and energy dissipation capacity under monotonic loading. This model, well known as Park and Ang's model, is a calibrated model and has been widely used in recent years. The damage index is expressed as a linear combination of the maximum deformation and the hysteretic

energy as follows:

$$D = \frac{\delta_m}{\delta_u} + \beta \int \frac{dE}{(Q_y \delta_u)} \qquad (2.2)$$

where D is the damage index, an empirical measure of damage (D>1 indicates total damage or collapse), δ_m is the maximum response deformation, δ_u is the ultimate deformation capacity under static loading, Q_y is the calculated yield strength, dE is the incremental dissipated hysteretic energy, and β is the coefficient for cyclic loading effect. The limiting value of D (i.e., damage capacity of a member) is lognormally distributed with a mean of approximately 1.0 and a standard deviation of 0.54.

Sasada et al. (1996) developed a practical way to assess damage to structures under severe earthquake motions. They proposed a method for damage estimation by the use of damage parameters that were obtained by using Park and Ang's damage index.

Nagata, Watanabe and Sugiura (1996) studied the effect of restoring force characteristics on the inelastic dynamic interaction of foundation-structure system. They simply modeled a bridge structural system by a three-degree-of-freedom system, allowing sway of the structure, sway and rocking of the foundation. The equation of motion for the 3DOF system, which was derived by considering bilinear restoring force characteristics, was solved numerically by Newmark's β method in order to obtain the inelastic dynamic response of foundation-structure system subjected to strong ground motions. They evaluated effects of both the yielding strength, and the tangential second stiffness of the bilinear restoring force on the structural damage. They found that the damage was concentrated at the weakest structural components and that the sway of structure might significantly affect the rocking of the foundation.

Sasada et al. (1996) studied effects of soil-structure interaction on the required strength of reinforced concrete pier under strong earthquake motions. They conducted inelastic response analysis for the sway-rocking 3DOF models subjected to strong artificial earthquake motions, and calculated the required yield strength ratios which were values of yield strength of the pier satisfying Park and Ang's damage index=1. Their numerical results showed that the required strength ratio was mainly influenced by the yield strength of the foundation and the ratio of the natural frequency for rocking of the foundation to those of sway of the foundation.

2.3 STRUCTURAL DAMAGE BY RECENT GREAT EARTHQUAKES

(1) The 1995 Hyogoken-Nanbu earthquake (The Kobe Earthquake)

An earthquake, with magnitude of 7.2 on the Richter scale, violently shook the city of Kobe, Awaji Island and other parts of the Hansin region in Japan on January 17th, 1995. This earthquake is called the 1995 Hyogoken-Nanbu earthquake. This earthquake was the first violently disastrous one with its fault line directly under a large city with modern urban infrastructures. The death toll caused by the earthquake was 5,472, the number of houses totally destroyed was 83,536 and those partially destroyed was 68,761. Fires broke out at 258 locations, and burned an area of 671,253m^2. The total damage is estimated to exceed ¥9 trillion (Japan Society of Civil Engineers, 1995).

The epicenter of this event was located approximately 15 km underground, just below the northern end of Awaji Island in Hyogo Prefecture. The length of the fault that ruptured in this event extended from the northern end of Awaji Island northeast through the city of Kobe. The fault rupture directed from the epicenter toward northeast. The concentration of the aftershock sequence following the main shock delineated the area of the fault rupture. Appearance of surface fault rupture was limited to about 9 km on the northern portion of Awaji Island. Measurements indicate that the two sides of the faults moved between 1.2 and 1.5 meters relative to one another.

The area that has a seismic intensity level of VII on the JMA (Japanese Meteorological Agency) scale was concentrated along the fault rupture as shown in Figure 2.1 (Editorial Committee for the Report on the Hanshin-Awaji Earthquake Disaster, 1998a). It is the first time when level VII has been recorded since the 1848 Fukui earthquake. The intensity level of VII is defined by JMA to be the level in which 30% or more of wooden houses collapse. In Figure 2.1, it is found that detail of distribution of the area of greatest devastation is affected by the directivity of the fault rupture movement. In the northeast side of the fault where the rupture arrived, the area of greatest devastation expanded.

Figure 2.2 shows recorded maximum accelerations of ground motions during the earthquake in Hanshin Region (Editorial Committee for the Report on the Hanshin-Awaji Earthquake Disaster, 1998b). The significance of a direct hit with a shallow fault line is that the ground motion in the vicinity of the rupture area is very high, while in even 20 to 30 km from the epicentral region the ground motion attenuates rapidly. Ground acceleration measurements in Kobe indicate that accelerations in the epicentral area were as high as 833 cm/sec^2, while measurements at stations 20 km from the area of fault rupture ranged 200 to 400 cm/sec^2. Also, it is found that the distribution of the area of PGA is affected by the directivity of the fault rupture movement. In the northeast side of the fault where the rupture arrived, the area of large PGA expanded.

Many kinds of civil structures such as bridges, viaducts, harbor facilities, pipelines, sewage

networks suffered severe damage by the earthquake. Roads and railways on the ground, shopping areas and parking lots under ground had been apparently damaged much less, however. Severe damage to subways was very local, and the majority of them suffered no damage.

The distribution of damage to buildings is described as follows (Department of Civil Engineering, Faculty of Engineering, Kobe University, 1995):

a) Topography of Kobe city may be classified into the Rokko Mountains, piedmont terraces, composite fans below the terraces, the old coastal strip, and reclaimed land along the sea. Total collapse of housing occurred on the composite fans.
b) A closer examination of the distribution of the damage in the composite fans shows that the damage was relatively small in areas close to the piedmont terraces.
c) The damage was also relatively small in the old coastal strips below the composite fans.
d) Ground liquefaction was observed on reclaimed land, but the damage to wooden frame housings in such areas was relatively small.
e) The damage to buildings was concentrated in a belt 0.7 to 1.2 km in wide, stretching from southwest to northeast along the foot of Rokko Mountains.
f) On Awaji Island, severe damage occurred in the towns of Hokutan and Ichinomiya, whereas only a small amount of damage to housing was observed in the town of Awaji that was close to the epicenter.

The locations of damaged roads and railways are shown in Figure 2.3 and Figure 2.4. Extensive damage occurred in viaduct sections of both roads and railways. The severity of the damage to roads and railways is strongly related to the ground conditions and positions of faults. Various types of damage were observed as follows:

a) Complete collapse of bridge piers
b) Dislocation of girders from piers
c) Failure of bridge piers
d) Tilt of bridge piers

Kobe Line of Hanshin Expressway is along the southern edge of the heavily damaged zone as shown in Figure 2.4. Viaducts of the Kobe line were supported with 718 piers. Damage to the piers, girders and shoes was investigated by Abe, Fujino and Abe (1999). The damage level to piers was generally very high in the Kobe Line, but the damage level was scattered along the route. According to Iemura et al. (1998), this may be partially because ground motion at each pier was different, and the analyzed maximum elastic acceleration acted on the piers varied from 0.65 to 1.52 g.

Many industrial facilities were seriously damaged during the earthquake. Almost all functions of the port of Kobe were incapacitated during the earthquake. Liquefaction occurred extensively in reclaimed coastal areas, and influenced damage to port facilities. Liquefaction induced ground settlements and destruction or deformation of quay walls around the shore. At Port Island, one of the

man-made islands in Kobe, ground settlements of 20 to 50 cm were found extensively over the island.

Almost all container cranes on Rokko Island, another man-made islands in Kobe, were damage seriously. Some cranes had completely overturned. The container crane columns on the seaward side stood on quay walls, and the movements of the quay walls in a seaward direction induced by liquefaction caused buckling of the steel frames of the cranes.

The earthquake caused damage to the electrical power supply, city gas supply, and telecommunications systems. Also, there occurred such damage as the tilting of utility poles and the severing of cables for the systems, and the failure of joints in gas delivery network.

.

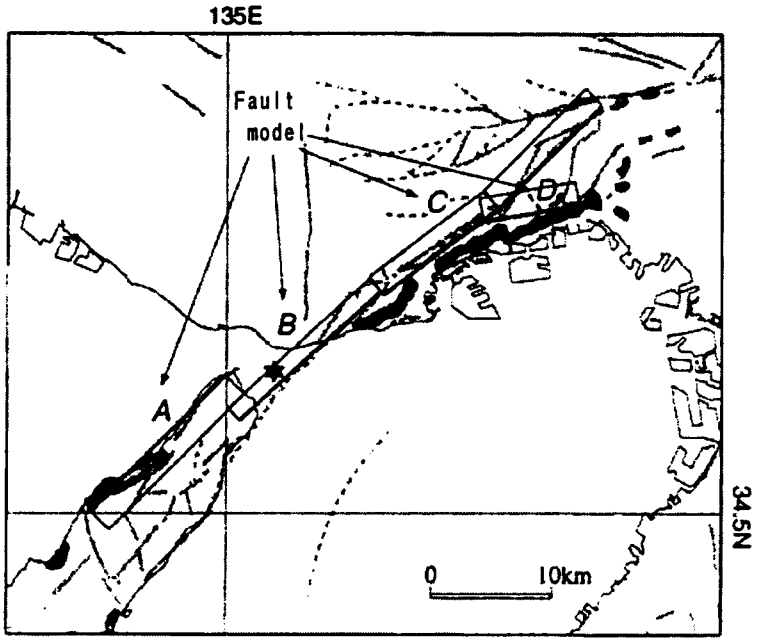

Figure 2.1 Fault model and area with the JMA Intensity level Ⅶ (the area is shaded)

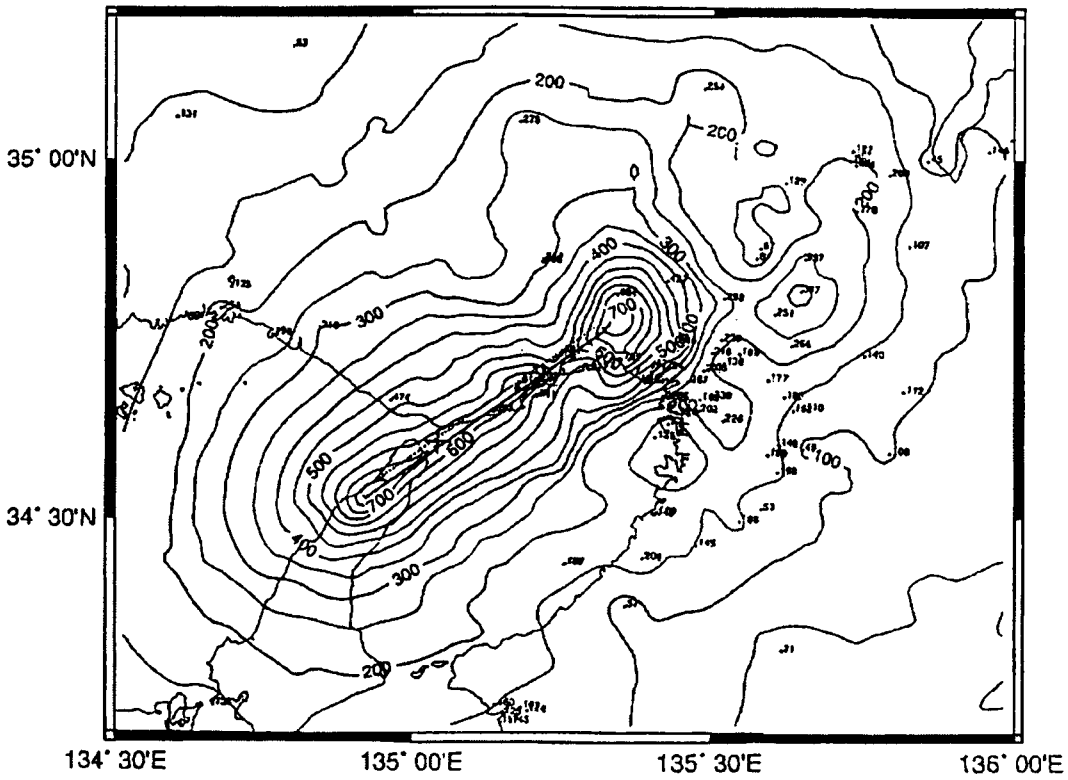

Figure 2.2 Distribution of horizontal peak ground accelerations

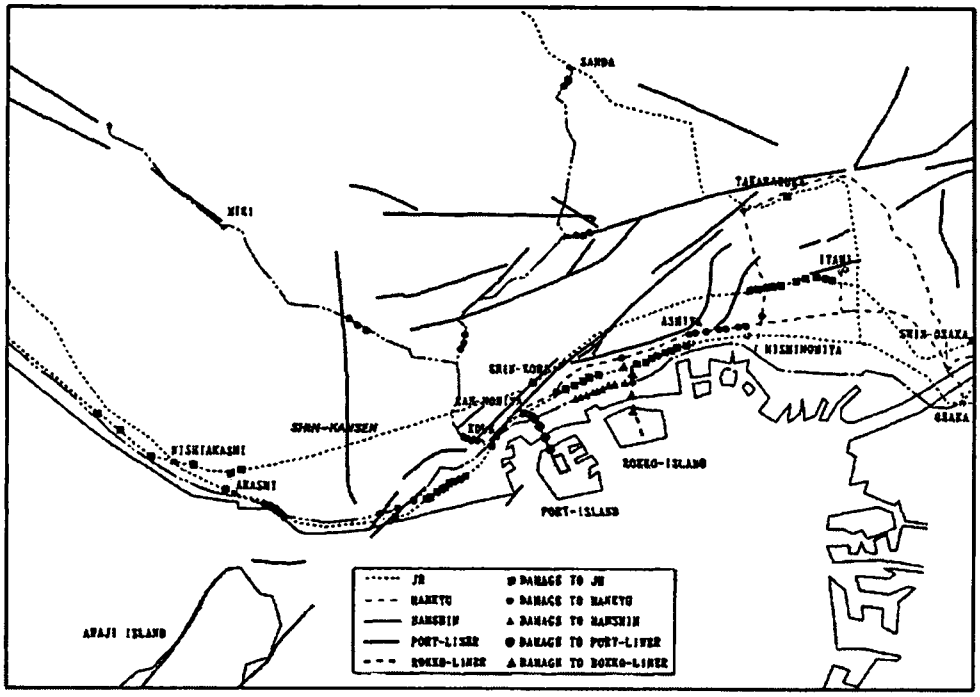

Figure 2.3 Location of damaged railway facilities (JSCE, 1995)

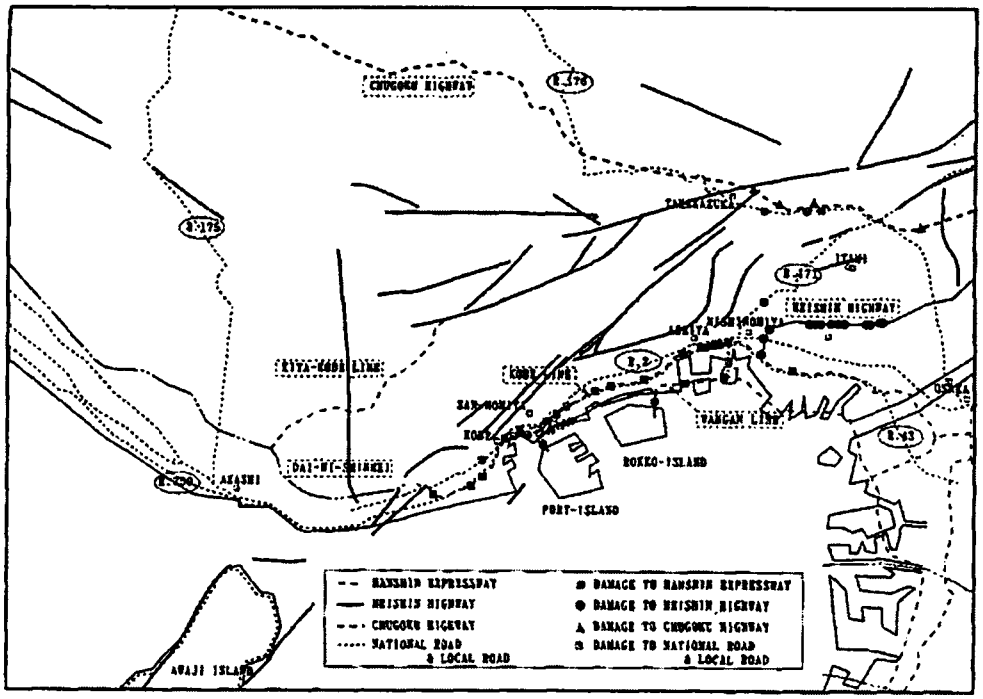

Figure 2.4 Location of damaged roads and bridges (JSCE, 1995)

(2) The 1999 Kocaeli earthquake, Turkey

A great earthquake occurred in Kocaeli Province, Turkey on August 17, 1999. The earthquake caused the collapse of more than 2,000 buildings, and the loss of more than 16,000 lives. The earthquake fault was observed on land from Yalova to Duzce, and the length of the fault was about 150 km. The displacement of the fault on the ground surface was measured from about 2 to 4 m. Disastrous damage to buildings, civil structures, industrial facilities was distributed along the fault.

The epicenter of the earthquake was at latitude 40.77 degrees, longitude 29.97 degrees, and at a depth of about 17 km. The fault rupture directed from the epicenter toward east. According to Earthquake Research Institute, University of Tokyo, source mechanism is thought to be right-lateral strike-slip fault. It is reported that the earthquake was induced by movement of two segments of the North Anatolian Fault.

Figure 2.5 shows recorded maximum accelerations of ground motions during the earthquake. The maximum accelerations of ground motions along the North Anatolian Fault are distributed from about 0.2 to 0.4 g. From this figure, it is found that detail of distribution of the peak ground motions is affected by the directivity of the fault rupture movement. In the east side of the fault where the rupture arrived, the area of large peak ground motions expanded.

A large number of buildings were perfectly broken by the fault movement. Several bridges, rails and embankments crossing the fault were completely collapsed by the lateral displacements of the fault.

Soil liquefaction widely occurred in the city of Adapazari and on the lake of Sapanca. The soil liquefaction inclined and/or sank many buildings, and broke buried pipes for water distribution.

Many 5 to 8 story-buildings were totally collapsed or heavily damaged. The natural periods of these buildings mostly coincide with the dominant periods of the ground motion (Japan Society of Civil Engineers, 1999). These structures were designed as moment-resistant frame structures with in-filled walls made of very brittle hollow bricks. Therefore, once they start to fail, they fail very quickly. Many buildings had a weak ground floor without shear-walls for shops or garages.

Motorways and rails run almost parallel to the fault, and crosses over it at several locations. The lateral displacement of the fault induced damage to bridges, rails and embankments.

Two highway bridges, Arifiye Overpass and Sakarya River Bridge, collapsed due to the displacement of the fault. There was extensive damage to reinforced concrete columns, parapet walls, reinforced concrete stoppers, bearings and prestressed concrete decks. It is thought that the main cause of the damage to roads and railways was ground surface faulting. The relative displacement at the ground surface along the fault rupture was observed to be about 4 m.

At Derince Port located very close to the epicenter, damage to quay walls was observed. The peak ground accelerations were estimated to be between 0.25 and 0.3 g during the earthquake.

Concrete cellular block walls moved toward the sea by about 0.7 m, and a large settlement in the backfill occurred of about 0.5 m. A crane with a capacity of 5 tons on a quay was overturned due to the settlement in the backfill during the earthquake. Boiled fine sands were found on the backfill ground, thus the soil liquefaction of backfill was thought to be one of the causes of the damage.

Several storage tanks for petroleum products in a national oil refinery plant were burned down. The tanks were damaged by high sloshing waves of storage liquid, which was caused by the long period components of the ground motion during the earthquake.

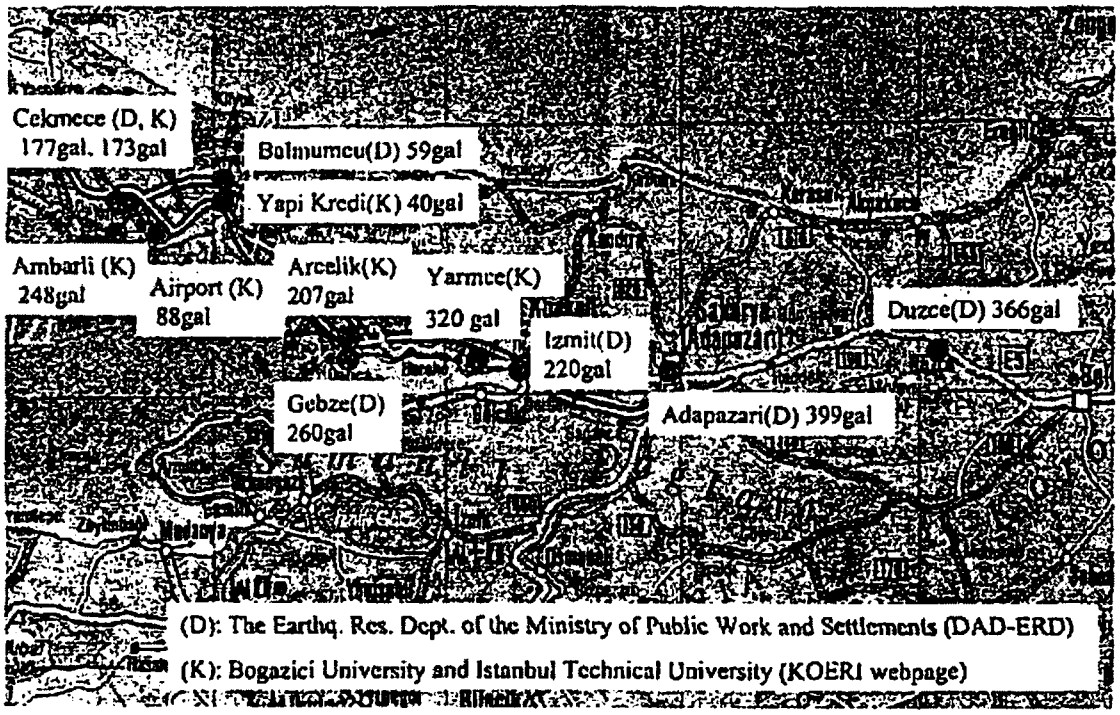

Figure 2.5 Distribution of horizontal peak ground accelerations (JSCE, 1999)

(3) The 1999 Chi-Chi earthquake, Taiwan

A major earthquake (M_W=7.6) occurred near the town of Chi-Chi in Nantou County, central Taiwan on September 21, 1999. According to the Taiwan's Interior Department, the earthquake caused about 2,000 deaths and about 10,000 injuries, and thousands of houses collapsed.

A seismic instrumentation program in Taiwan was implemented by the Central Weather Bureau (CWB). More than 700 strong observation stations are distributed and maintained. About 70% of them were triggered during the earthquake.

The epicenter of the earthquake was at latitude 23.85 degrees, longitude 120.81 degrees, and at a depth of about 7 km. According to Earthquake Research Institute, University of Tokyo, source mechanism is thought to be a reverse dip slip fault. It is thought that the earthquake was induced by the movement of the Chelongpu Fault in N-S direction along the foothills of the Central Range. The fault is 80 km in length, 40 km wide with 30-degree dip angle. The maximum dislocation at the ground surface was measured to be 6.5 m.

In Figure 2.6 and 2.7, recorded accelerations of ground motions during the earthquake in Taiwan (CWB, 1999) are shown. The recorded maximum accelerations of ground motions along the Chelongpu Fault are distributed between 300 and 800 cm/ sec^2.

In the whole area of Taiwan, more than 14,000 buildings suffered damage. In Nantou and Taichung Prefecture, in the epicentral region, more than 12,000 buildings were damaged and almost half of them collapsed. In Taichung City, more than 1,000 buildings was damaged, almost half of them totally collapsed.

Wufung is one of the towns across the Chelongpu Fault, and is located about 8 km south from Taichung City. The reconnaissance teams organized by the Japan Society of Civil Engineers made a comprehensive survey in Wufung, and investigated the correlation between the degree of structural damage and structural factors such as structural type, the number of stories, and location (Japan Society of Civil Engineers, 1999). They investigated the degree of damage to buildings in some blocks, based on Damage Level Criteria from the European Macroseismic Scale. According to the results, 5.8 % of 812 buildings collapsed. There was heavy damage found mainly to 2 and 4 story RC buildings and one-story masonry buildings. In Wufung, several buildings were severely damaged by ground surface ruptures along the Chelongpu Fault. Some buildings tilted due to differential settlements of their foundations.

At Dali City in the neighborhood of Taichung City, some of many condominium buildings collapsed. Damage to buildings was caused by large ground motions and/or ground surface faulting. The peak ground accelerations observed in the epicentral region were greater than 0.4 g. Many ground surface ruptures appeared along the Chelongpu Fault and induced differential settlement of building foundations.

According to the report from the Transportation Department of the Taiwanese Government, 10 bridges were severely damaged and 30 bridges were in need of repair. The majority of the damage to transportation facilities was caused by ground surface faulting and several structures were damaged by strong ground shaking. The displacement of ground surface faulting was reported to be about 2 to 9 m in the vertical direction and 2 to 3 m in the horizontal direction. Such huge displacements of the surface faulting caused falling-off of superstructures or complete overturning of substructures in highway bridge systems crossing the fault.

Swi-Wei Bridge, a simply supported concrete girder bridge, collapsed. The main cause of the bridge collapse is thought to be the ground surface faulting. Another simply supported concrete girder bridge, Bei-Fon Bridge, collapsed. The fault ran across the bridge and caused the collapse.

A cable-stayed bridge under construction was seriously damaged during the earthquake in the epicentral area. The bridge is located in Chi-Chi, and crosses over the Juo-Suei-Shi River. The span of the bridge is about 110 m, and the main tower is about 50 m high. One cable failed and the main tower suffered flexural and torsional cracks from the earthquake.

Port and harbor facilities in Taichung were damaged during the earthquake. The port of Taichung is located along the west coast of the central part of Taiwan. The epicentral distance to the port of Taichung is approximately 55 km.

In power transformation facilities, the Chungliao switching yard was seriously damaged during the earthquake. Insulators and bushings for the extra-high voltage switching facilities were damaged. The causes are thought to be both great ground shaking and ground surface faulting. According to the survey by the Taiwan Power Company, approximately 200 transmission steel towers were damaged.

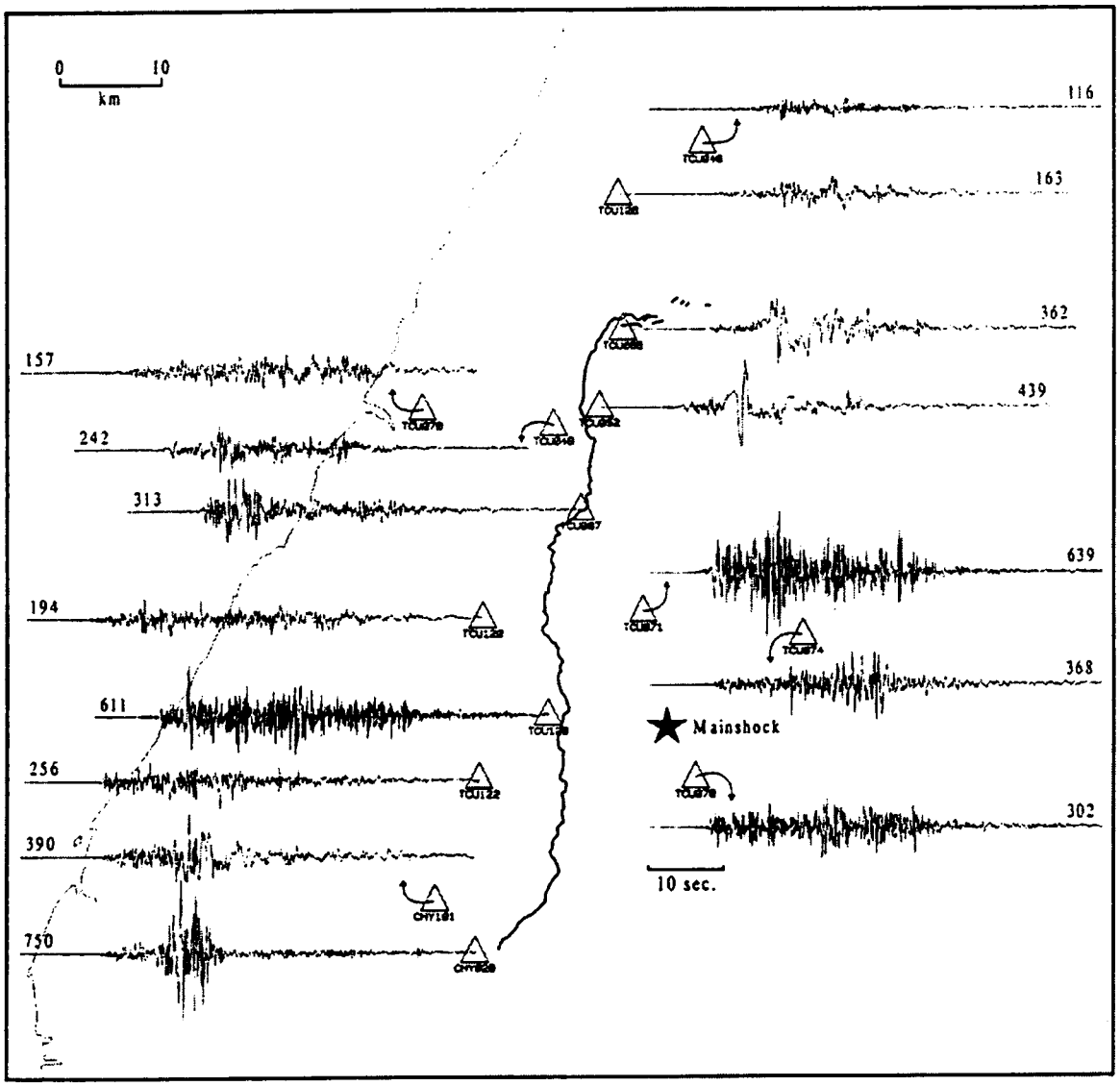

Figure 2.6 North-south components of recorded accelerations of ground motions

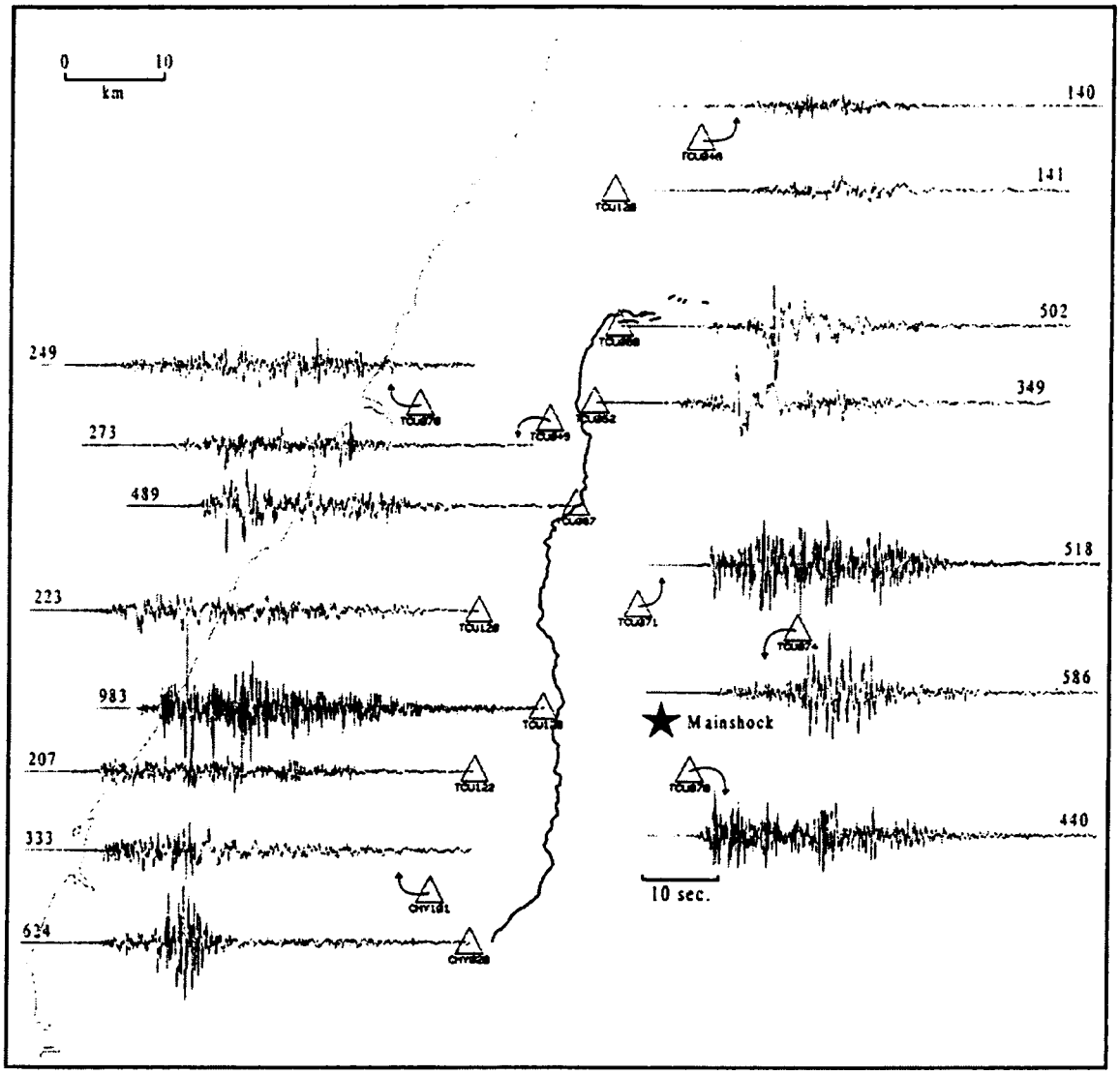

Figure 2.7 East-west components of recorded accelerations of ground motions

CHAPTER 3

DEFINITION OF DAMAGE SPECTRAUM OF GROUND MOTIONS

3.1 INTRODUCTION

The most important aspect of ground motion during a earthquake is its effect on structures, i.e., the stresses and deformations or the amount of damage it will produce. In this chapter, a damage spectrum of ground motion during an earthquake is introduced to estimate its damage potential. The damage spectrum is defined here as damage indices of single-degree-of-freedom system with natural periods ranging 0.05 to 5.0 sec. The damage index proposed by Park and Ang (1985) and a bilinear model as a force-displacement relationship are used to calculate the damage spectrum.

3.2 DEFINITION OF DAMAGE SPECTRUM

Structural damage depends on the characteristics of the structure as well as the ground motions. Thus, we must select an appropriate damage measure that reflects the characteristics of a structure. The damage index proposed by Park and Ang (1985) is an appropriate tool to evaluate the damage of concrete structures during earthquakes.

This index is expressed as a linear combination of the maximum normalized deformation and the hysteretic energy dissipation as follows:

$$D = \frac{\delta_m}{\delta_u} + \beta \int \frac{dE}{(Q_y \delta_u)} \qquad (3.1)$$

where D is the damage index, an empirical measure of damage, δ_m is the maximum response deformation, δ_u is the ultimate deformation capacity under static loading, Q_y is the calculated yield strength, dE is the incremental dissipated hysteretic energy, and β is the coefficient for cyclic loading effect. $D \geqq 1$ indicates total damage or collapse. $0<D<0.7$ indicates the slight damage, and $0.7<D<1.0$ indicates severe damage (Park and Ang, 1985). The limiting value of D (i.e., damage capacity of a member) is lognormally distributed with a mean of approximately 1.0 and a standard deviation of 0.54.

D(T,h) is defined to be the damage spectra for SDOF system with a bi-linear force-deformation characteristics subjected to a specified ground motion. For a given structural period T and damping h, D(T,h) is equal to the Park and Ang's damage index (Sunasaka, 1998, Sunasaka, Toki and Kiremidijian, 2001). The bi-linear model is shown in Figure 3.1 and the

parameters of the SDOF system and the damage index are shown in Table 3.1. The yield strength is set to be 40% of the weight of the SDOF and the ultimate deformation capacity is set to be four times that of the yield deformation. Park and Ang et al. (1985) studied the value of the parameter β in equation (3.1). Based on their study, it is appropriate to assume that the value of β in equation (3.1) is 0.05, when the force-displacement relationship is bi-linear.

Figure 3.2 shows a schematic explanation of the definition of the damage spectrum. The inelastic response of a SDOF system with natural period T_i subjected to a strong ground motion during a great earthquake (Figure 3.2(a)) is evaluated first. Then the damage index is calculated by using the inelastic response analysis of the SDOF system with natural period T_i. The damage spectrum is plotted in Figure 3.2(b) where the vertical axis shows damage indices and the horizontal axis shows natural periods T_i of the SDOF system ranging from 0.05 to 5.0 sec.

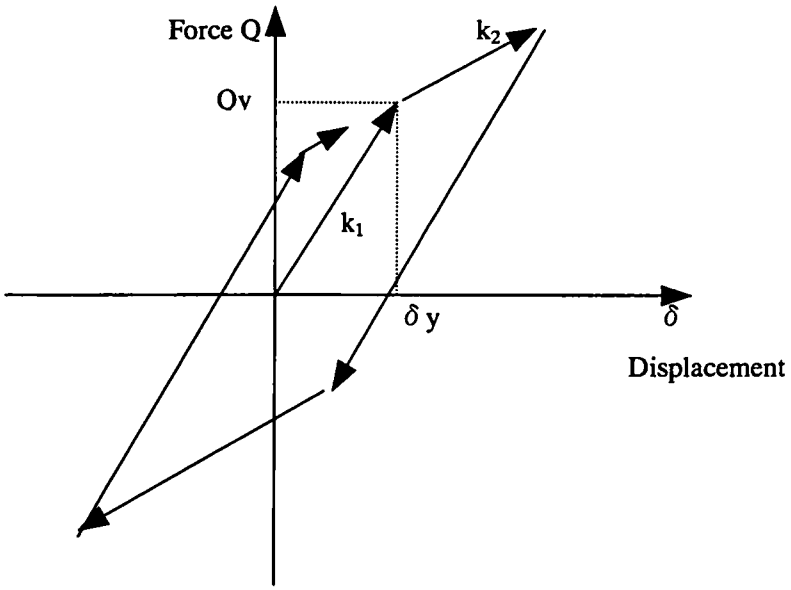

Figure 3.1 Bilinear force-displacement relationship

Table 3.1 Basic parameters for analysis

SDOF Model	damping ratio h	0.05
	second stiffness k_2	$0.05k_1$
	yield strength Qy	0.4W
Damage Index	coefficient β	0.05
	ultimate deformation capacity δu	$4\delta y$

k_1: initial stiffness, W: weight of the SDOF, δy: yield deformation

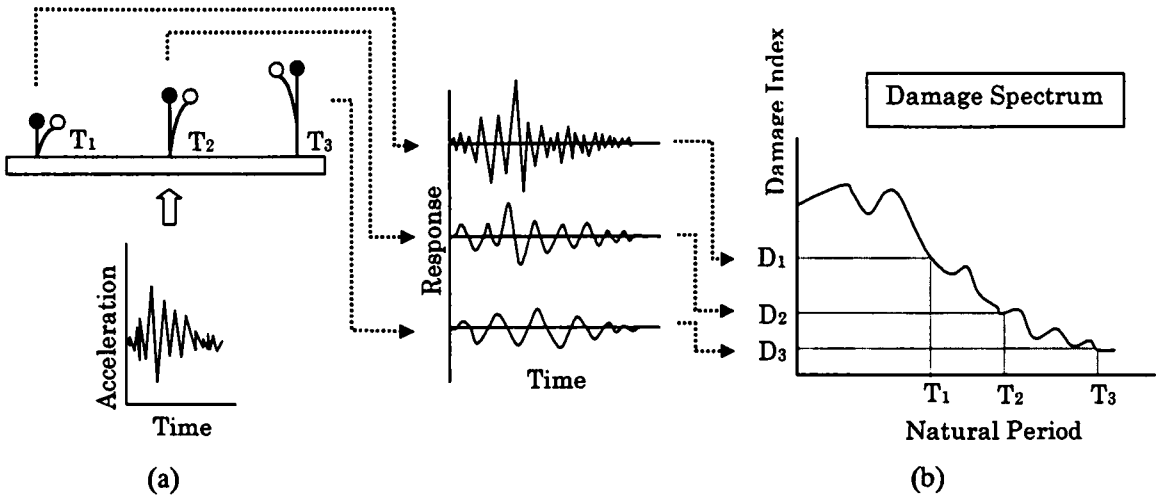

Figure 3.2 Schematic explanation of definition of damage spectrum

3.3 CHARACTERISTICS OF DAMAGE SPECTRA

For a demonstration of damage spectra, two representative recorded ground motions, i.e. the ground motion recorded at El Centro during the 1940 earthquake and the ground motion recorded at JMA Kobe during the 1995 Hyogoken-Nanbu earthquake, are selected. The acceleration time histories of the ground motions are shown in Figure 3.3. The damage spectra of the two ground motions, according to the definition described above and the elastic response spectra are shown in Figure 3.4. The response spectrum of the ground motion recorded at JMA Kobe are much larger than those at El Centro, but it is difficult to suppose directly the effect they will have on structures. As shown in Figure 3.4, the damage indices of the ground motion observed at El Centro are smaller than 1 for all natural periods range. Therefore the ground motion is supposed to have very small damage potential against all structures. As for the SDOF systems with the natural periods less than about 0.7 sec., the damage indices of the ground motion at JMA Kobe during the 1995 Hyogoken-Nanbu earthquake are greater than 1. Therefore the ground motion is supposed to have very large damage potential for structures with natural periods less than about 0.7 sec.

In Figures 3.5 to 3.7, the required yield strength ratio spectra in view of damage index are shown. The required yield strength spectrum demonstrates the relationship between the natural period of SDOF and the ratio of the required yield strength to the weight of the SDOF so as to satisfy a safety level presented by the damage index.

Figure 3.5 shows the required yield strength ratio spectra so as to satisfy the damage index=1.0 for various ratios μ of the ultimate deformation capacity under static deformation, δ u, to the yield deformation, δ y, of the SDOF. Figure 3.6 shows the required yield strength ratio spectra for the damage index=1.0 and 0.7 in the case of μ=4. Figure 3.7 shows the required yield

strength ratio spectra to satisfy the damage index=1.0 with β in Equation(3.1) of 0.05 and 0.0. In the case of the parameter β =0.0, the required yield strength ratio spectra is the same as that to satisfy ductility=4.0.

In Figures 3.8 and 3.9, parametric studies on damage spectra of ground motions recorded at El Centro and at JMA are shown, respectively. The values of the parameters that are not explicit in the figures are the same as those shown in Table 3.1. It is found that the yield strength Qy and the ultimate deformation capacity δ u have a strong effect on the damage spectrum and that the parameter β, the damping ratio h and the ratio of second stiffness to initial stiffness k_2/k_1 have a considerable effect on the damage spectrum.

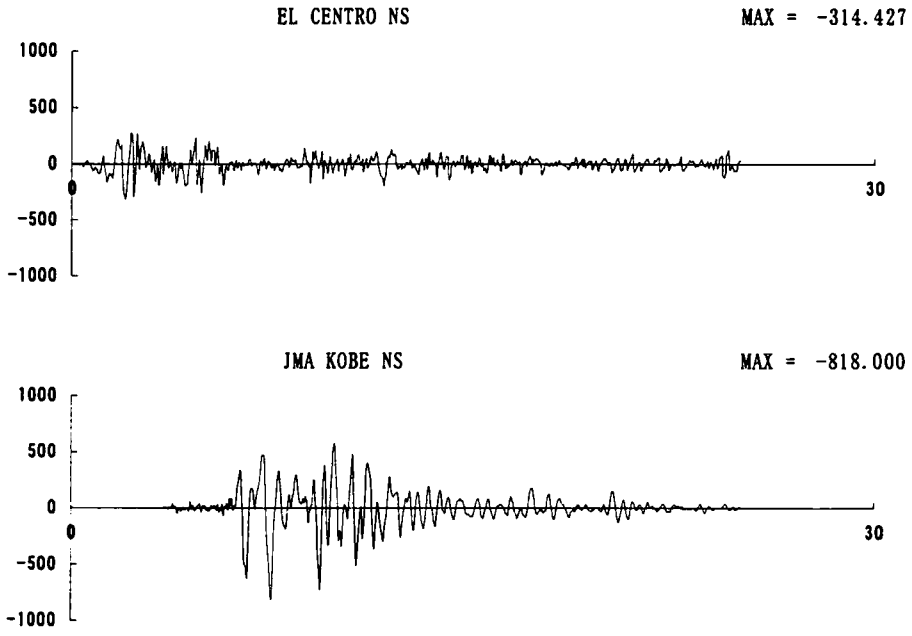

Figure 3.3 Acceleration time histories of the ground motions

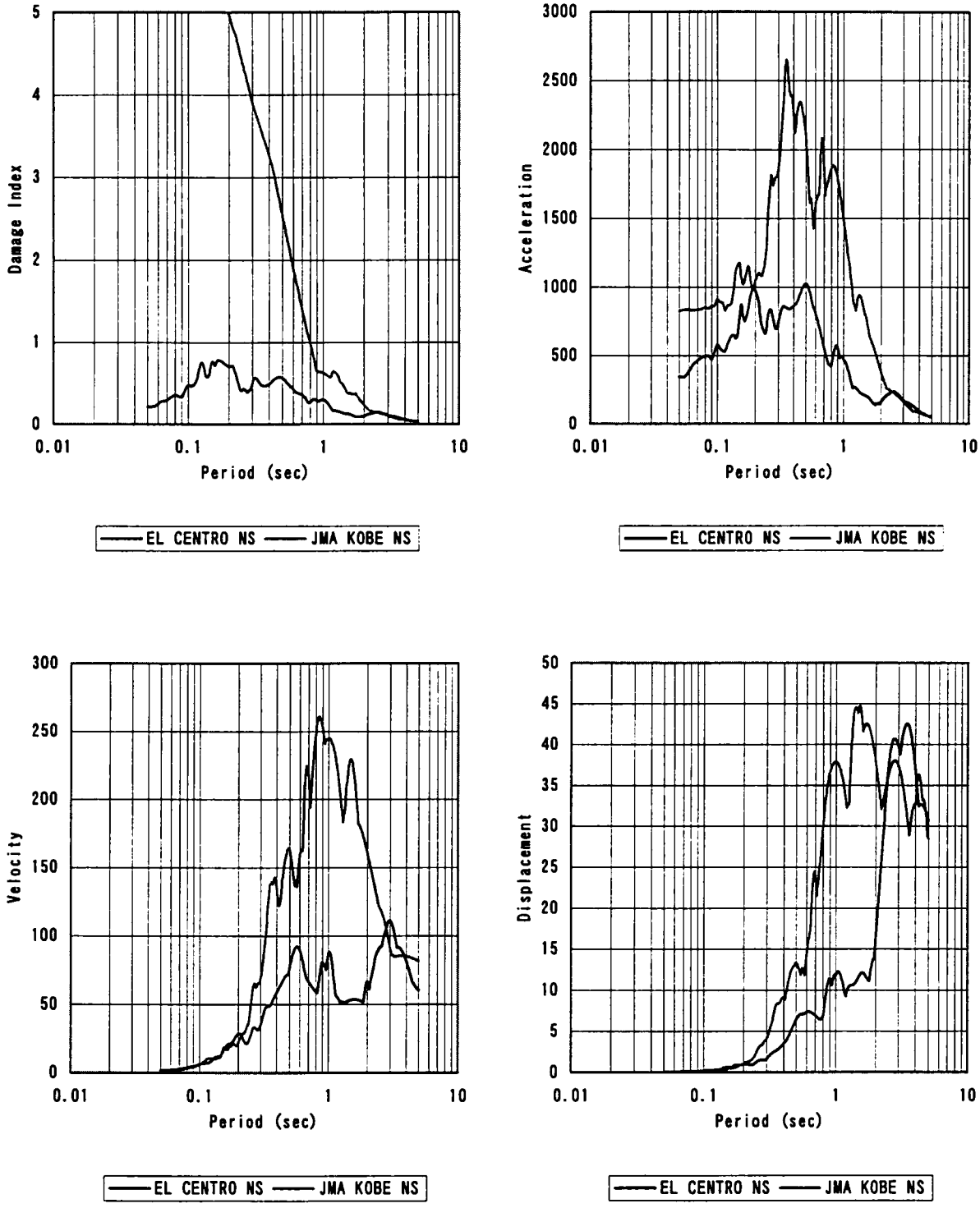

Figure 3.4 Damage spectra and response spectra of ground motions recorded at El Centro and JMA Kobe

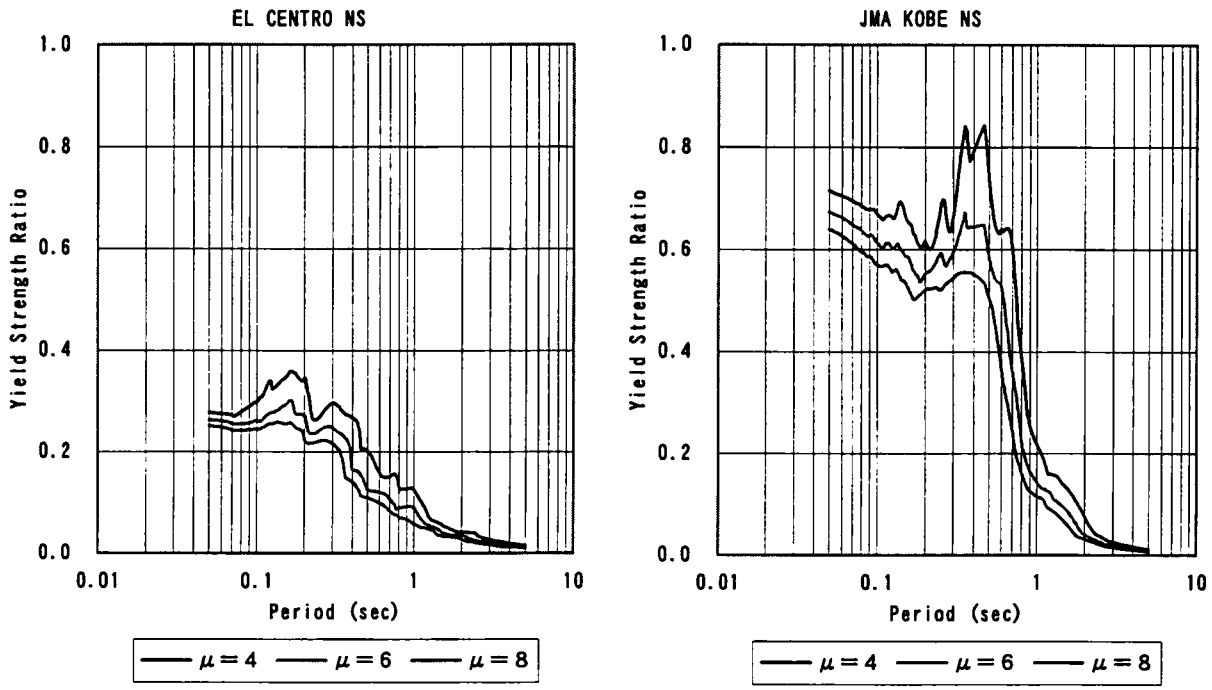

Figure 3.5 Required yield strength ratio spectra in view of damage index (Damage index=1.0)

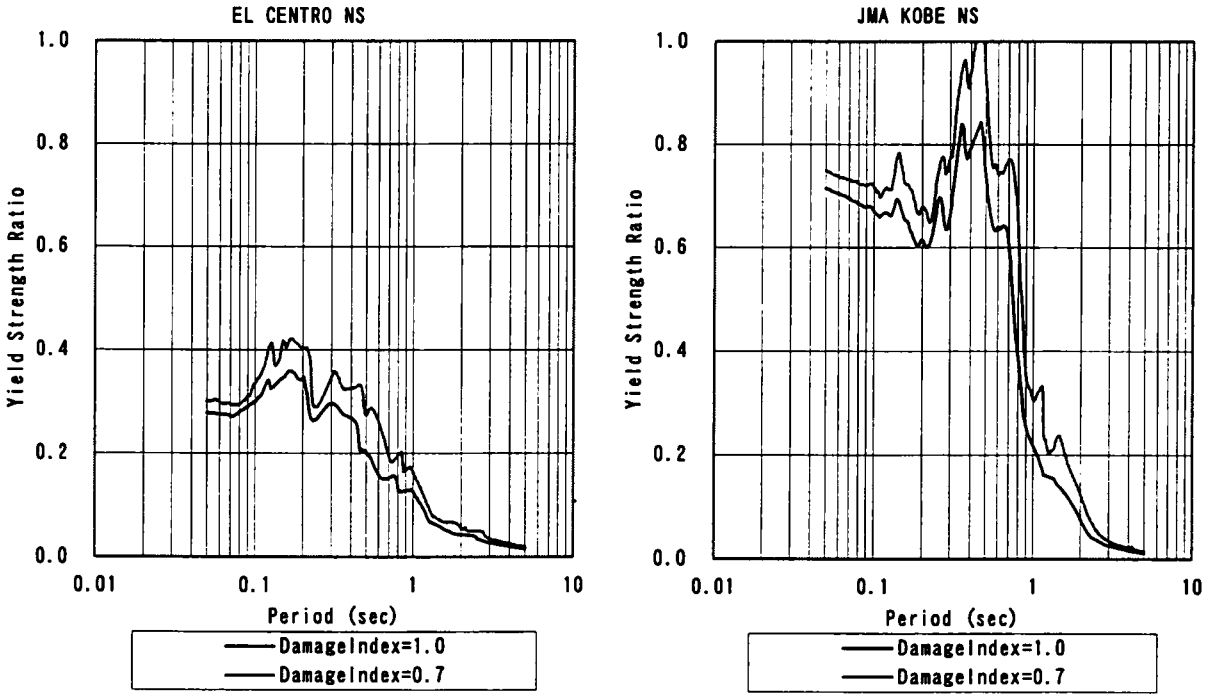

Figure 3.6 Required yield strength ratio spectra in view of damage index (Damage index=1.0, 0.7)

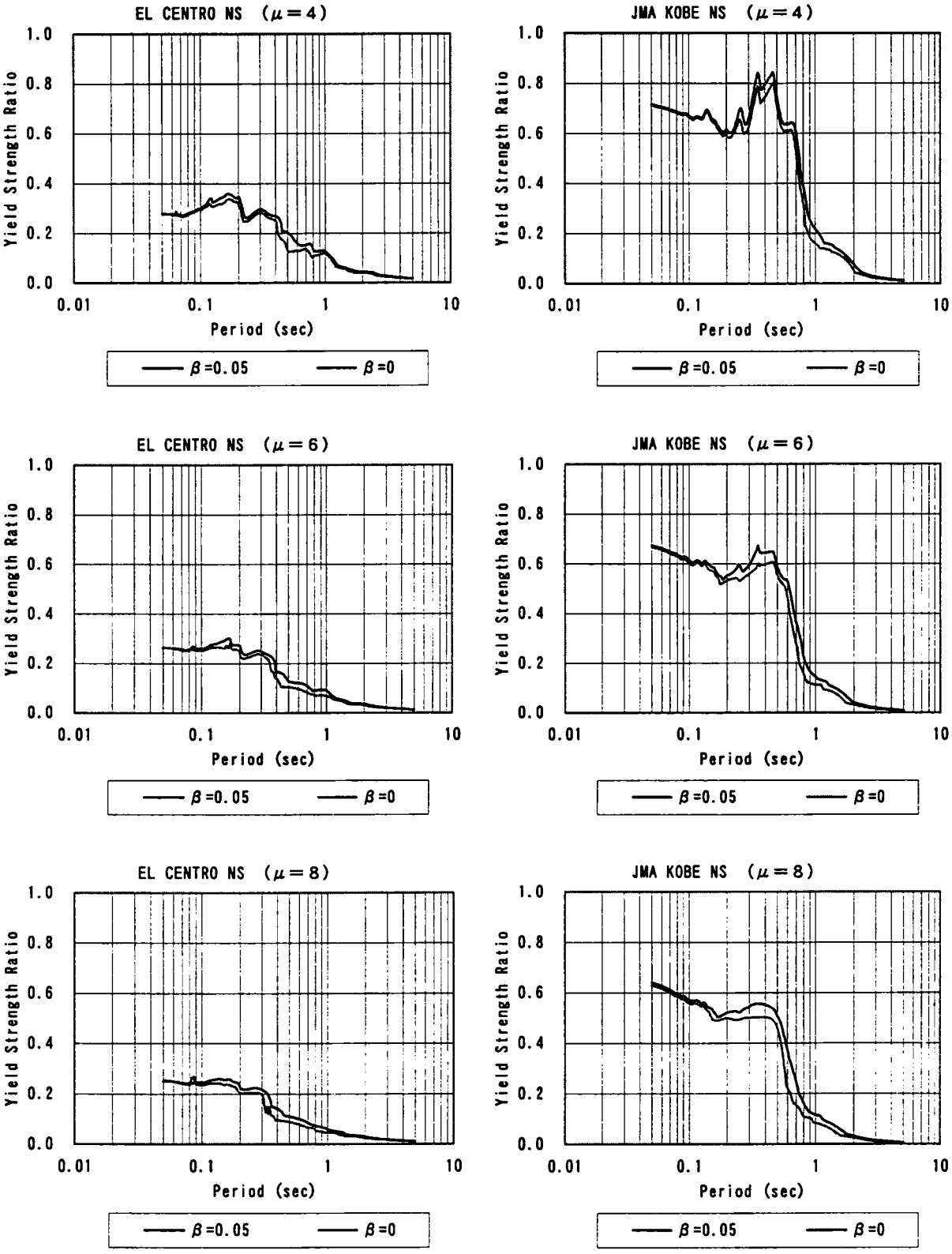

Figure 3.7 Required yield strength ratio spectra in view of damage index (Damage index=1.0)

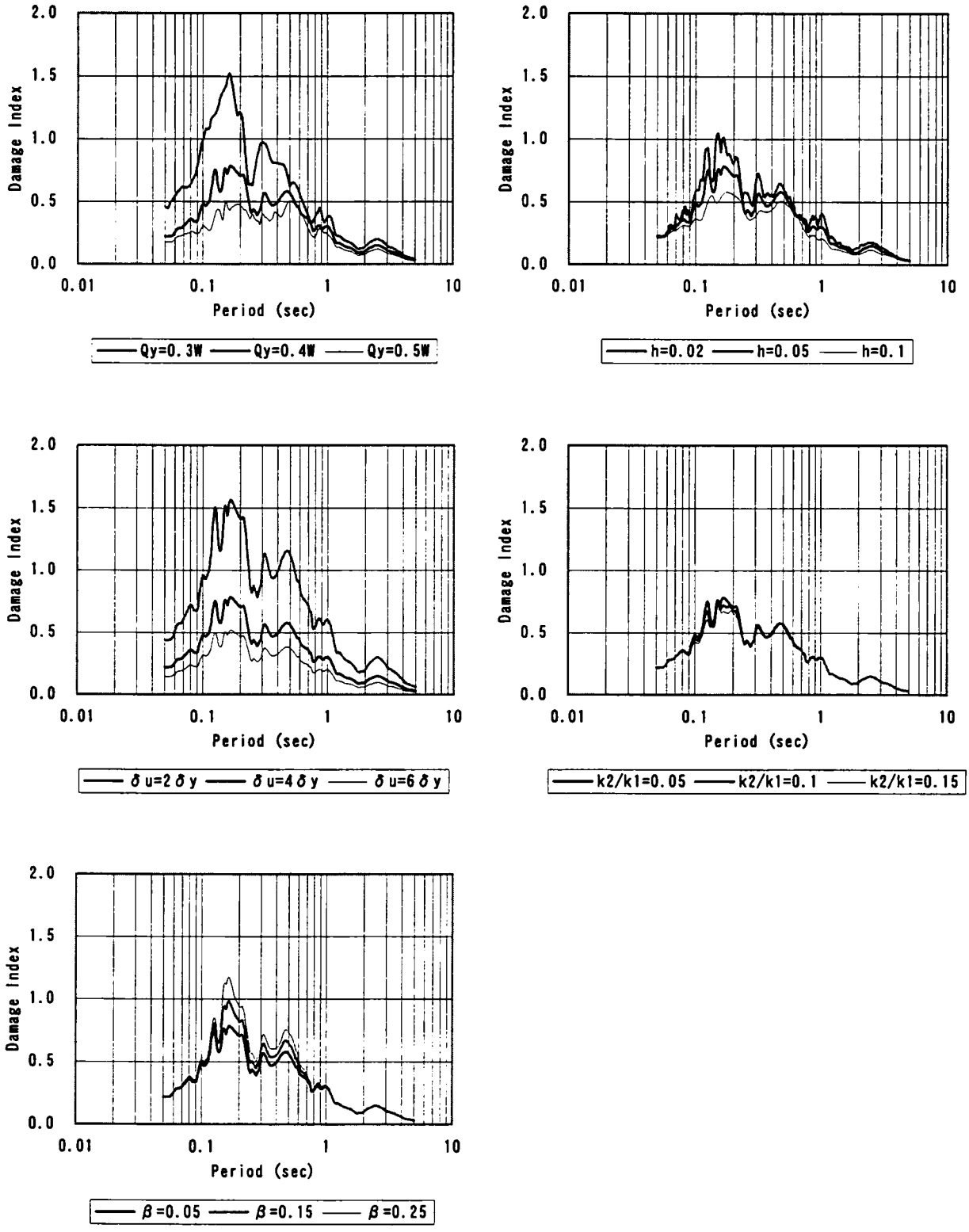

Figure 3.8 Parametric studies on damage spectra of ground motions recorded at El Centro

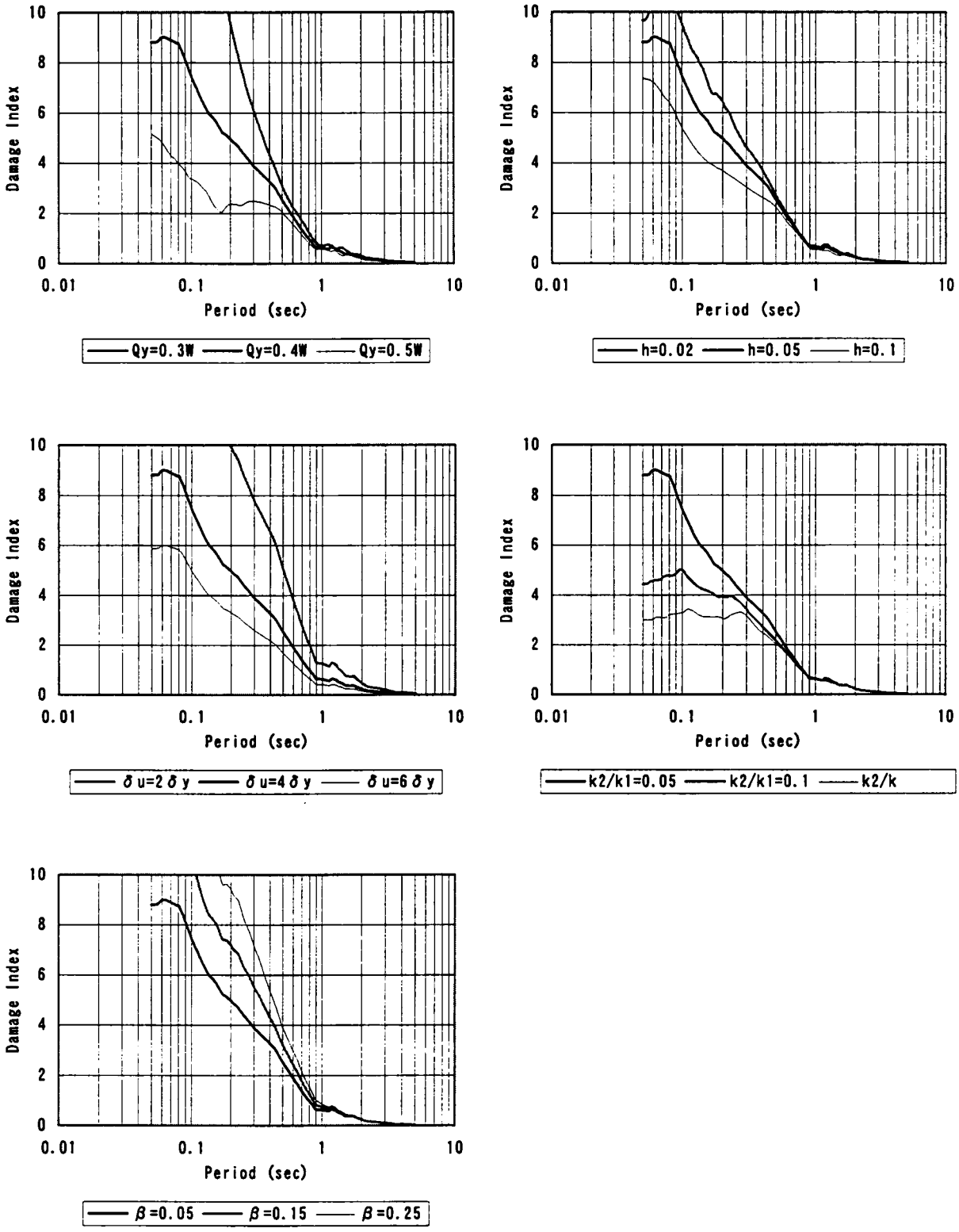

Figure 3.9 Parametric studies on damage spectra of ground motions recorded at JMA

CHAPTER 4

DAMAGE POTENTIAL OF GROUND MOTIONS DURING PAST GREAT EARTHQUAKES

4.1 INTRODUCTION

As summarized in Chapter 2, very severe damage to engineering structures was caused during recent great earthquakes including the 1995 Hyogoken-Nanbu earthquake, the 1999 Kocaeli earthquake in Turkey, and the 1999 Chi-Chi earthquake in Taiwan. In Chapter 3, damage spectra of ground motions are defined and characteristics of damage spectra are described.

In this chapter damage potential of ground motions during recent great earthquakes including the 1995 Hyogoken-Nanbu earthquake, the 1999 Kocaeli earthquake in Turkey, 1999 Chi-Chi earthquake in Taiwan and damage potential of earthquake ground motions that have been used for design purpose are described.

4.2 DAMAGE POTENTIAL OF THE 1995 HYOGOKEN-NANBU EARTHQUAKE

Structural damage in Kobe during the 1995 Hyogoken-Nanbu earthquake was concentrated in a belt 0.7 to 1.2 km wide stretching from southwest to northeast along the foot of the Rokko Mountains as shown in Figure 4.1. Figure 4.2 shows the recorded ground motions at JMA Kobe, Fukiai (FKI), Kobe University (KBU) and NTT during the Hyogoken-Nanbu earthquake in or around the heavily damaged zone shown in Figure 4.1. Figure 4.3 shows the damage spectra of the ground motions (Sunasaka, 1996, Sunasaka, 1997, Sunasaka, 1998). The damage spectrum of the ground motion recorded at FKI in the heavily damaged zone is the largest in the recorded ground motions for almost all natural periods. The damage indices of the ground motion recorded at FKI are larger than 1.0 at natural periods smaller than about 1.2 sec, and the damage indices of the ground motion recorded at JMA Kobe are larger than 1.0 at natural periods smaller than about 0.7 sec. These results agree with the fact that 45 percents of 158 viaducts piers with natural periods ranging 0.4 to 0.9 sec. collapsed in this zone (Japan Society of Civil Engineers, 1996a). The damage spectra of ground motions recorded at KBU and NTT outside of the heavily damaged zone are smaller than 1.0 in all natural period range, however.

To estimate the amplification characteristics of ground motions in the heavily damaged zone in the city of Kobe during the Hyogoken-Nanmu earthquake, Motosaka and Nagano (1996) performed wave-propagation analyses of a deep irregular underground structure model with vertical discontinuity. The incident waveform at bedrock was estimated by deconvolution analysis using the

observed record at Kobe University. Figure 4.4 shows the two-dimensional model of the underground structure orthogonal to the Rokko Fault plane along the Rokko Mountains. Figure 4.5 shows the configuration of shallow surface layers. Figure 4.6 shows the simulated ground motions by Motosaka and Nagano (1996) at ground surface points P1 to P8 shown in Figure 4.5. Ground surface points P4 to P6 are located in the heavily damaged zone, and P4 among them is located in the most heavily damaged zone between JR and the Hanshin Railway Line (HR). The ground motions in the heavily damaged zone were amplified due to the focusing effect in the deep irregular underground structure as well as in the shallow surface layers.

The damage spectra of the simulated ground motions are calculated and showed in Figure 4.7. According to this figure, the damage spectra of the simulated ground motions at ground surface points P4 to P7 located in the heavily damaged zone are relatively large. Among them, the largest is the damage spectra of the ground motion at P4 located between JR and the Hanshin Railway Line. The damage indices of the ground motions at the point are larger than 1.0 at natural periods smaller than about 1.5 sec, and the damage indices of the ground motions at points P5 to P7 are larger than 1.0 at natural periods smaller than about 0.7 sec. These results agree with the fact that 45 percents of 158 viaducts piers with natural periods 0.4 to 0.9 sec of JR collapsed in the zone (Japan Society of Civil Engineers, 1996a). The damage spectra of ground accelerations at P1 and P2 are smaller than 1.0 for all natural periods. The intensity of the damage spectra of ground accelerations increases with distance from the Rokko Mountains to P4. Beyond P4, the intensity of the damage spectra of ground accelerations decreases with distance from the Rokko Mountains. These results demonstrate that the damage spectra well correlate with the structural damage, and that the concentration of structural damage in the nallow zone stretching from southwest to northeast along the foot of the Rokko Mountains is mainly explained by the geological deep ground conditions of Kobe.

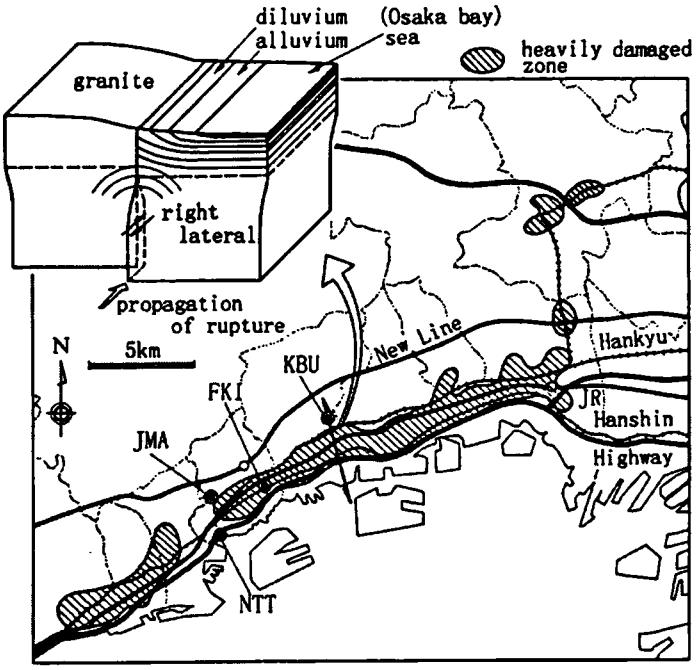

Figure 4.1 Heavily damaged zone in Kobe City and schematic diagram of underground structure

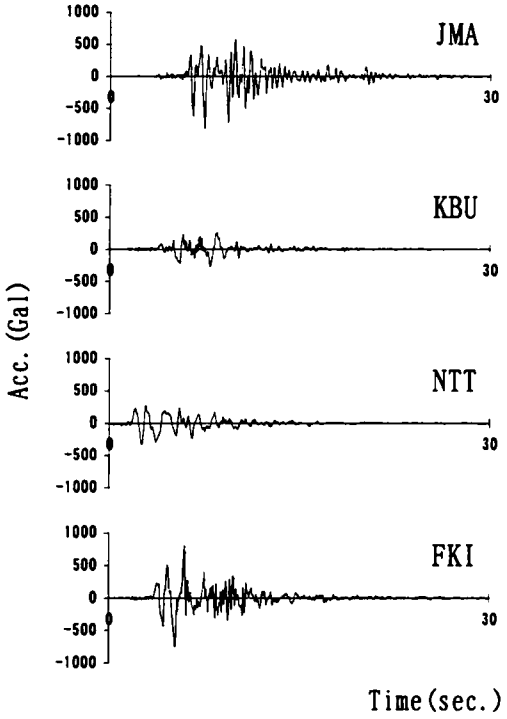

Figure 4.2 Recorded ground accelerations at JMA, KBU, FKI and NTT During Hyogoken-Nanbu earthquake

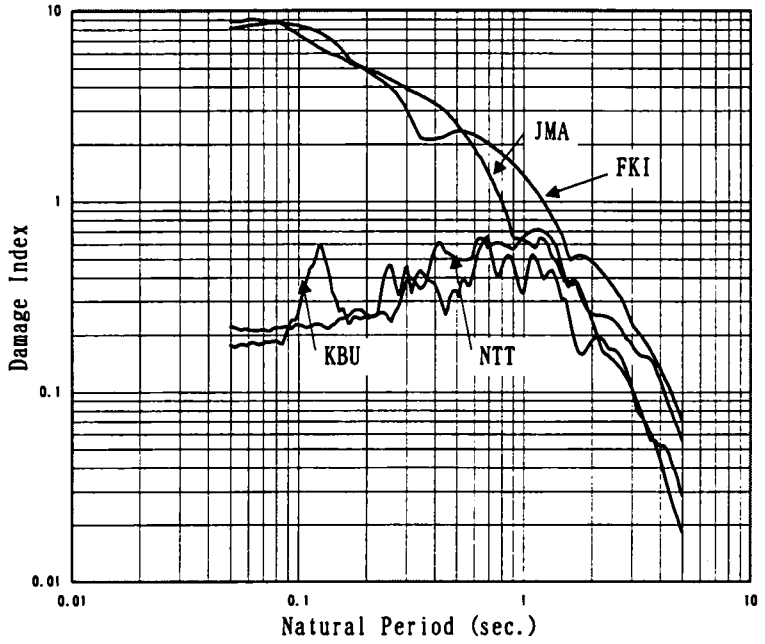

Figure 4.3 Damage spectra of ground motions at JMA, KBU, FKI and NTT

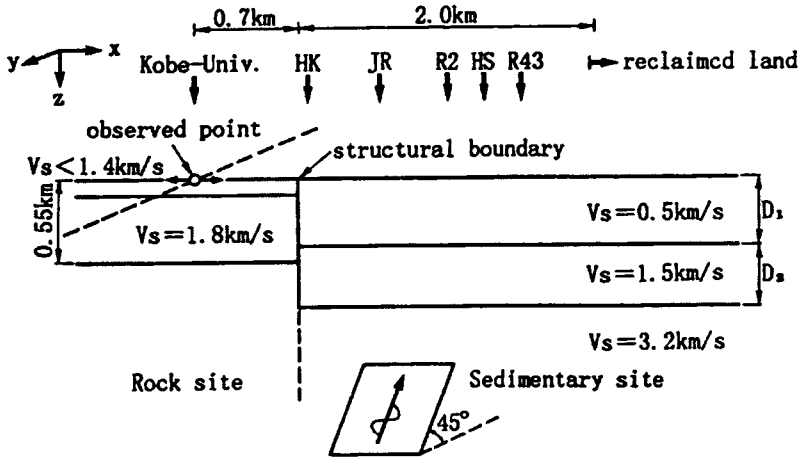

Figure 4.4 Two-dimensional model of deep irregular underground structure orthogonal to Rokko Fault line

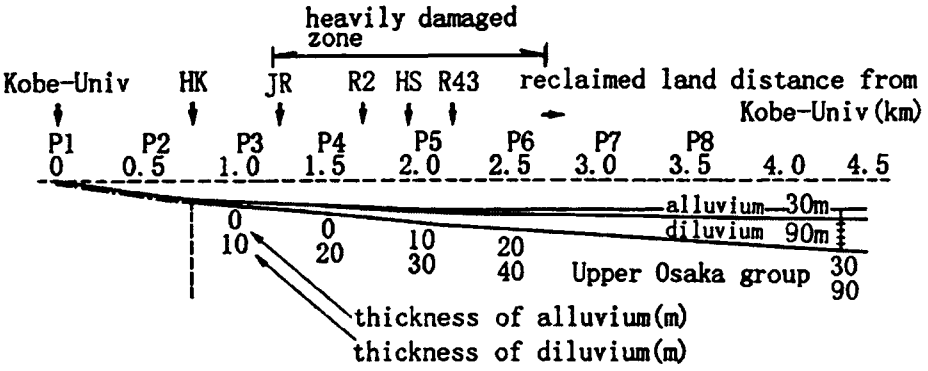

Figure 4.5 Configuration of shallow surface layers

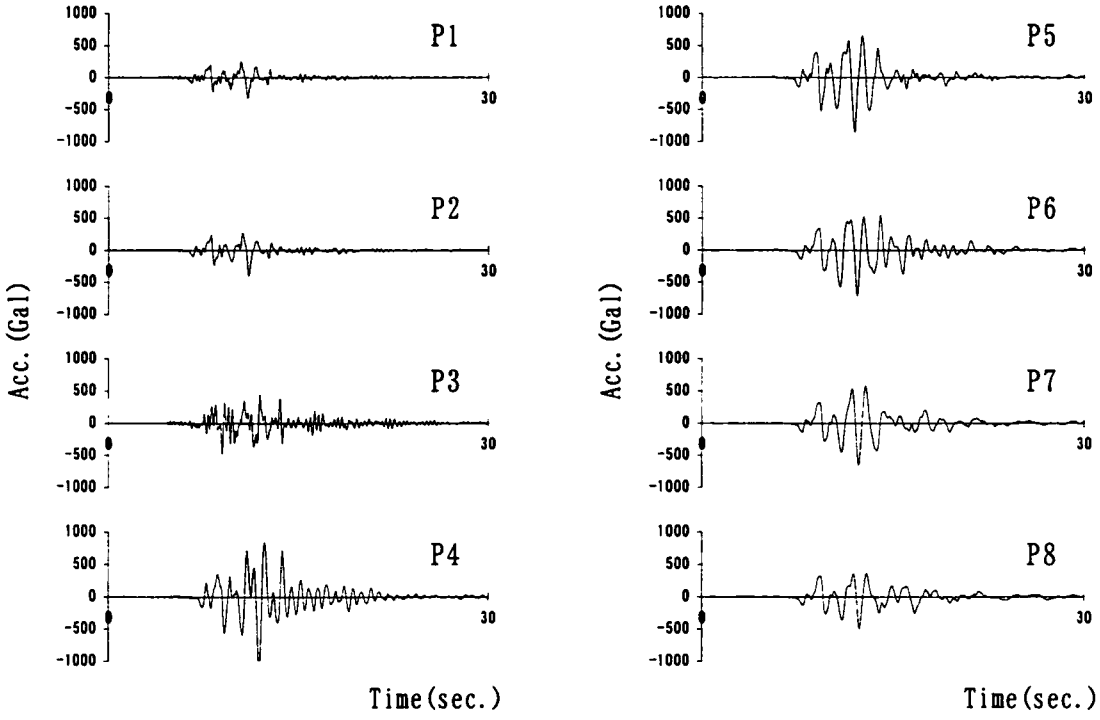

Figure 4.6 Simulated ground accelerations by Motosaka and Nagano (1996)

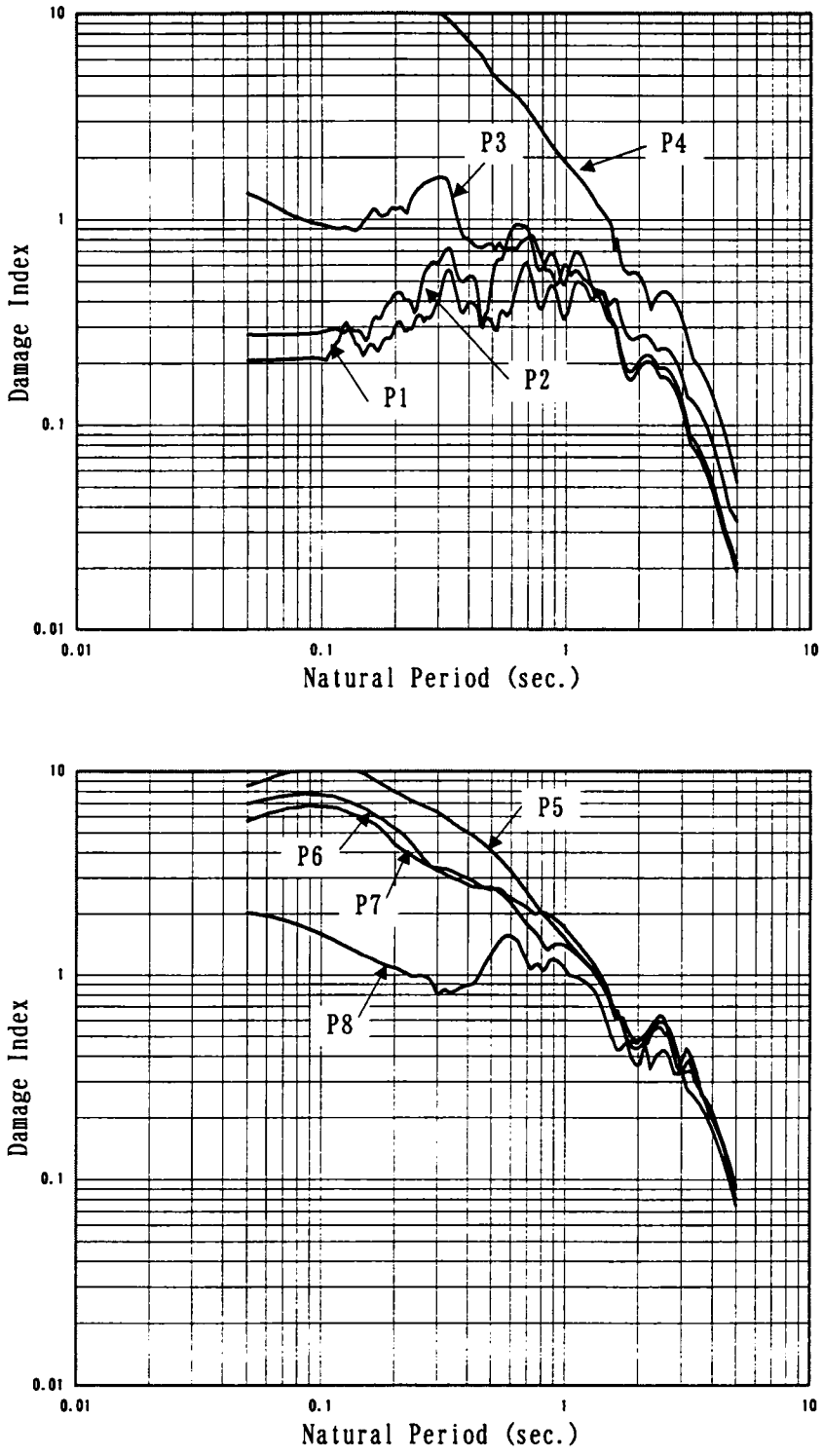

Figure 4.7 Damage spectra of simulated ground motions during Hyogoken-Nanbu earthquake

4.3 DAMAGE POTENTIAL OF THE 1999 KOCAELI EARTHQUAKE, TURKEY

Figure 4.8 shows the recorded acceleration time histories of the ground motions at Duzce (DZC), Gebze (GBZ), Izmit (IZT) and Sakarya (SKR) along the North Anatolian Fault during the 1999 Turkey earthquake. It is thought that the maximum accelerations of ground motions about 0.2 to 0.4 g are small in contrast to the severe structural damage. The elastic acceleration response spectra are shown in Figure 4.9. Based on those figures, it is found that the predominant periods of the ground motion are distributed from 0.1 to 0.4 sec. and that the maximum acceleration response are about 1000 and 1500 cm/sec^2 for NS component at DZC and EW component at SKR, respectively. The small acceleration response suggests that the damage potential of the ground motions are relatively small.

Figure 4.10 shows the damage spectra of the recorded ground motions at DZC, GBZ, IZT and SKR. It is found from Figure 4.9 and Figure 4.10 that the shapes of the acceleration response spectra are very similar to those of the damage spectra. However, the sharpness of the damage spectra is emphasized around damage index of 1.0. Damage indices of ground motions at GBZ and IZM are much smaller than 1.0 for all natural periods. Damage indices of ground motions at DZC and SKR are larger than 1.0 for narrow period range from 0.1 to 0.2 sec. This means that the damage potential of ground motions during the Kocaeli earthquake is relatively small.

Some of structural damage was directly caused by the fault movement, liquefaction or liquefaction-induced large ground displacements. In spite of relatively small damage spectra of the observed ground motions during the earthquake, however, many structures were severely damaged by ground motions during the earthquake. This is thought to imply poor earthquake-resistant capacity of the structures in Turkey. Many collapsed or heavily damaged apartment buildings had 5-8 stories. The natural periods of these buildings range between 0.2 and 0.4 sec., and mostly coincided with the predominant periods of the ground motions. These structures were designed as moment-resistant frame structures with in-fill walls made of hollow bricks. The diameters of reinforcing bars were mostly between 8 and 16 mm and bars were generally of smooth types (Japan Society of Civil Engineers, 1999). These poor earthquake-resistant capacities of the structures would be the reason why many structures were severely damaged by ground motions during the earthquake in spite of relatively small damage spectra of the ground motions.

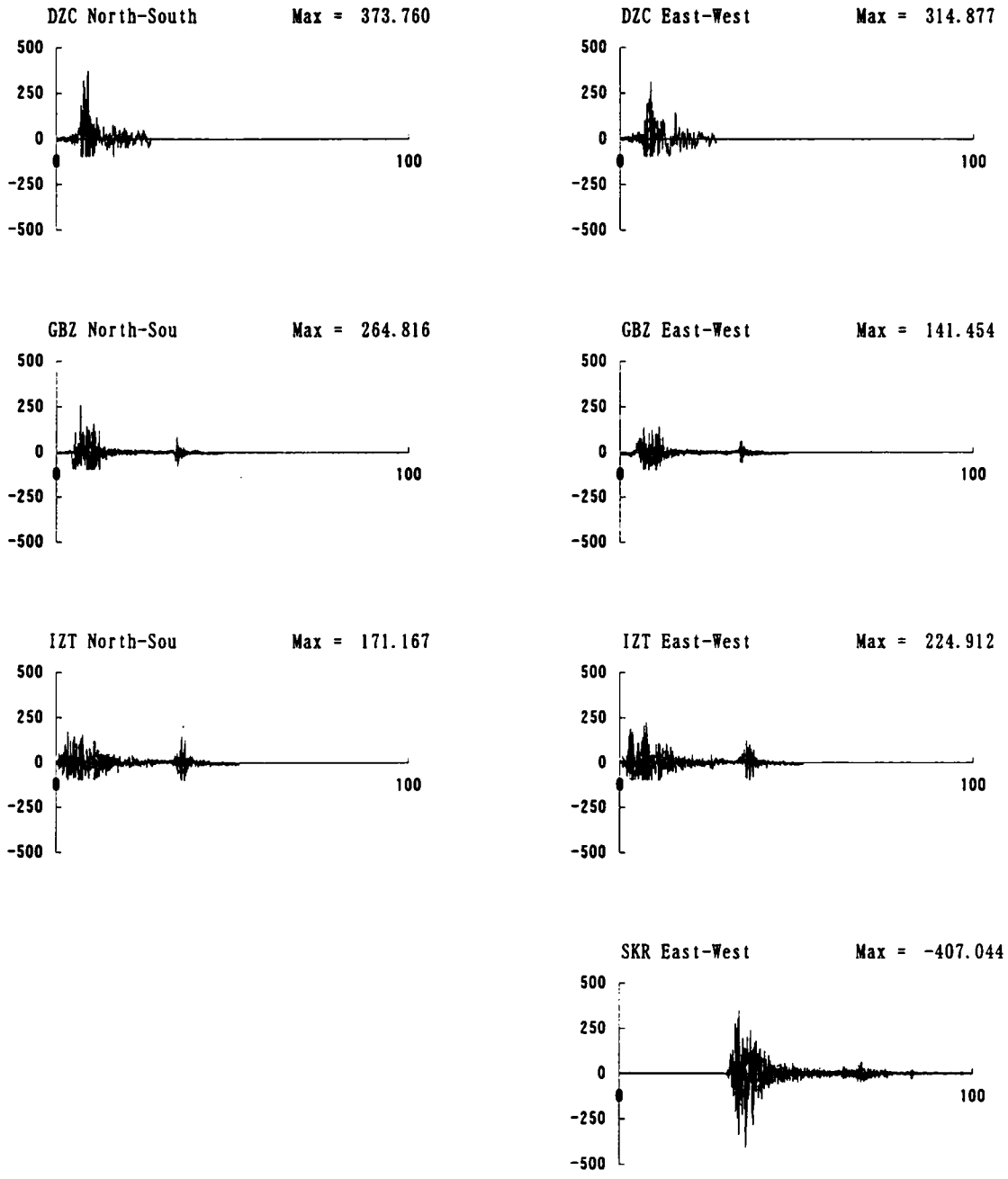

Figure 4.8 Recorded acceleration time histories at DZC, GBZ, IZT and SKR during the Kocaeli earthquake

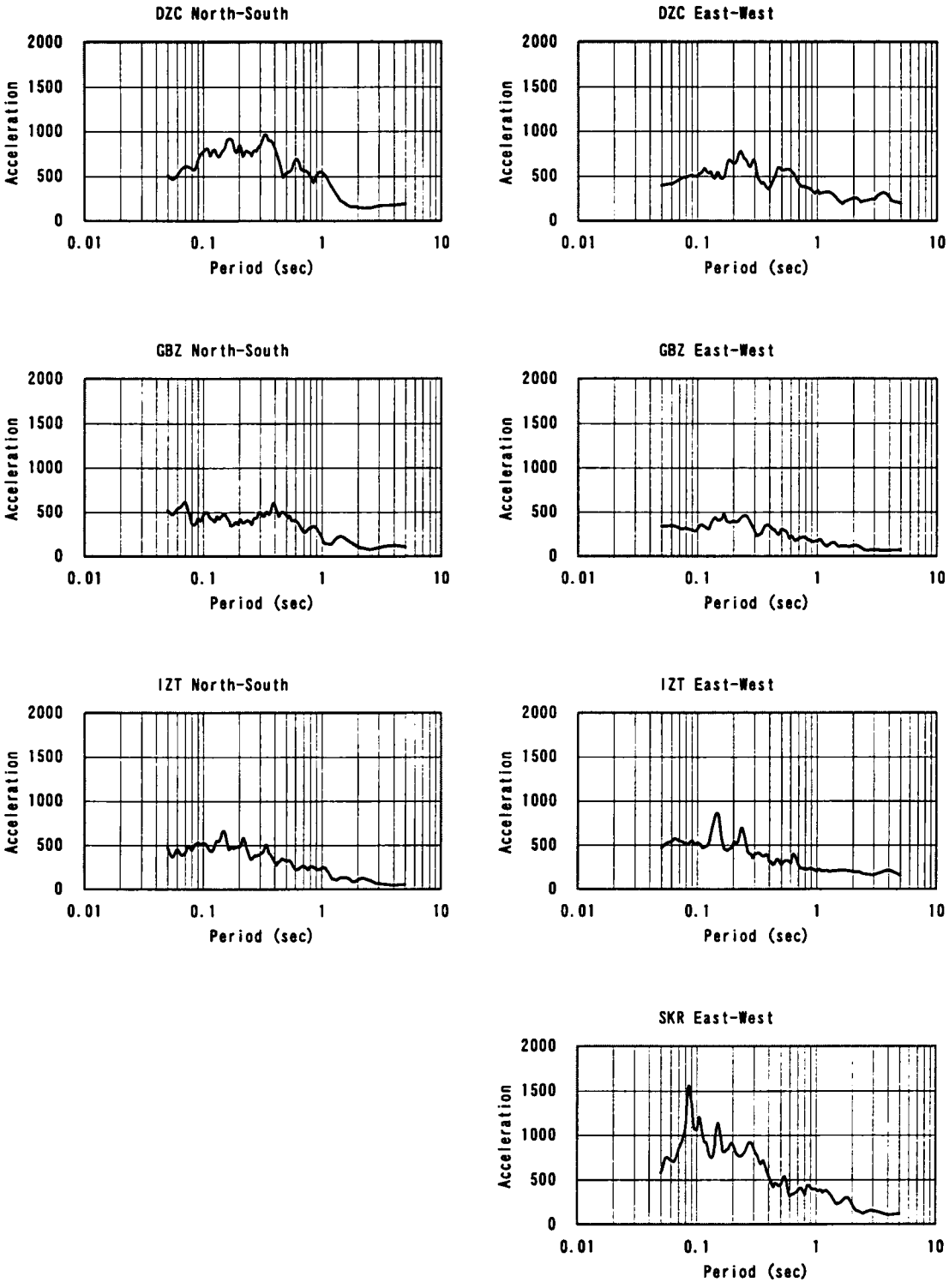

Figure 4.9 Acceleration response spectra of the recorded ground motions during the Kocaeli earthquake

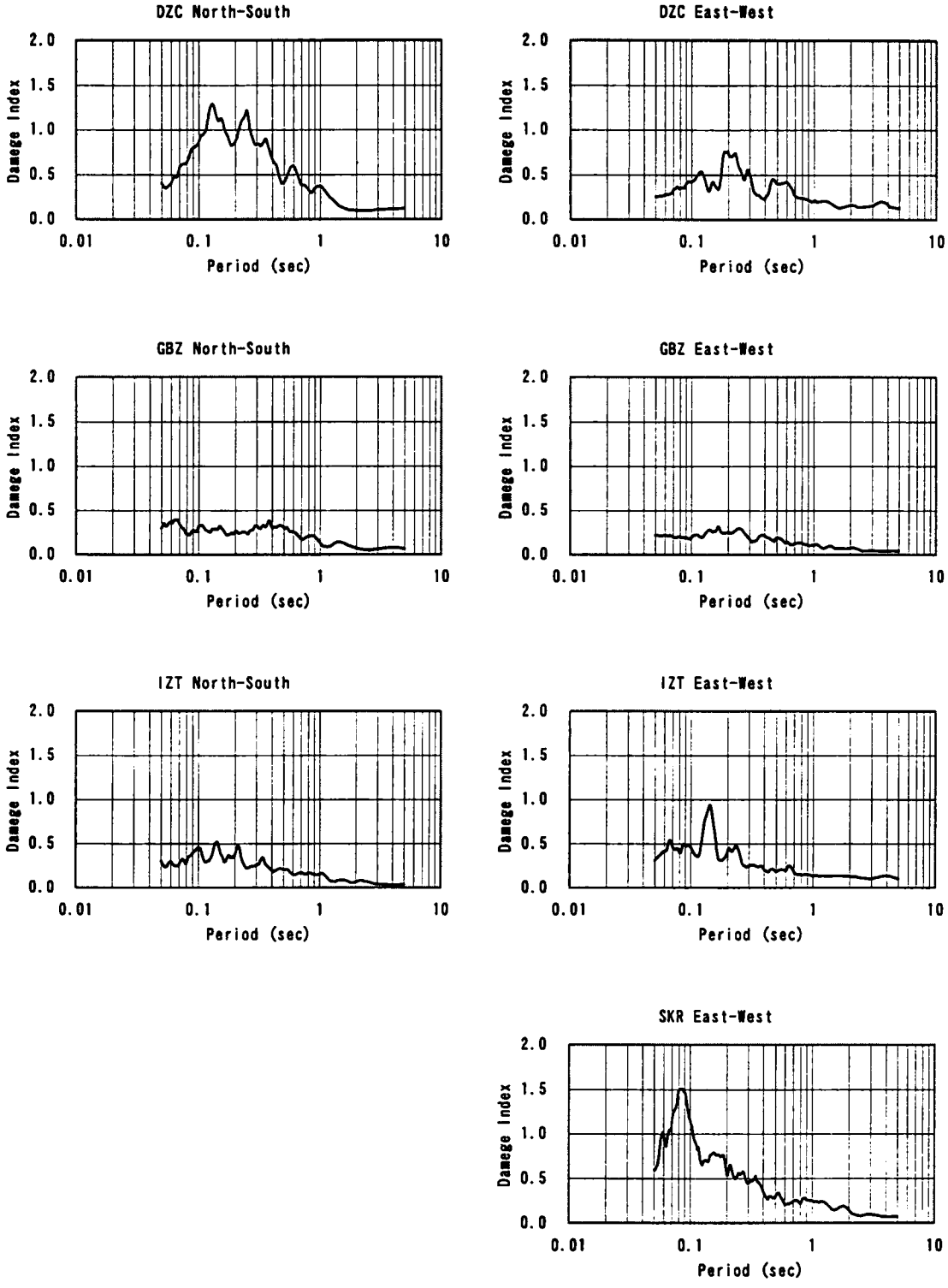

Figure 4.10 Damage spectra of the recorded ground motions during the Kocaeli earthquake

4.4 DAMAGE POTENTIAL OF THE 1999 CHI-CHI EARTHQUAKE, TAIWAN

Ground motion records during the Chi-Chi earthquake were retrieved from the free-field accelerographs by the Central Weather Bureau (CWB). In Figures 4.11, the recorded ground motions at the stations located relatively close to the fault are shown. In this figure, integrated velocities and displacements of ground motions from the acceleration records are showed, too. Along the northern end of the fault, very simple waveforms are observed. At the southern end of the fault, a large ground motion with very short duration is observed. Very large ground motions with long duration and high frequencies are observed in the middle of the fault.

The damage spectra of ground motions at the stations are shown in Figure 4.12 (Sunasaka, Toki and Kiremidejian, 2001). The damage spectra of the EW component at station TCU068 and the NS component at station TCU052 in the northern part and eastern side of the fault are fairly large for natural periods less than around 1.0 sec., while their waveforms are very simple and the maximum accelerations are relatively small. These fairy large damage spectra appear to correspond to the ground motions recorded at stations where many civil engineering structures suffered severe damage. The damage spectra of ground motions at station CHY028 in the southern part and western side of the fault are much larger than 1.0 for the natural periods less than about 0.9 sec., while the ground motions have fairly large PGA and short duration. The damage spectra of ground motions at stations TCU129 and TCU065 in the middle part of the fault are larger than 1.0 for the natural periods less than about 0.7 sec., while the ground motions have long duration and high frequencies.

The locations of the stations that are very close to the fault can be classified into six parts as shown in Table 4.1. Unfortunately, there are no stations in the southern part and eastern side of the fault. The selected ground motions in Table 4.1 are representatives of those damage spectra that are the largest in each location along the fault. Station TCU068 is located in the northern part and eastern side of the fault where the rupture arrived. The ground motion observed at the station has relatively low PGA, low dominant frequency, and then high damage potential for relatively long natural periods around 1.0 sec. Station CHY028 is located in the southern part and western side of the fault where the rupture extended. The ground motion observed at the station has large maximum acceleration and very short duration, and its damage potential is very large for natural periods less than 0.9 sec. Stations TCU065 and TCU129 are located at the middle of the fault. In spite of the large maximum acceleration and long duration of the ground motions observed at the stations, the damage potential is high only for the short natural periods. The tendency that the ground motions observed on eastern side of the fault have larger damage spectra, peak ground velocities (PGV), and peak ground displacements (PGD) than those on western side of the fault can also be observed in Table 4.1.

Table 4.1 Features of ground motions observed along the Chelungpu fault

Location along the Chelungpu fault		Ground motion	Max. natural period (sec) when damage index ≧ 1.0	PGA (cm/sec^2)	PGV (cm/sec)	PGD (cm)
northern part	eastern side	TCU068 (EW)	1.0	468	147	101
	western side	TCU067 (EW)	0.5	482	71	32
middle part	eastern side	TCU065 (EW)	0.7	722	115	67
	western side	TCU129 (EW)	0.6	832	47	26
southern part	eastern side	-	-	-	-	-
	western side	CHY028 (NS)	0.9	678	86	27

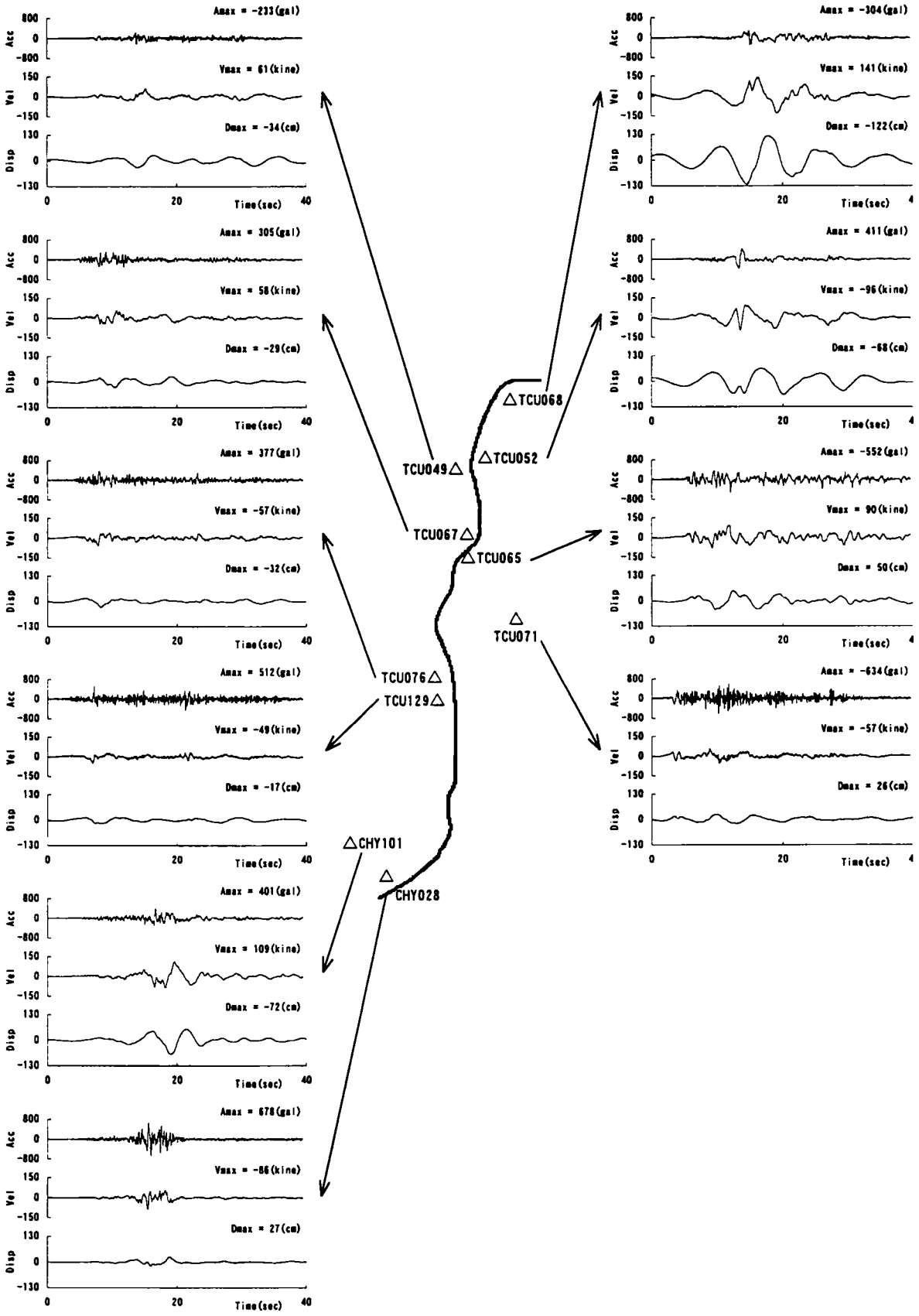

Figure 4.11(a) North-south components of ground motions during the Chi-Chi earthquake

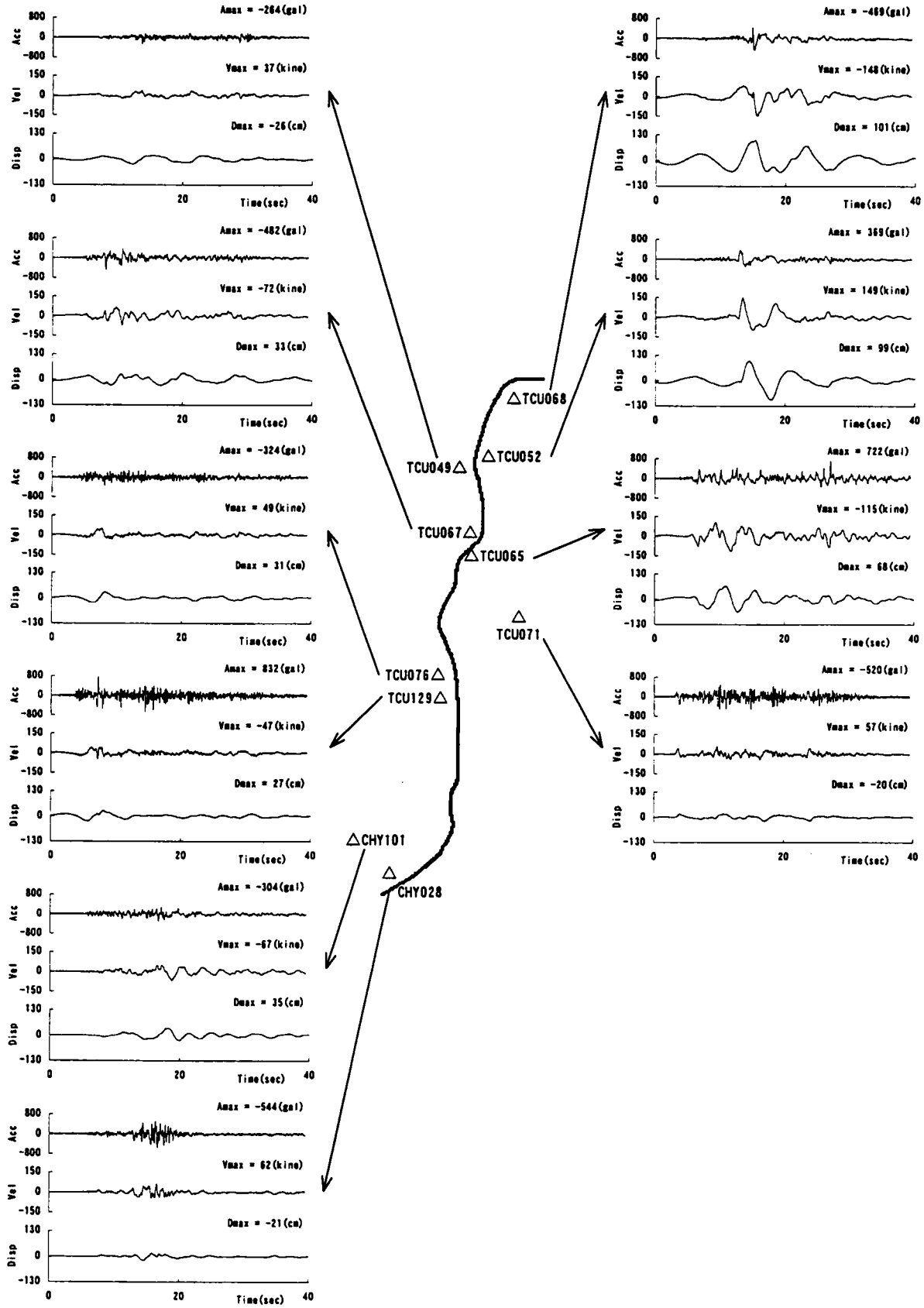

Figure 4.11(b) East-west components of ground motions during the Chi-Chi earthquake

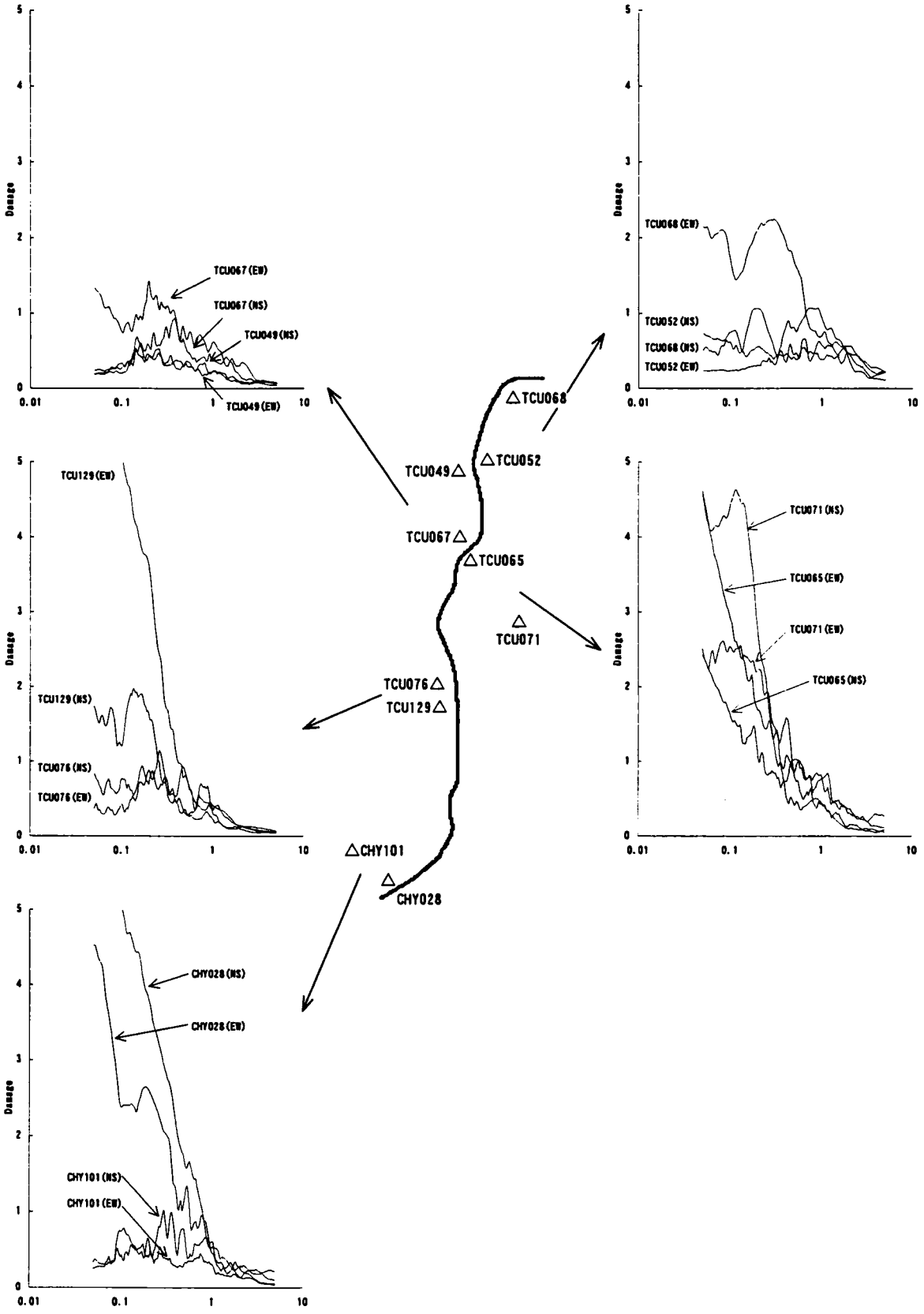

Figure 4.12 Damage spectra of recorded ground motions along the Chelungpu fault

4.5 DAMAGE POTENTIAL OF GROUND MOTIONS FOR DESIGN PURPOSE

The 1995 Hyougoken-Nanbu earthquake caused severe damage to many structures that had been thought to be designed according to proper earthquake-resistant design. Damage to modern engineering structures was beyond engineers' expectation. This has been forcing engineers and researchers to revise the earthquake-resistant standards and to reevaluate ground motion potential during great earthquakes.

In 1996, the Special Task Committee of Earthquake Resistance of Civil Engineering Structures issued the JSCE Recommendations on Earthquake Resistance of Civil Engineering Structures (JSCE, 1996b). Major subjects of the recommendations follow:

i) Two levels of earthquake motions, i.e., Level I and Level II design motions should be incorporated. The Level I design motions account for moderate seismic loads at the site from random sources. The Level II design motions are induced by deterministic sources near the site. There would be many difficulties in generating the proper Level II design motions at the site by using simulation techniques, however. For these cases, standard Level II motions may be specified on the basis of recorded near-source ground motions during earthquakes, e.g. the 1995 Hyogoken-Nanbu earthquake.

ii) For structural design or structural safety evaluation against the Level II motions, it is basically required to estimate the inelastic deformations and ultimate strengths.

According to the recommendations, many seismic codes for civil engineering structures including highway bridges, railway facilities, water and sewer facilities have been revised. The Japanese Design Specifications of Highway Bridges were revised in 1996 (Japan Roads Association, 1996). In this revision, Level II design motions include two types of ground motions: Type I and Type II ground motions. Type I ground motions are induced by inter-plate earthquakes that occurred at boundaries between tectonic plates relatively far from affected areas. Type II ground motions are induced by near-source type earthquakes that occurred at faults very close to affected areas. The acceleration response spectra of Type I ground motions were statistically determined by considering estimated ground motions in Tokyo during the 1923 Kanto earthquake with a magnitude of 8.0 and epicentral distance of 50 km. The 1923 Kanto earthquake claimed the largest number of lives in Japan, and was thought to be one of the inter-plate earthquakes that occurs at the boundary between tectonic plates. The acceleration response spectra of Type II ground motions were statistically determined by considering ground motions recorded in Kobe during the 1995 Kyogoken-Nanbu earthquake.

In this section, damage spectra of ground motions that have been used for design purpose and

the required yield strength in view of damage indices of structures are calculated, and damage potential of them are studied.

Before the 1995 Hyougoken-Nanbu earthquake caused severe damage to various structures, some observed and/or artificial ground motions had been used in dynamic design process of civil engineering structures in Japan. Representative ground motions are as follows:

(1) Observed ground motions at El Centro during the 1940 Imperial Valley earthquake

(2) Observed ground motions at Taft during the 1952 Kern County earthquake

(3) Observed ground motions at Hachinohe during the 1968 Tokachioki earthquake

(4) Observed ground motions at Kaihoku Bridge during 1978 Miyagiken-Oki earthquake

(5) Observed ground motions at Itajima Bridge during 1968 Hyuganada-Oki earthquake

(6) Artificial standard ground motions for highway bridges (Japan Road Association, 1990)

Time histories of these ground motions are shown in Figure 4.13. The maximum accelerations of these ground motions range from 0.2 to 0.3 g. Damage spectra of these ground motions are shown in Figure 4.14. Almost all damage indices are smaller than 1 for all natural periods.

Figure 4.15 shows acceleration response spectra and damage spectra of ground motions that are adjusted to design of nuclear power plants that have had one of the most severe earthquake resistant design standards in Japan until the 1995 Hyogoken-Nunbu earthquake. The ground motions are defined at bedrock. It is found from the figures that the shapes of the damage spectra of the ground motions are slightly different from the corresponding acceleration response spectra.

As described above, since the 1999 Hyogoken-Nanbu earthquake, almost all earthquake resistant design standards for civil engineering structures have been revised. The experience of the 1995 Hyogoken-Nanbu earthquake have forced civil engineers to introduce the design ground motions with Intensity Level II into the revised standards. In Figure 4.16, samples of design ground motions with Intensity Level II for earthquake resistant design of highway bridges in Japan (Japan Road Association, 1996) are shown. These ground motions are classified by type of earthquake and type of ground. The damage spectra of the ground motions are shown in Figure 4.17. The response spectra of the ground motions are shown in Figure 4.18. Figure 4.17 demonstrates that the damage spectra of Type I design ground motions are relatively small and that the damage spectra of Type II design ground motions are very large. It is suggested that the Type I design ground motions are too small as for Level II design ground motions and that additional study of Type I ground motion is needed. Also it is suggested that the Type II design ground motions are possibly too large to be used in the whole country because they were defined based on the observed ground motions during the 1995 Hyogoken-Nanbu earthquake. Based on the comparison between Figure 4.17 and Figure 4.18(a), shapes of the damage spectra are very similar to those of the acceleration response spectra for Type I design ground motions, but shapes of the damage spectra are significantly different from those of the acceleration response spectra for Type II design ground motions. Based on Figure 4.18,

acceleration response spectra of Type II design ground motions are larger than those of Type I ground motions, velocity response spectra of Type I ground motions are similar to those of Type II design ground motions, and displacement response spectra of Type I design ground motions are larger than those of Type II design ground motions in longer natural periods than about 2 sec.

In Figures 4.19 to 4.21, the required yield strength ratio (Qy/W) so as to satisfy a safety level with the damage index=1.0 are shown for the ground motions described above. In each figure, three lines are plotted for three values of the parameter μ =4, 6, 8: the parameter μ is the ratio of the ultimate deformation capacity under static loading (δ u) to the yield deformation (δ y). As shown in Figure 4.19, the required yield strength ratio for the conventional design ground motions are less than about 0.4, except the ground motion recorded at Itajima Bridge. Figure 4.20 shows that the required yield strength ratios for the design ground motions at bedrock for nuclear power plants are less than about 0.5. As shown in Figure 4.21, the required yield strength ratios of Type I design ground motions for highway bridges are less than about 0.4, whereas those of Type II design ground motions are about 0.4 to 0.7 for natural periods of less than 1.0.

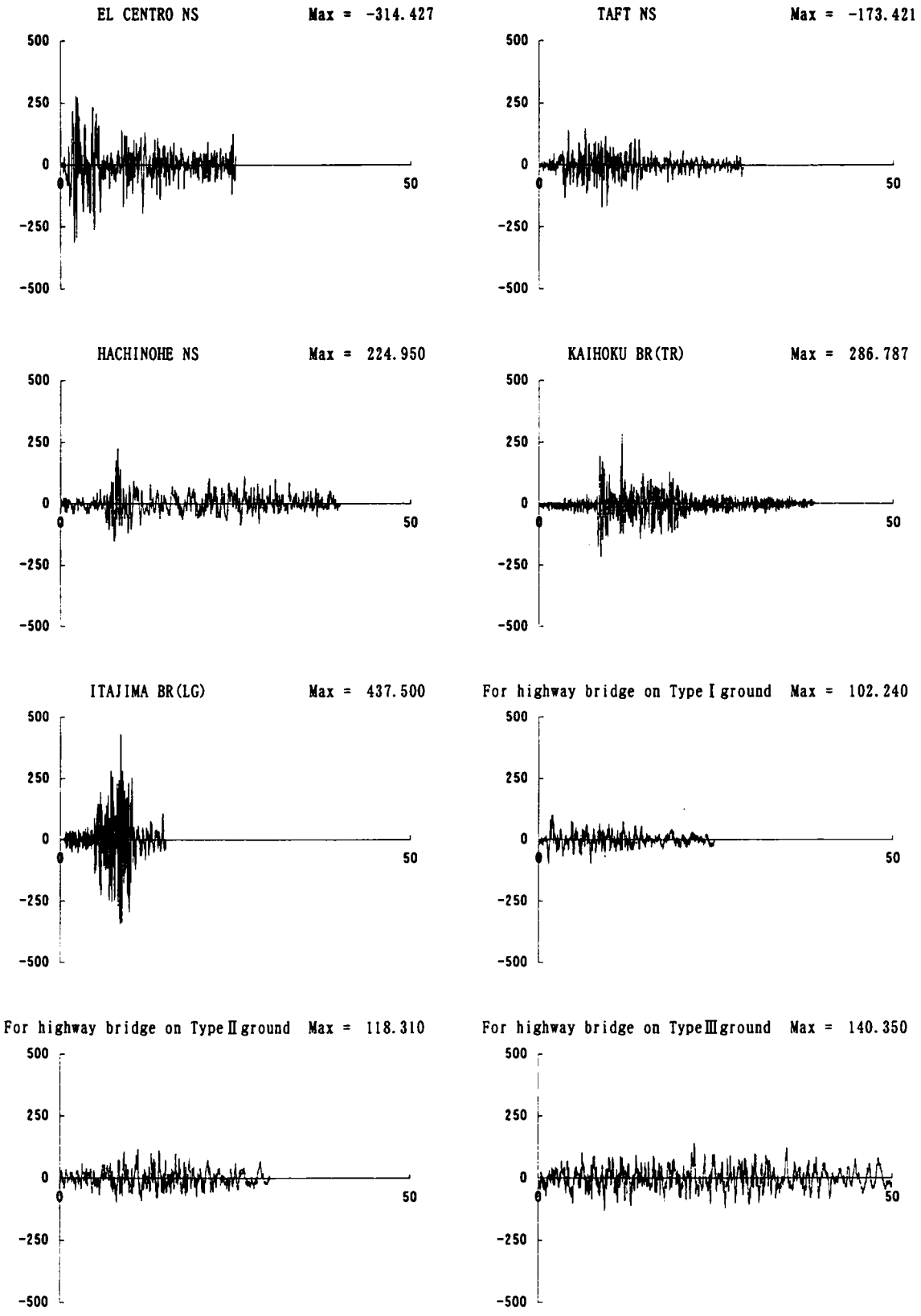

Figure 4.13 Acceleration time histories of ground motions for design purpose

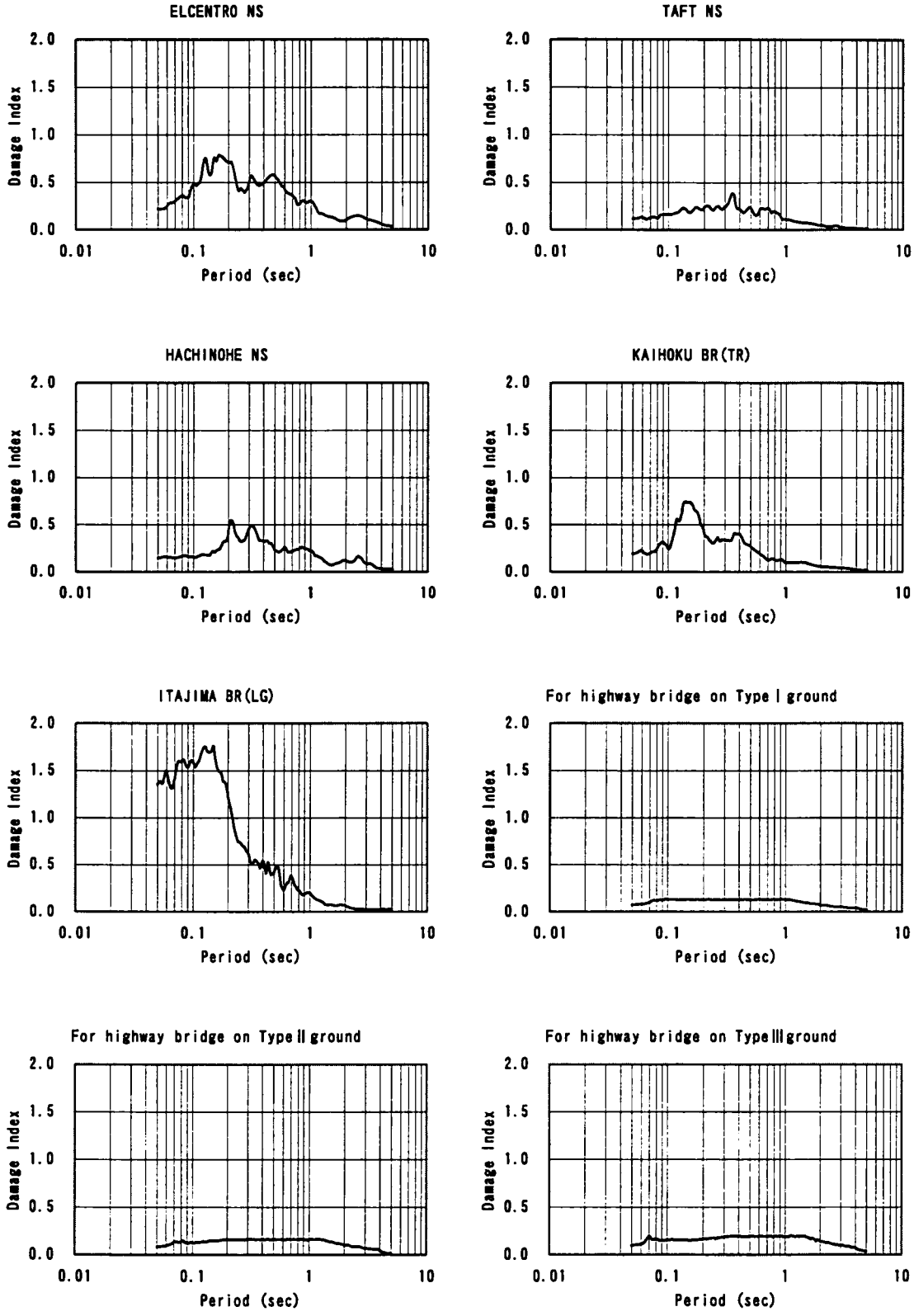

Figure 4.14 Damage spectra of ground motions for design purpose

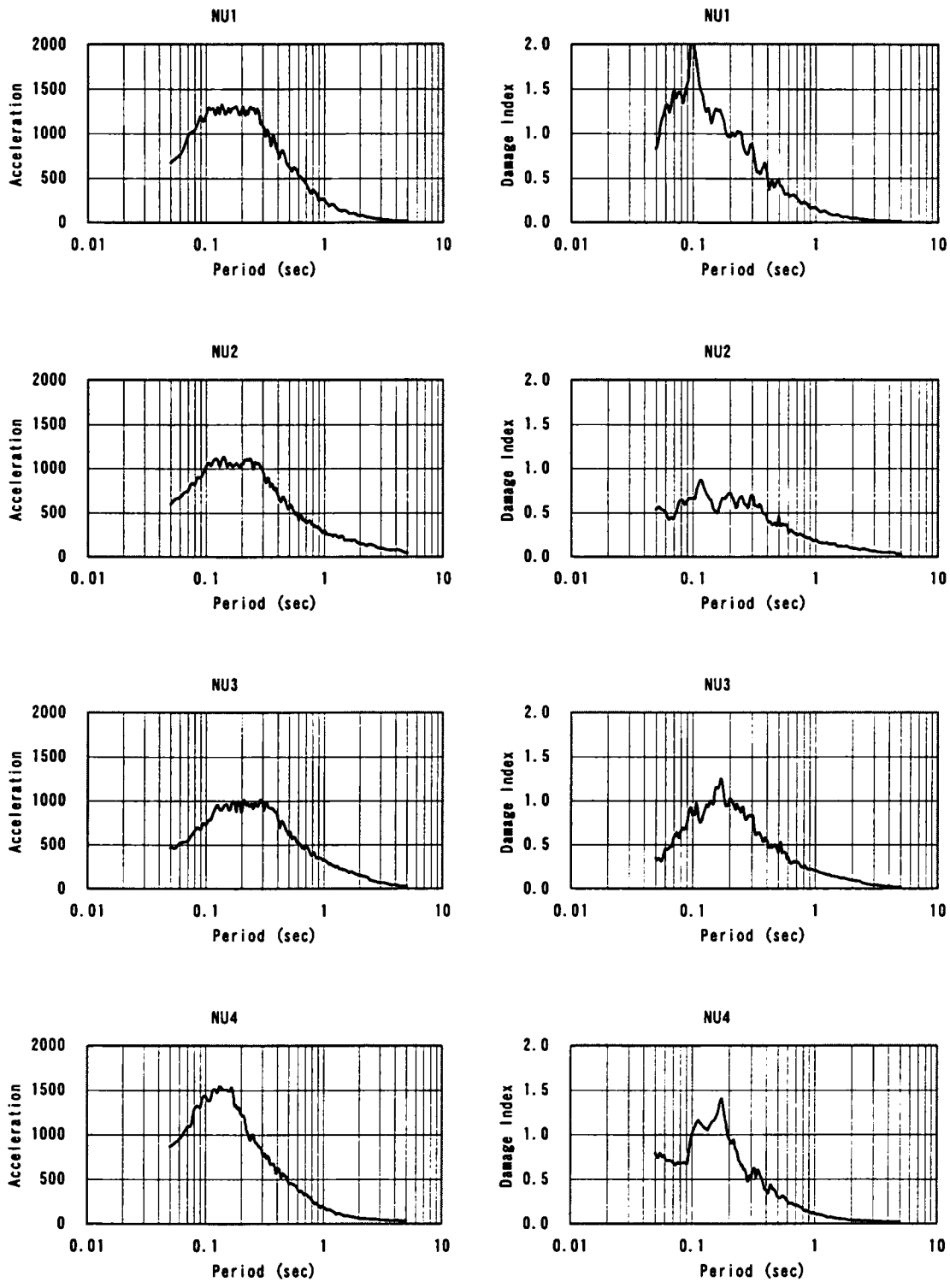

Figure 4.15 Acceleration response spectra and damage spectra of the design ground motions for nuclear power plants

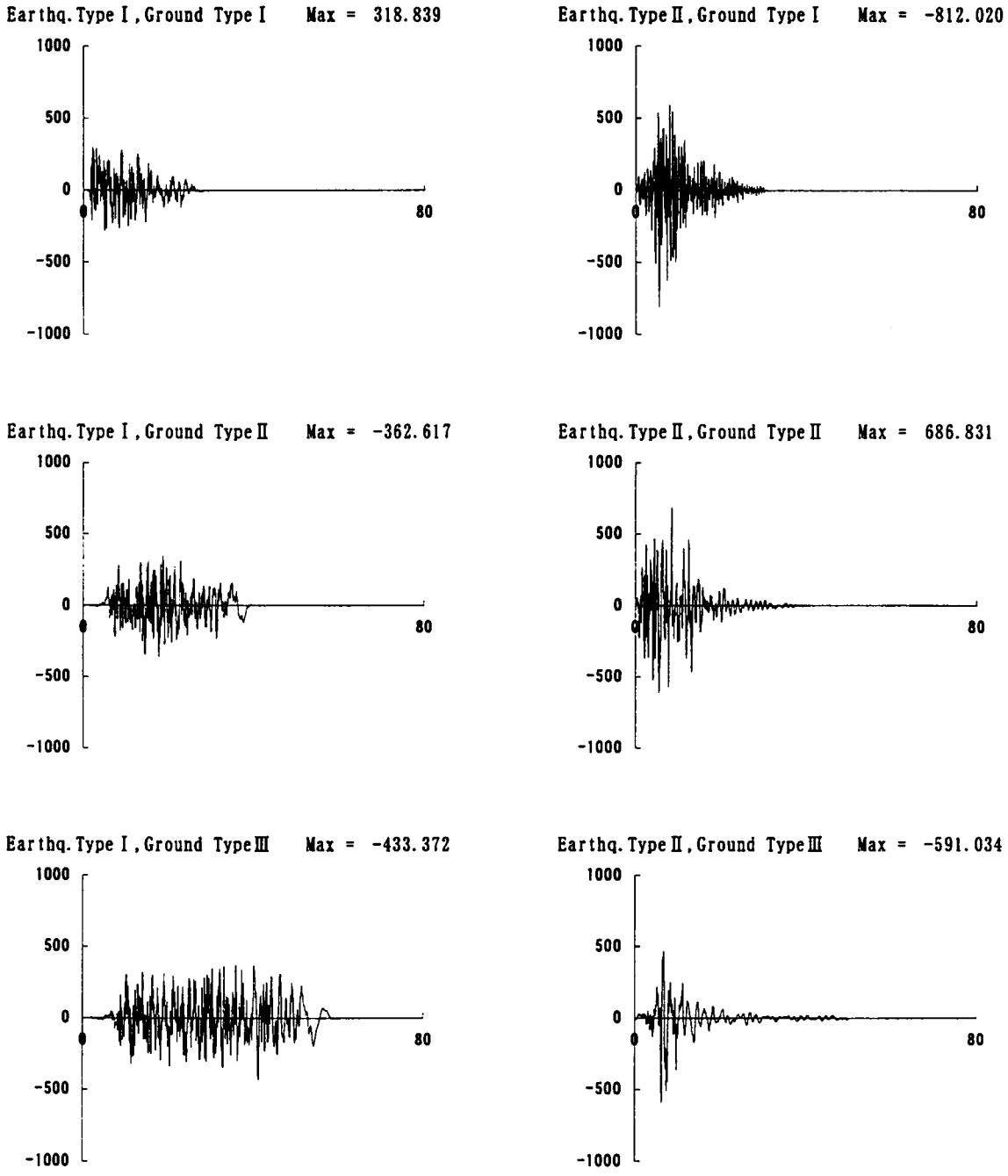

Figure 4.16 Acceleration time histories of Level II design ground motions for highway bridges

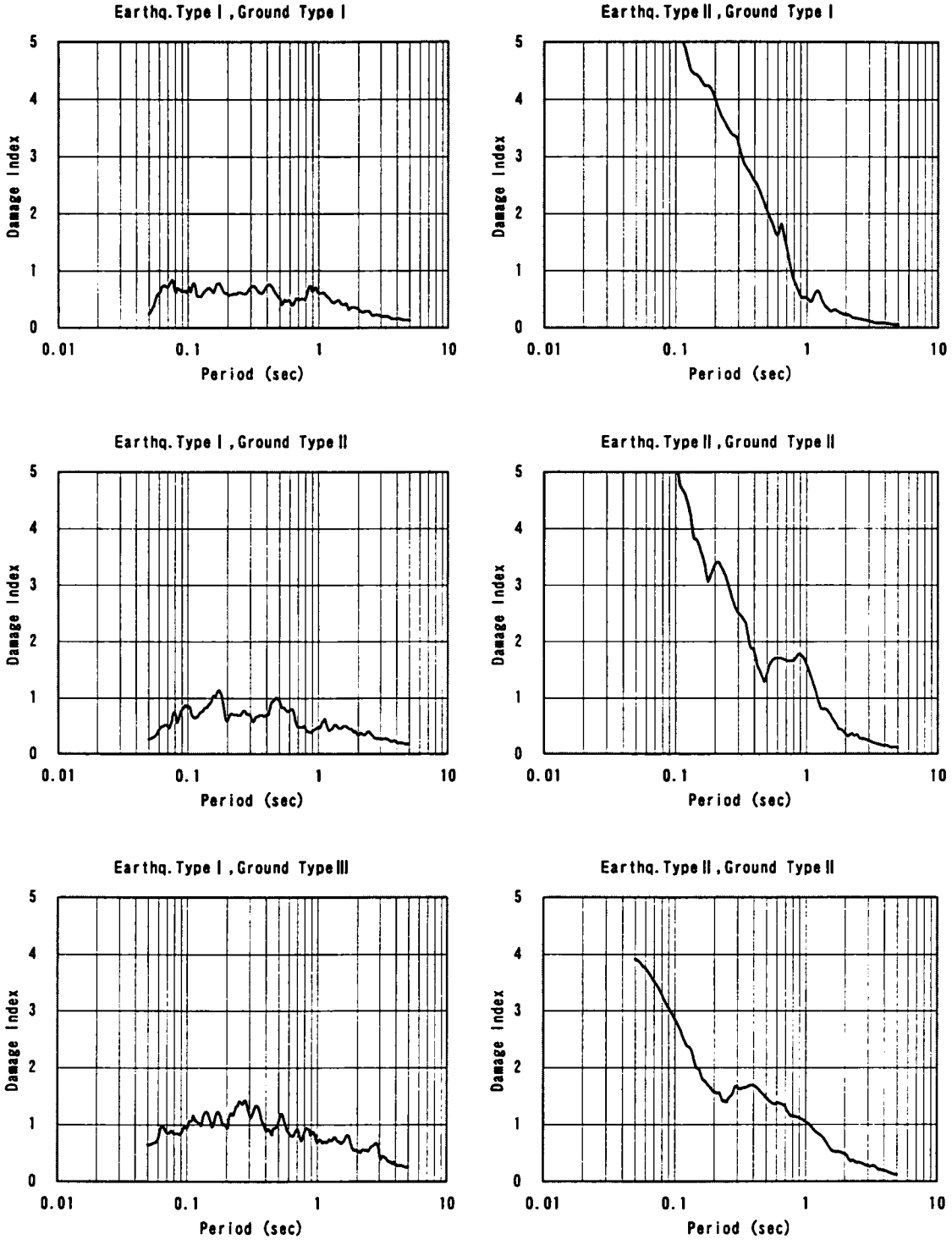

Figure 4.17 Damage spectra of Level II design ground motions for highway bridges

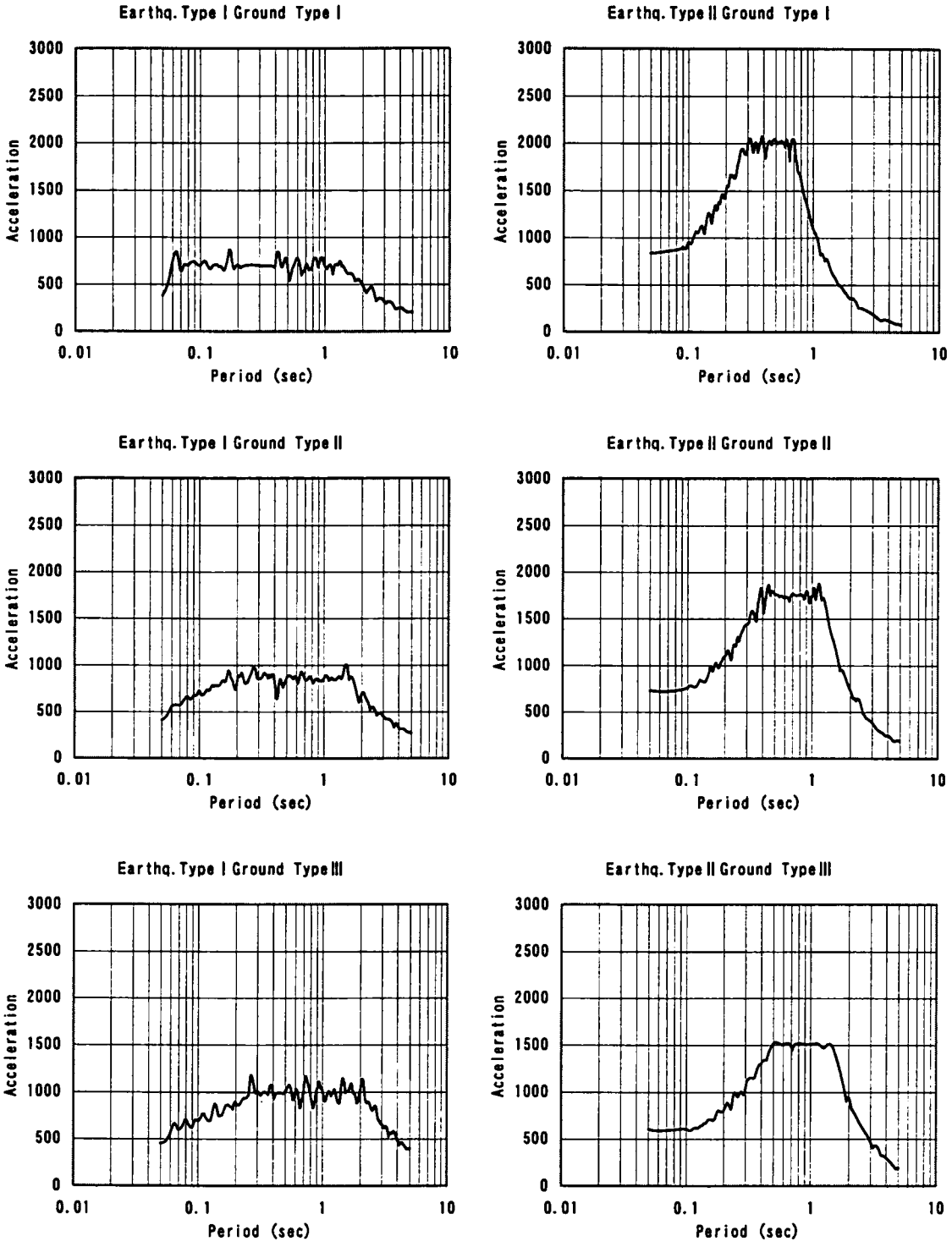

Figure 4.18(a) Response spectra of Level II design ground motions for highway bridges (acceleration)

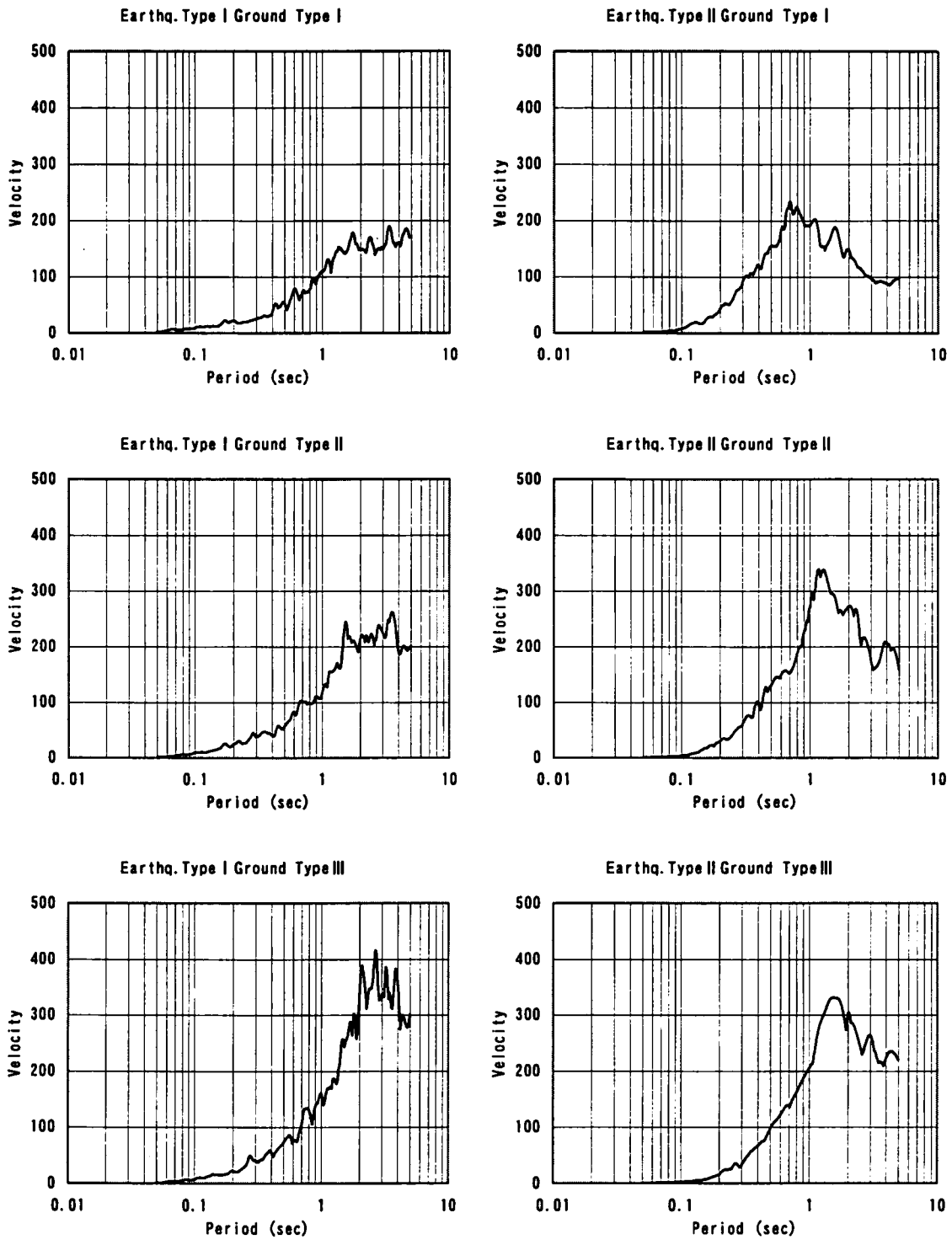

Figure 4.18(b) Response spectra of Level II design ground motions for highway bridges (velocity)

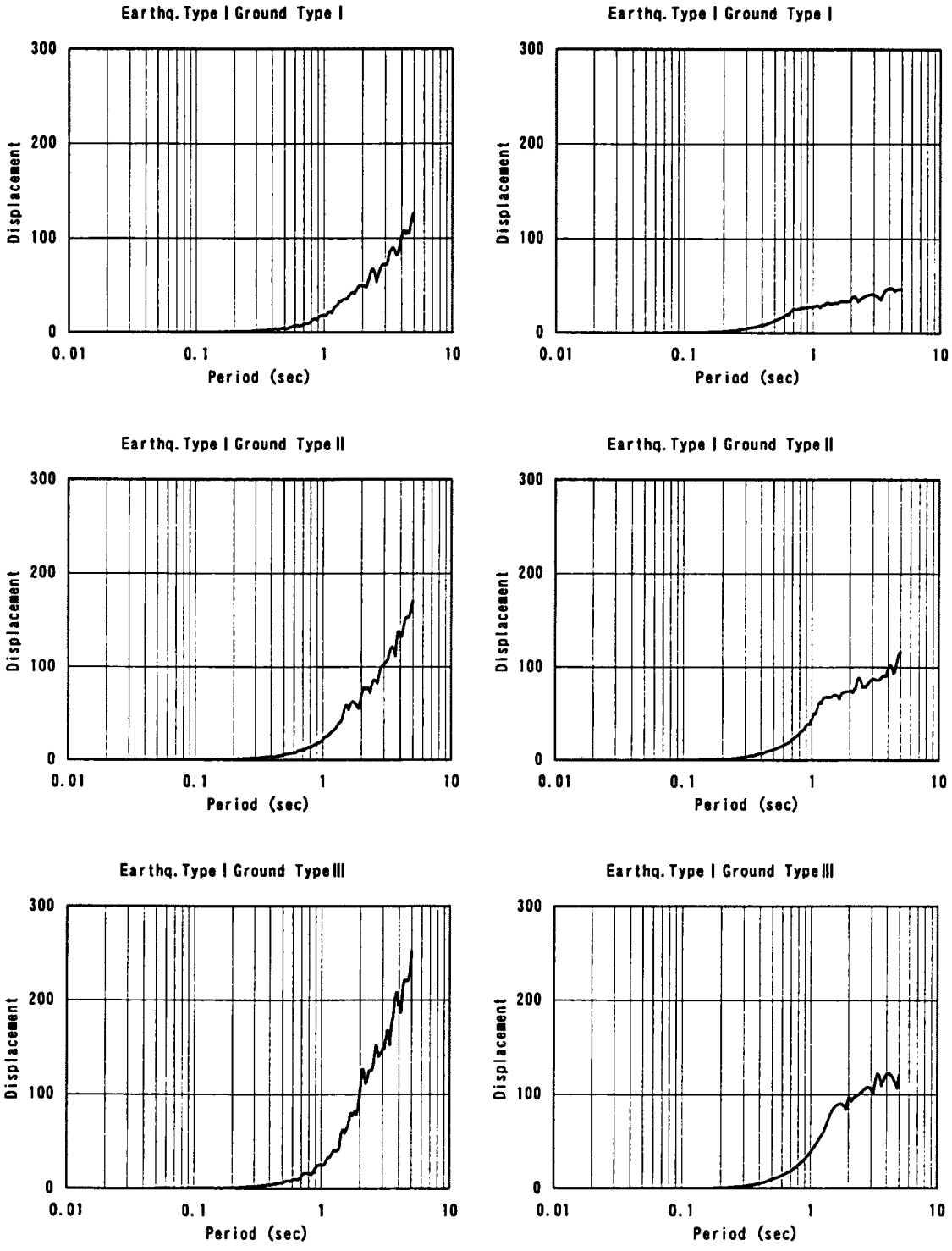

Figure 4.18(c) Response spectra of Level II design ground motions for highway bridges (displacement)

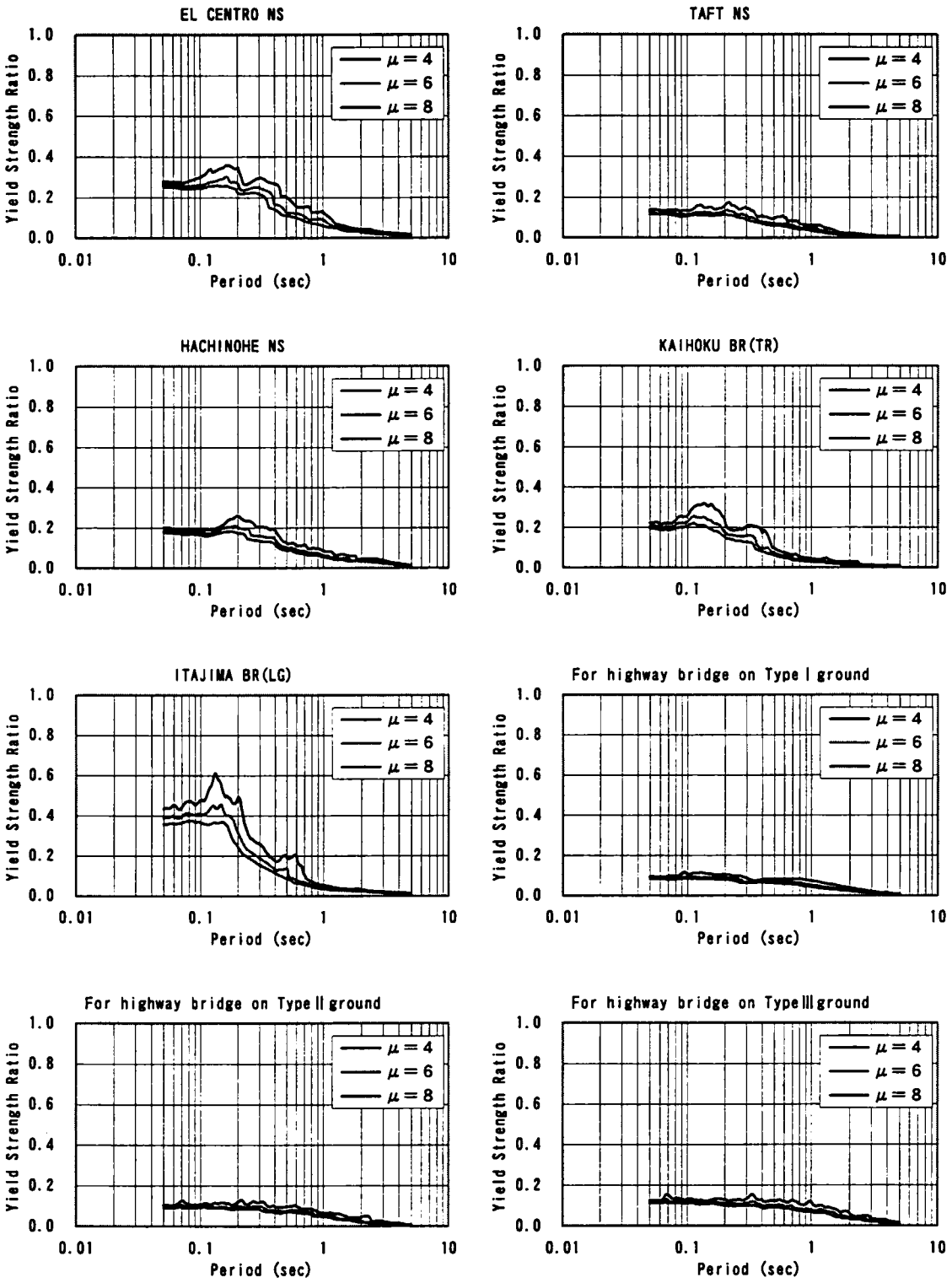

Figure 4.19 Required yield strength ratio of ground motions for design purpose

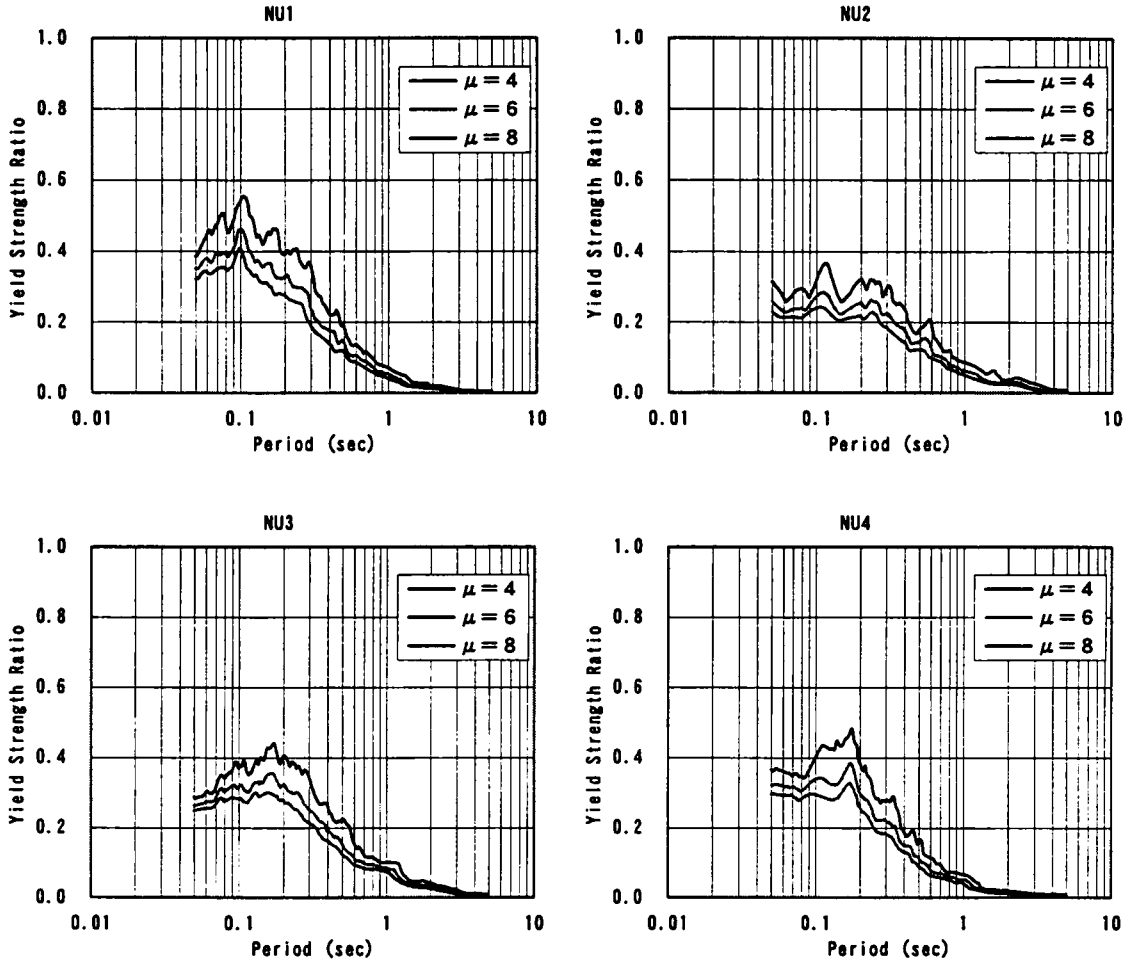

Figure 4.20 Required yield strength ratio of design ground motions for nuclear power plants

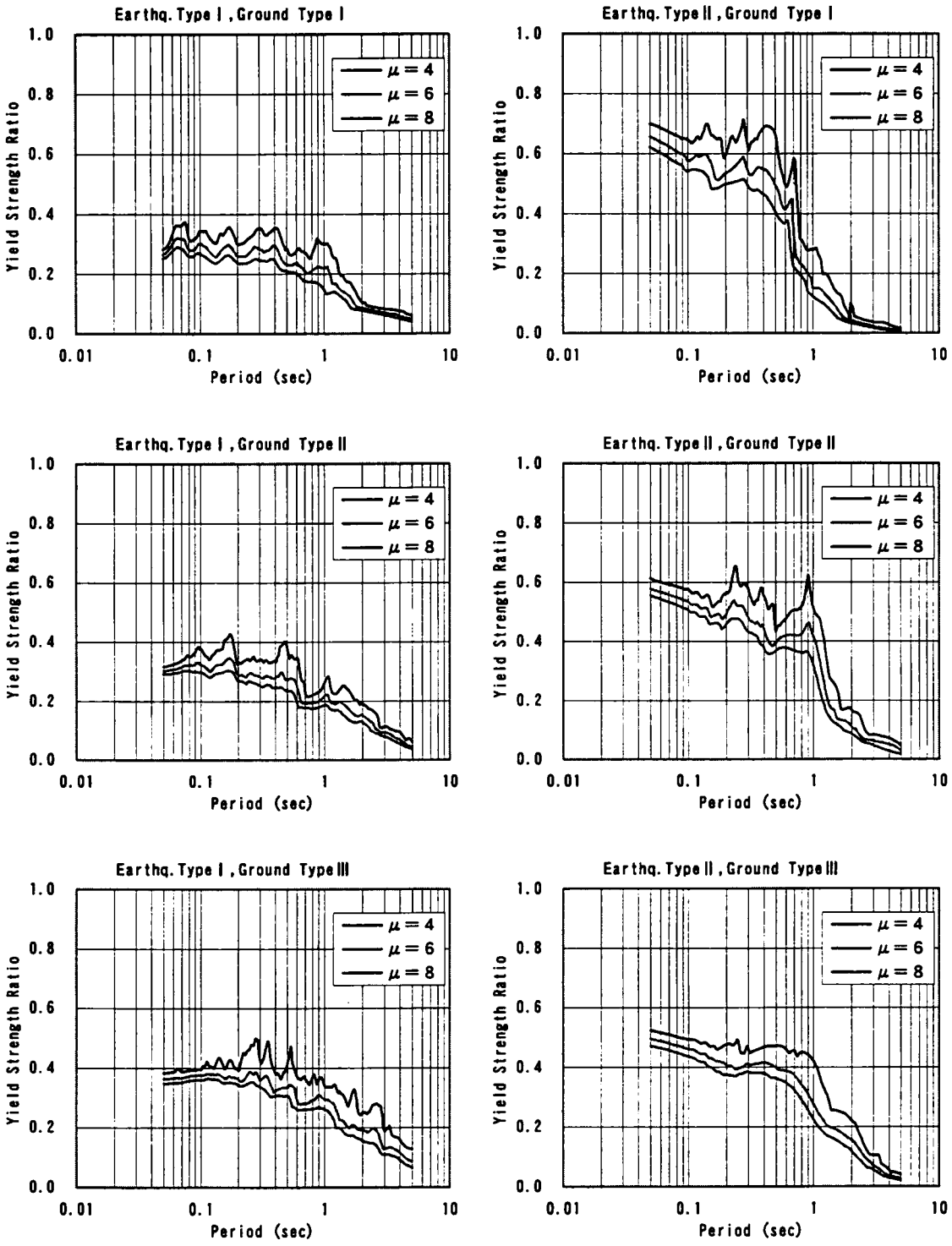

Figure 4.21 Required yield strength ratio of Type II design ground motions for highway bridges

4.5 CONCLUSIONS

(1) Structural damage in Kobe during the 1995 Hyogoken-Nanbu earthquake was concentrated in a belt 0.7 to 1.2 km wide stretching from southwest to northeast along the foot of the Rokko Mountains. The damage spectrum of the ground motion recorded in the heavily damaged zone is the largest among those of the recorded ground motions in almost all natural periods range. The damage indices of the ground motion recorded in and around the heavily damaged zone are larger than 1.0 at natural periods smaller than about 1.0 sec. These results well agree with the fact that 45 percents of 158 viaducts piers with natural periods ranging 0.4 to 0.9 sec. collapsed in the zone (Japan Society of Civil Engineers, 1996a). The damage spectra of ground motions recorded outside of the heavily damaged zone are smaller than 1.0 in all natural periods.

(2) To estimate the amplification characteristics of ground motions in the heavily damaged zone in the city of Kobe during the Hyogoken-Nanmu earthquake, Motosaka and Nagano (1996) performed wave-propagation analyses of a deep irregular underground structure model with vertical discontinuity for incident plane waves. The simulated ground motions in the heavily damaged zone were amplified due to the focusing effect in the deep irregular underground structure as well as in the shallow surface layers. The damage spectra of the ground motions simulated by Motosaka and Nagano (1996) are calculated and studied. The damage spectra of the simulated ground motions at ground surface points in the heavily damaged zone are relatively large. Among them, the largest is the damage spectrum of the ground motion at a point located between JR and the Hanshin Railway Line. The intensity of the damage spectra of ground accelerations decreases with distance from the center of the heavily damaged zone. These results demonstrate that the damage spectra well correlate with the structural damage, and that the concentration of structural damage in the narrow zone stretching from southwest to northeast along the foot of the Rokko Mountains is mainly explained by the geological deep ground structure in Kobe.

(3) The damage spectra of the recorded ground motions at Duzce (DZC), Gebze (GBZ), Izmit (IZT) and Sakarya (SKR) during the 1999 Turkey earthquake have been studied. Damage indices of ground motions at GBZ and IZM are much smaller than 1.0 for all natural periods. Damage indices of ground motions at DZC and SKR are larger than 1.0 for a narrow period range around 0.1 sec. In spite of relatively small damage spectra of the observed ground motions during the earthquake, structural damage was very severe. This is thought to imply poor earthquake-resistant capacity of the structures in Turkey.

(4) Damage spectra of the recorded ground motions at the stations very close to the Chelongpu Fault during the 1999 Taiwan earthquake have been studied. Station TCU068 is located in the northern part and eastern side of the fault where the rupture arrived. The ground motion observed at that station has a relatively low PGA, low dominant frequency, and high damage potential for relatively

long natural periods around 1.0 sec. Station CHY028 is located in the southern part and western side of the fault where rupture arrived. The ground motion observed at the station has a large maximum acceleration, a very short duration, and its damage potential is very large for natural periods less than 0.9 sec. Stations TCU065 and TCU129 are located at the middle of the fault. In spite of the large maximum acceleration and long duration of the ground motions observed at the stations, the damage potential is high only for short natural periods less than 0.6 sec. The ground motions observed on eastern side of the fault have larger damage spectra, peak ground velocities (PGV), and peak ground displacements (PGD) than those on western side of the fault.

(5) Damage potential of ground motions that have been used for design purpose was studied. It was found that damage potential of the conventional design ground motions that had been used before the 1995 Hyogoken-Nanbu earthquake is very small. The required yield strength ratios for the conventional design ground motions are less than about 0.4. It is found that the damage potential of design ground motions at bedrock for nuclear power plants is not very large in comparison with that of the conventional design ground motions. Since the 1995 Hyogoken-Nanbu earthquake, almost all earthquake resistant design codes of civil engineering structures have been revised. Two levels of design ground motions, i.e., Level I and Level II have been incorporated. The Level I design motions account for moderate seismic loads at the site from random sources. The Level II design motions are induced by deterministic sources near the site. Damage potential of design ground motions of the Japanese Design Specifications of Highway Bridges revised in 1996 was studied. In this specification, Level II design motions includes two types of ground motions: Type I ground motions which would be induced by inter-plate earthquakes that occurred at boundaries between tectonic plates relatively far from affected areas, and Type II ground motions which would be induced by near-source type earthquakes that occurred at faults very close to affected areas. Damage spectra of the design ground motions demonstrated that damage spectra of Type I design ground motions are relatively small and that damage spectra of Type II design ground motions are very large. The required yield strength ratios of Type I design ground motions are less than about 0.4, whereas those of Type II design ground motions are ranging from 0.4 to 0.7 for natural periods less than 1.0. It is suggested that the Type I design ground motions are too small as for Level II design ground motions and that additional study of Type I ground motion is needed. Also it is suggested that the Type II design ground motions are possibly too large to be used in the whole country because they were determined based on the observed ground motions during the 1995 Hyogoken-Nanbu earthquake.

CHAPTER 5

DAMAGE POTENTIAL OF GROUND MOTIONS IN LARGE AREA

5.1 INTRODUCTION

As observed from the 1995 Hyogoken-Nanbu earthquake and the 1999 Chi-Chi earthquake, damage to structures in a large area is greatly affected by the location of the fault, the geological structure of the site and the fault rupture mechanism. The prediction of damage over a large area subjected to a large scenario earthquake has become an important and valuable tool used by many governors in their disaster mitigation planning.

In this chapter, a methodology for the evaluation of damage potential during a large earthquake in a large area is presented. Then, an application of the method to Kawasaki City located in the southern part of Kanto, in Japan, is described (Sunasaka, Toki and Kiremidejian, 2001).

5.2 METHODOLOGY FOR DAMAGE POTENTIAL OF GROUND MOTIONS IN LARGE AREA

To estimate the damage potential of ground motions in a large area is very important for disaster mitigation and preparedness purposes. The ground motion potential in large area can be evaluated using the damage spectra of ground motions as defined in Chapter 3. In this chapter, relatively easy but reasonable procedure is applied as follows:

(1) divide the large area into a mesh, for example 500x500 (m) square cells
(2) make soil profile model for each cell in the mesh
(3) classify surface ground conditions according to the soil profile for each cell
(4) select or simulate input ground motions at bedrock
(5) obtain surface ground motions by response analysis of the soil profile for each cell
(6) calculate damage spectra for the ground motions
(7) develop damage distribution maps for different structural period ranges

5.3 EVALUATION OF DAMAGE POTENTIAL OF GROUND MOTIONS IN KAWASAKI CITY

5.3.1 GROUND CONDITIONS IN KAWASAKI CITY

As an example, the methodology described above is applied to the evaluation of ground motion potential in Kawasaki located in the southern part of Kanto, in Japan (see Figure 5.1).

Kawasaki City is divided into a mesh of 500x500 (m) square cells. The topography in Kawasaki City was assessed, the surface ground conditions were obtained, and 30 soil profile models were developed and applied to the mesh (Kawasaki City, 1988). Ishii et al. (1999) classified surface ground conditions into six groups according to their natural periods, and selected five representative soil profile models for each group as shown in Table 5.1. The distribution of the predominant periods of the soils is shown in Figure 5.2.

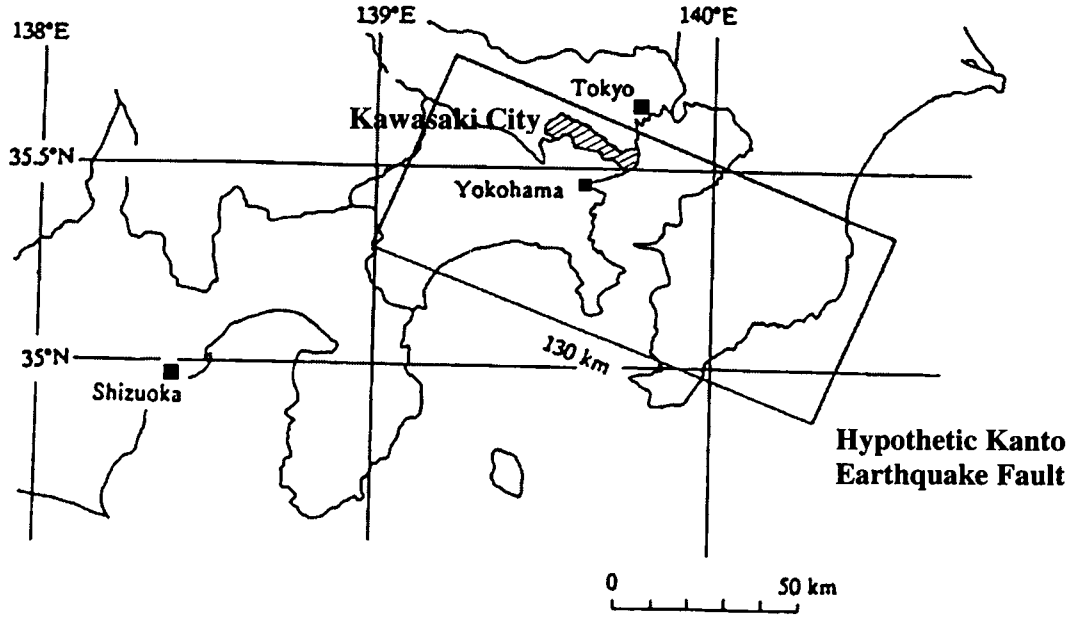

Figure 5.1 Location of Kawasaki City, and hypothetical Kanto earthquake fault

Table 5.1 Classified surface ground groups

Surface ground group	Natural period (sec)	Soil profile model (Kawasaki City, 1988)
A	$T \leqq 0.2$	LM1, LM10, DS1, DS2, DS3
B	$0.2 < T \leqq 0.4$	AS3, AG2, AG3, AG5, AG6
C	$0.4 < T \leqq 0.6$	AC6, AC8, AC9, AC10, AC16
D	$0.6 < T \leqq 0.8$	AS6, AS13, AS14, AS15, AS17
E	$0.8 < T \leqq 1.0$	AC17, AC18, AC22, AC28, AC35
F	$1.0 < T$	AS27, AS29, AS31, AS32, AS34

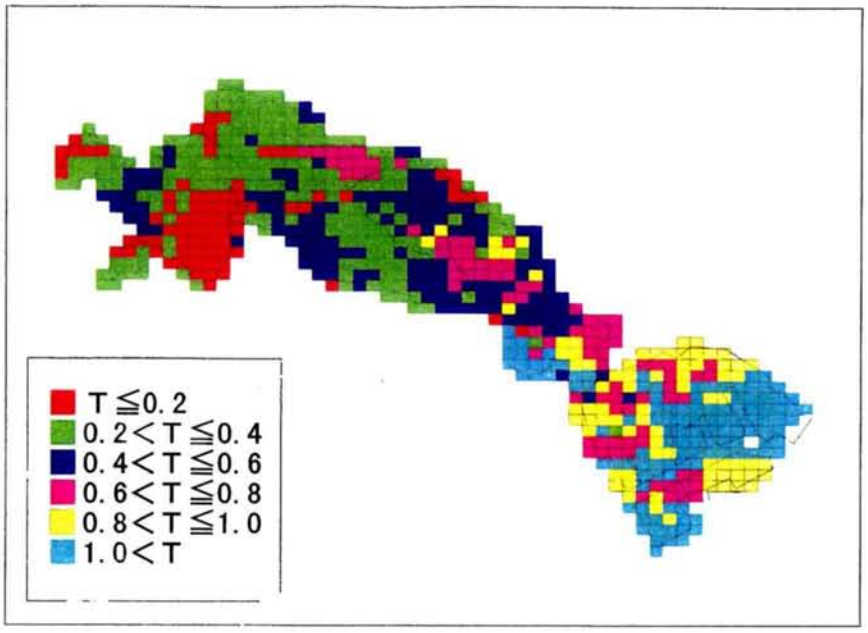

Figure 5.2 Distribution of surface ground group in Kawasaki City

5.3.2 PARAMETRIC STUDIES ON DAMAGE POTENTIAL

In this section, parametric studies on damage potential of ground motions during several types of earthquakes are conducted. Table 5.2 shows the selected ground motion records at bedrock. The ground motion time histories are shown in Figure 5.3. The ground motions at Izumi and Kobe JMA were recorded during near-source type earthquakes that occurred at faults very close to affected areas. The ground motions at Sutsu and Las Tortolas were observed during inter-plate earthquakes that occurred at boundaries between tectonic plates far from affected areas. The peak ground accelerations of the ground motions recorded at Izumi and Kobe JMA are larger than those of the ground motions recorded at Sutsu and Las Tortolas. On the other hand, the durations of the ground motions recorded at Sutsu and Las Tortolas are longer than those of the ground motions recorded at Izumi and Kobe JMA. The acceleration response spectra normalized by PGA are shown in Figure 5.4. The predominant periods of the ground motion recorded at Izumi are very short and around 0.1 sec. On the other hand, the predominant periods of the ground motion recorded at Kobe are relatively long and range from 0.25 to 1.0 sec. This suggests that individual characteristics of frequency components of the ground motions are different each other in the case of near-source type

earthquake. The predominant periods of the ground motions recorded at Sutsu and Las Tortolas during inter-plate type earthquakes range from 0.15 to 1.0 sec.

In the case studies, the peak ground accelerations of the input bedrock motions for the response analyses of grounds are modified to 200 and 500 cm/sec^2. The ground response analysis program SHAKE was used to obtain surface ground motions for the soil profile models.

Figure 5.5 and Figure 5.6 show the damage spectra of the calculated ground motions for the input motions with the PGA modified to 200 and 500 cm/sec^2, respectively. Three lines in each figure are the average and average$\pm$standard deviation (σ) of five damage spectra of ground motions at the five soil profile models shown Table 5.1. Based on Figure 5.5, in the cases of input motions with PGA of 200 cm/sec^2, the average damage spectra are smaller than 1 for almost all natural periods during near-source type earthquakes, and the average damage spectra of some surface ground groups are larger than 1 for special natural periods during inter-plate type earthquakes. Also, in these cases the deviations of the damage spectra on each surface ground group are relatively small. On the other hand, based on Figure 5.6, in the cases of the input motions with PGA of 500 cm/sec^2, the average damage spectra are larger than 1 for natural periods shorter than the particular values that depend on the earthquake type and surface ground group. Also, in these cases the deviations of the damage spectra on each surface ground group are very large.

In order to demonstrate visually the damage potential of the ground motions, the average damage indices for the selected natural periods in all meshes in Kawasaki City are shown in Figure 5.7 and Figure 5.8. It is found from Figure 5.7, in the cases of input motions with PGA of 200 cm/sec^2, that the damage indices in the whole of Kawasaki City are smaller than 1 for almost all natural periods during near-source type earthquakes, and that the damage indices in the mountain side are larger than 1 for the natural period of 0.25 sec. during the cases of inter-plate type earthquakes. On the other hand, it is found from Figure 5.8, in the cases of input motions with PGA of 500 cm/sec^2, that the distributions of the damage indices in of Kawasaki City are very complicated and depend on the earthquake type and natural periods. Based on these figures, the following points on the damage potential of ground motions in a large area during earthquakes are emphasized:

(1) Damage potential in a large area greatly depends on the type of earthquake. The ground motions induced by inter-plate type earthquakes might have wide frequency contents. These kinds of ground motions would have great damage potential in a large area.

(2) Damage potential of ground motions depends on the ground conditions. Distribution of damage indices in a large area would be very complex according to the distribution of the ground conditions.

Table 5.2 Selected ground motion records

Type of earthquake	Name of earthquake	Date	Magnitude	Observation site	Direction	PGA (cm/sec^2)
near-source type	Kagoshimaken-Hokuseibu	1997.3.26	6.3	Izumi	NS	535
	Hyougoken-Nanbu	1995.1.17	7.2	Kobe JMA	NS	818
inter-plate type	Hokkaido Nanseioki	1993.7.12	7.8	Sutsu	NS	216
	Chile	1985.3.3	7.8	Las Tortolas	N26W	139

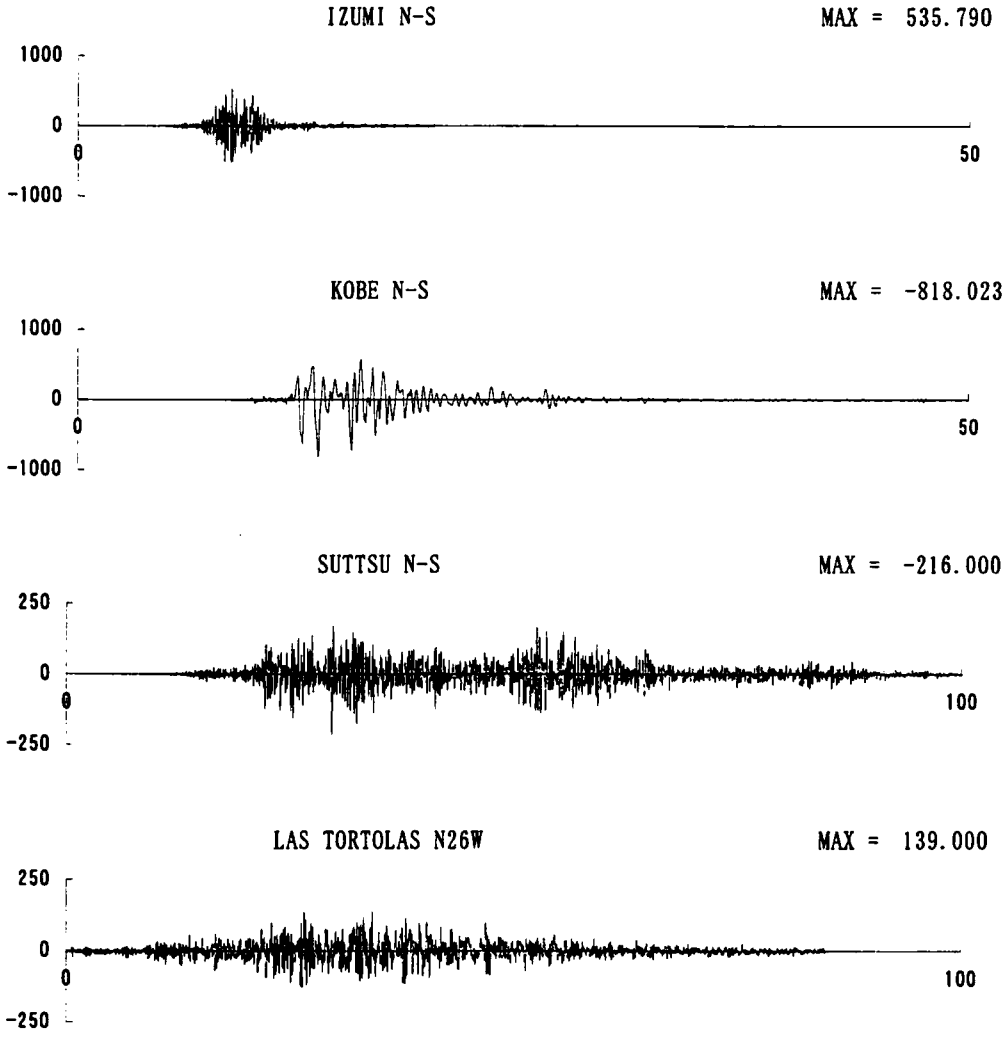

Figure 5.3 Selected input ground motion records at bedrock

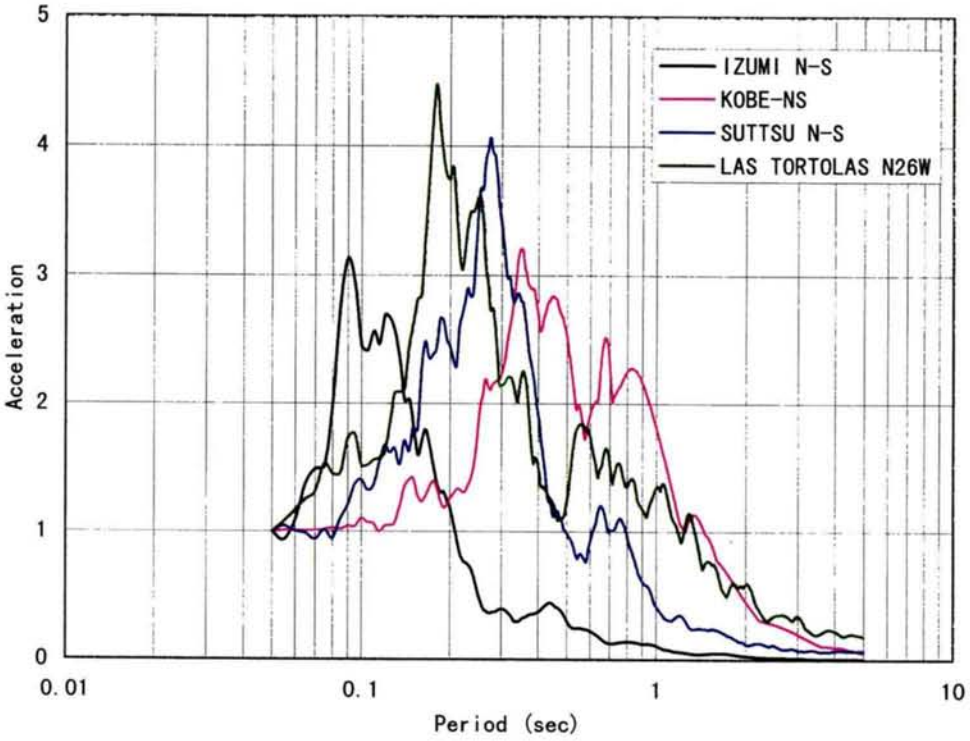

Figure 5.4 Normalized acceleration response spectra of selected ground motions

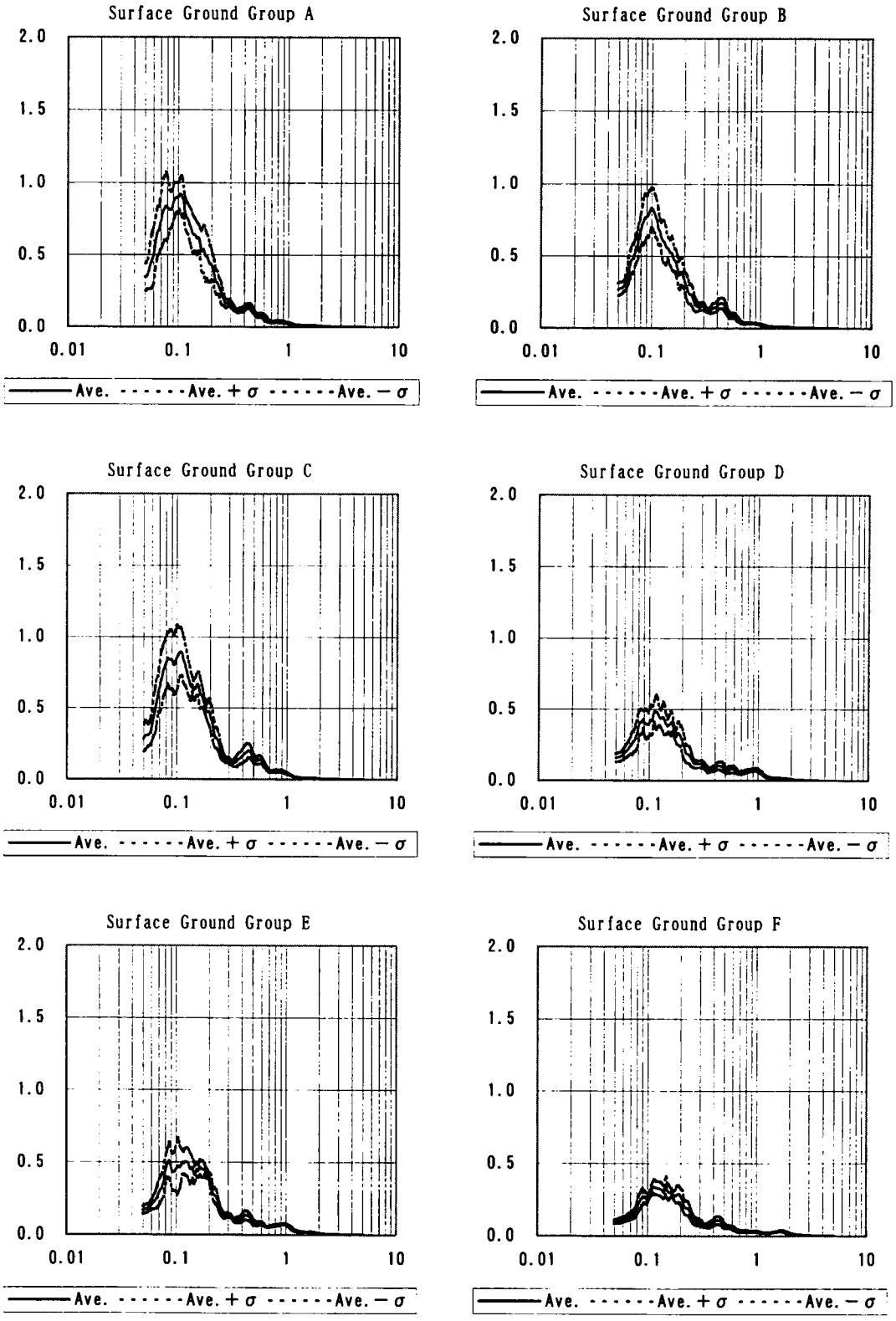

Figure 5.5(1) Damage spectra of ground motions at 6 ground groups
(input motion: Izumi, PGA:200Gal)

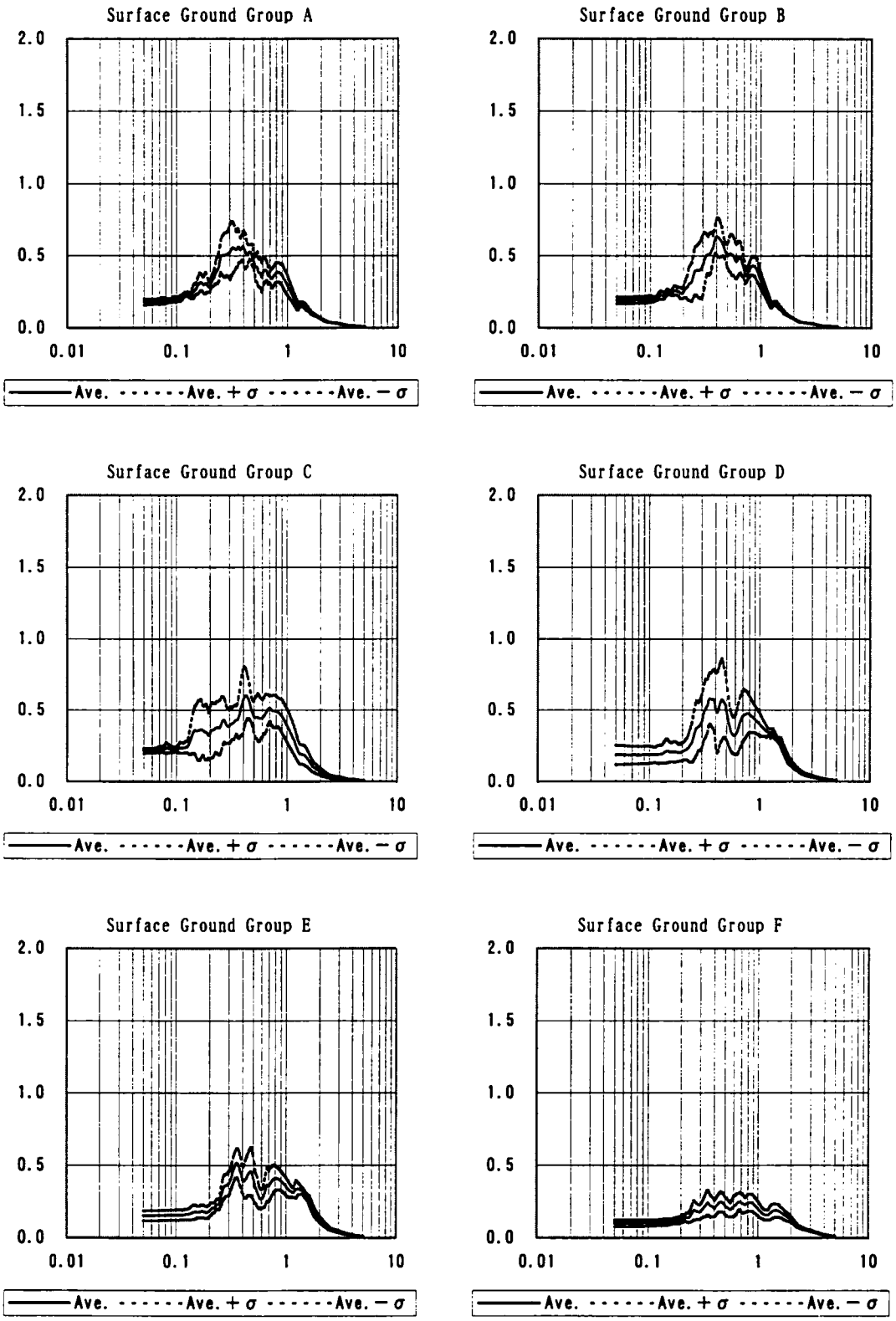

Figure 5.5(2) Damage spectra of ground motions at 6 ground groups
(input motion: Kobe JMA, PGA:200Gal)

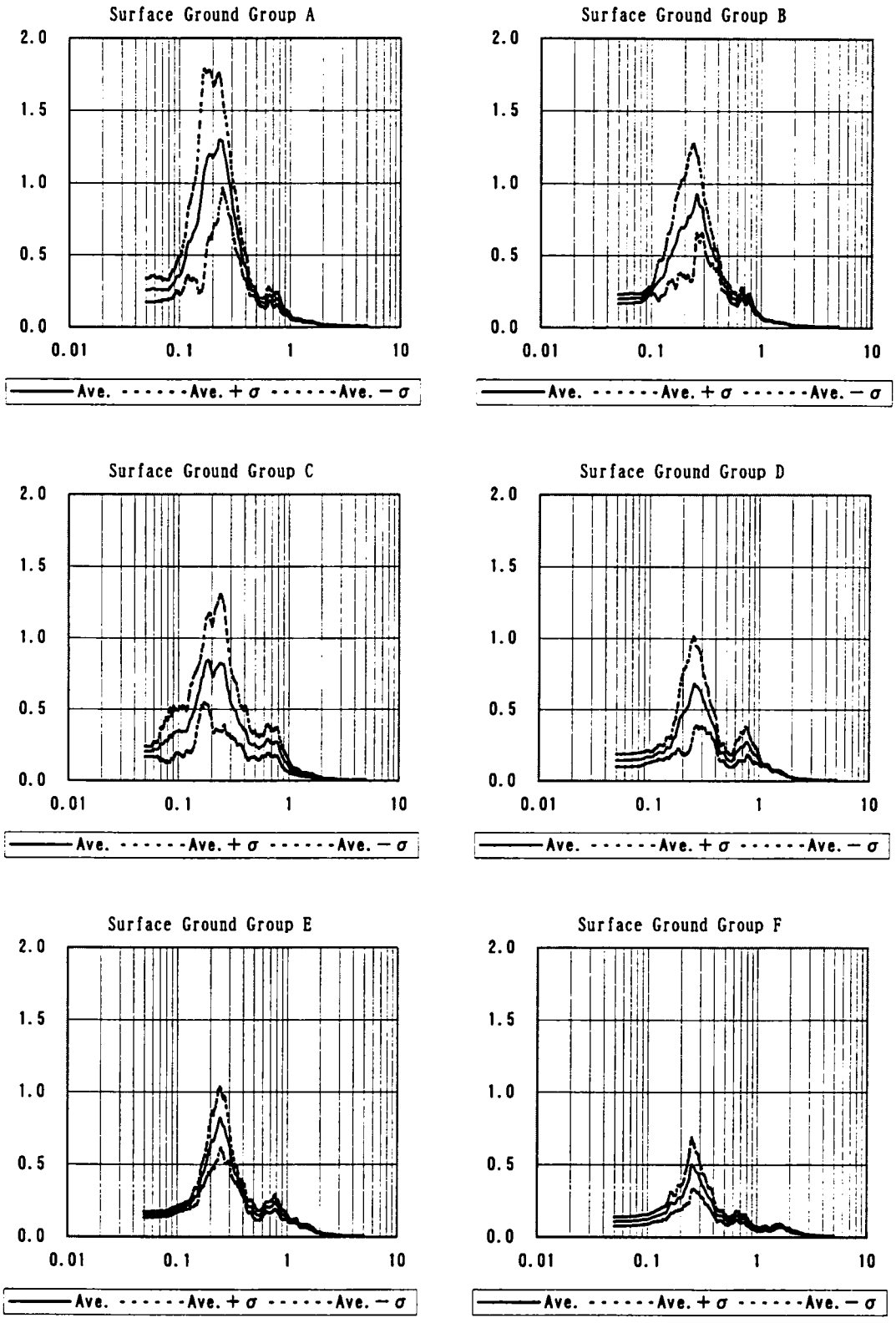

Figure 5.5(3) Damage spectra of ground motions at 6 ground groups
(input motion: Sutsu, PGA:200Gal)

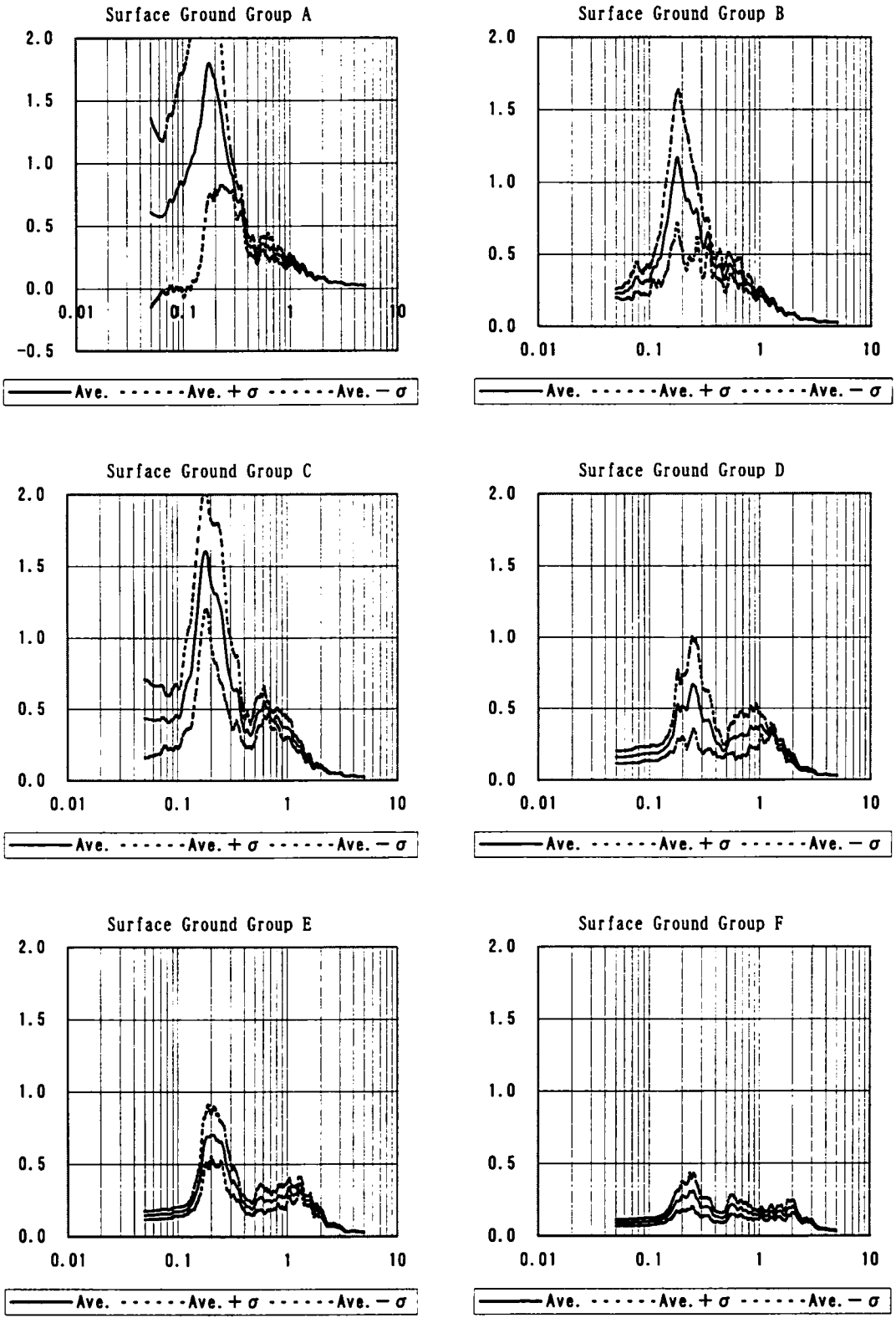

Figure 5.5(4) Damage spectra of ground motions at 6 ground groups
(input motion: Las Tortolas, PGA:200Gal)

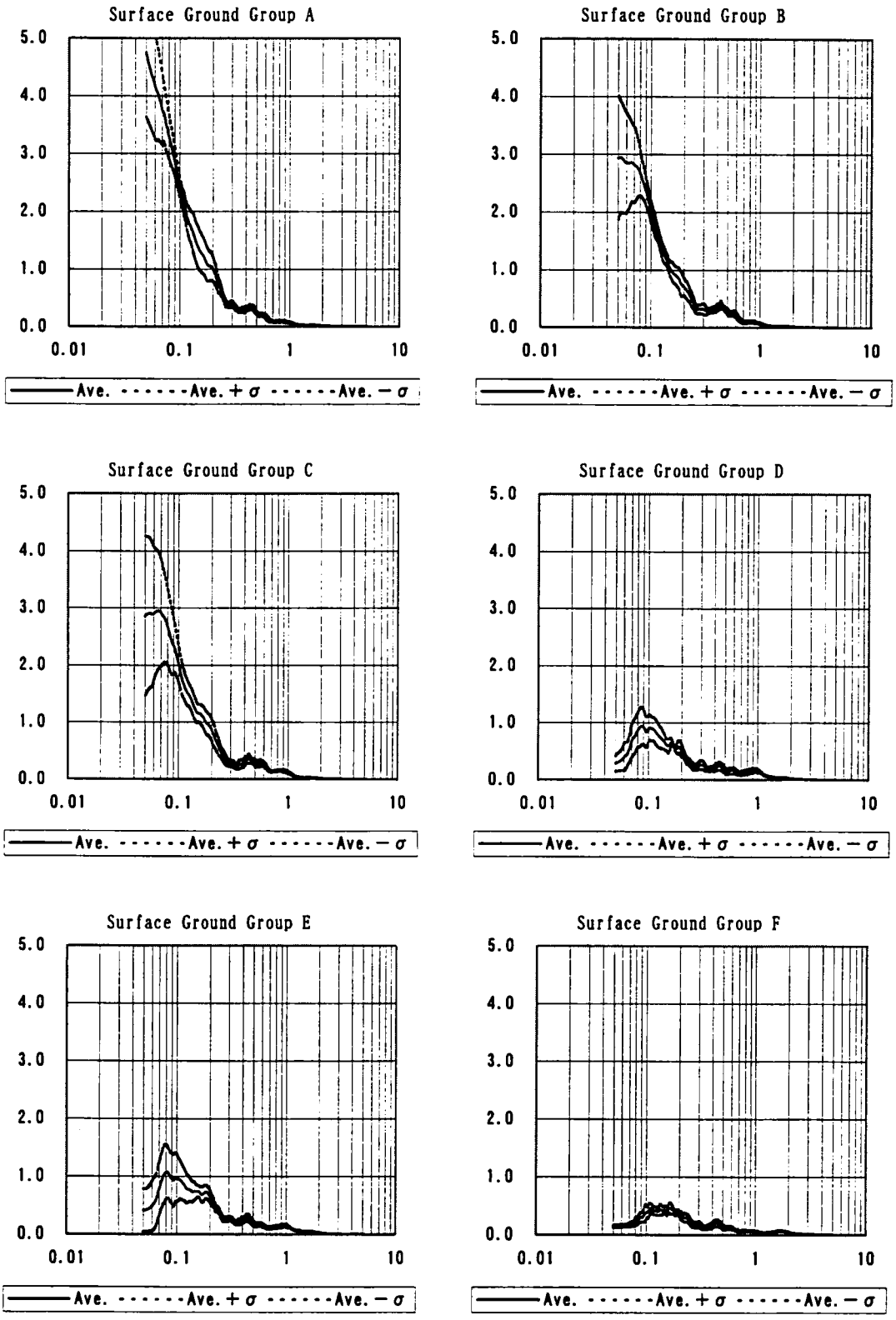

Figure 5.6(1) Damage spectra of ground motions at 6 ground groups
(input motion: Izumi, PGA:500Gal)

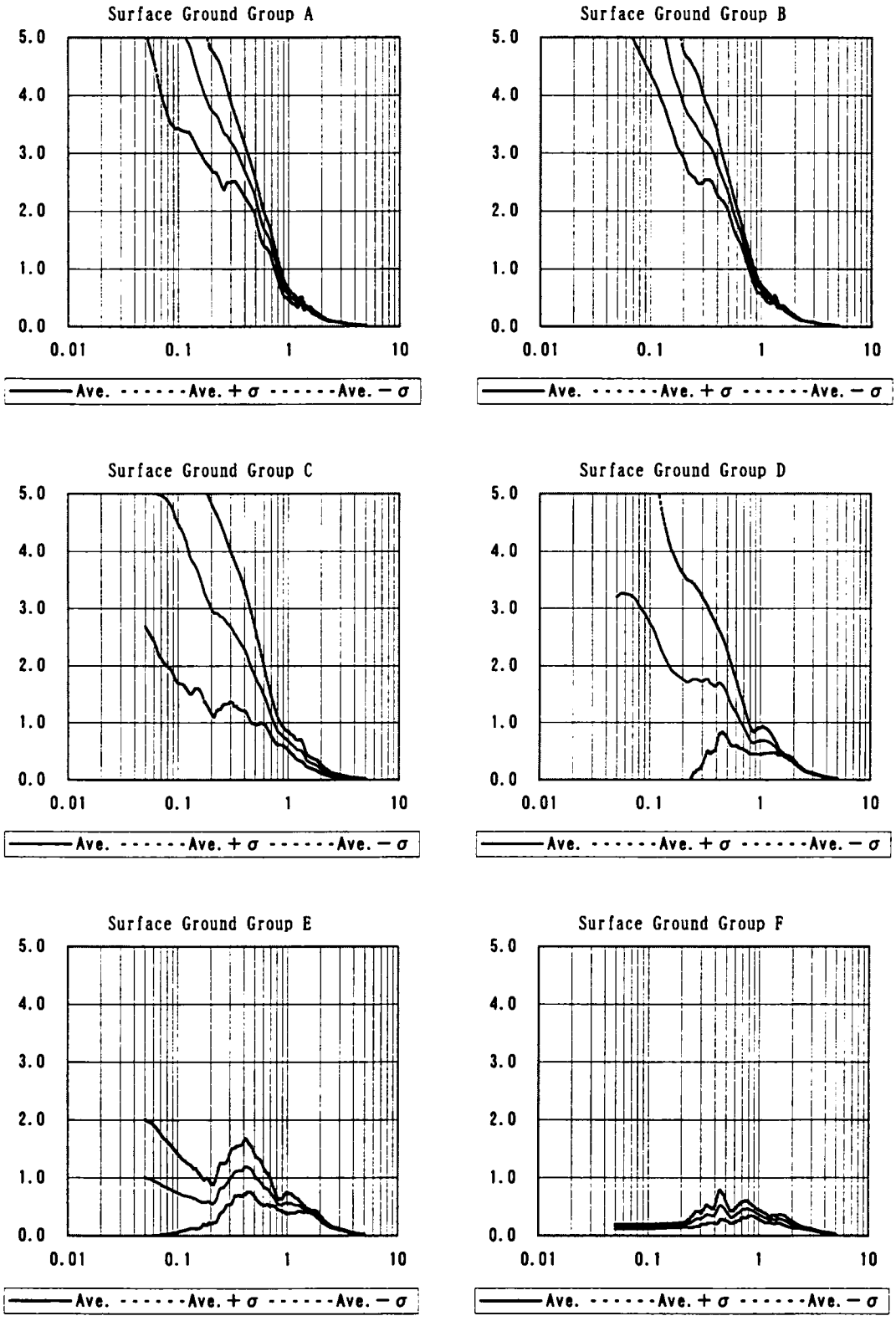

Figure 5.6(2) Damage spectra of ground motions at 6 ground groups
(input motion: Kobe JMA, PGA:500Gal)

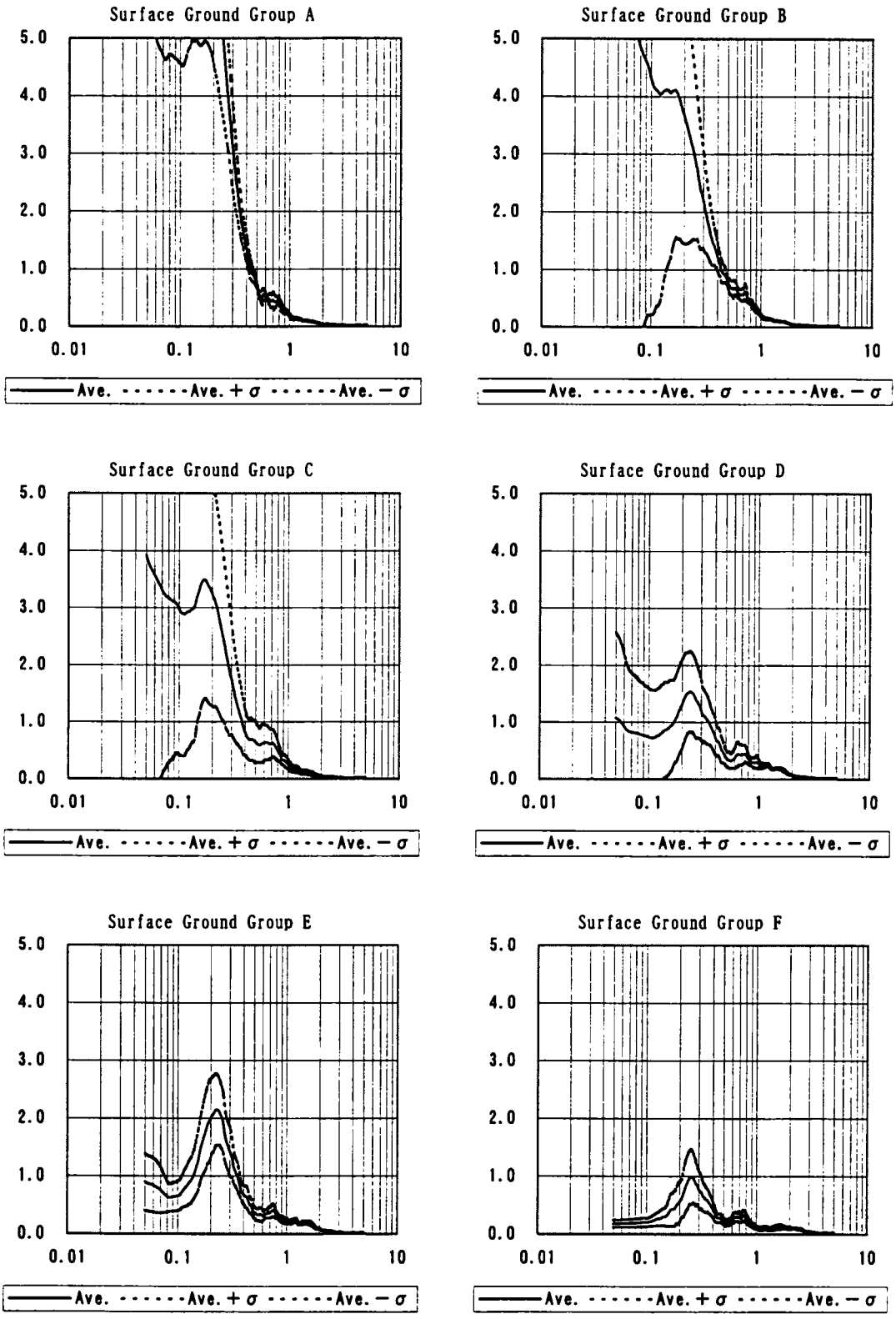

Figure 5.6(3) Damage spectra of ground motions at 6 ground groups
(input motion: Sutsu, PGA:500Gal)

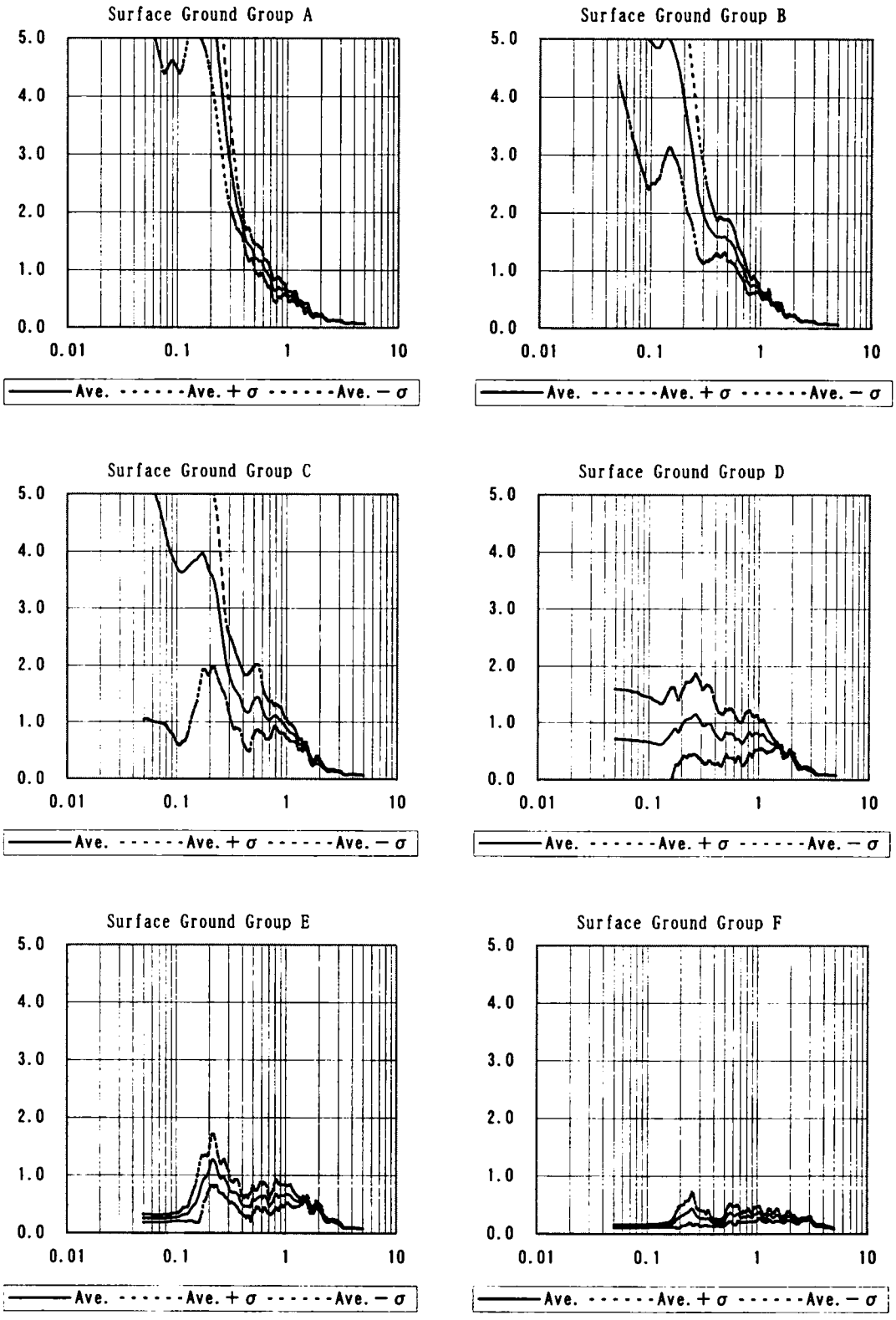

Figure 5.6(4) Damage spectra of ground motions at 6 ground groups
(input motion: Las Tortolas, PGA:500Gal)

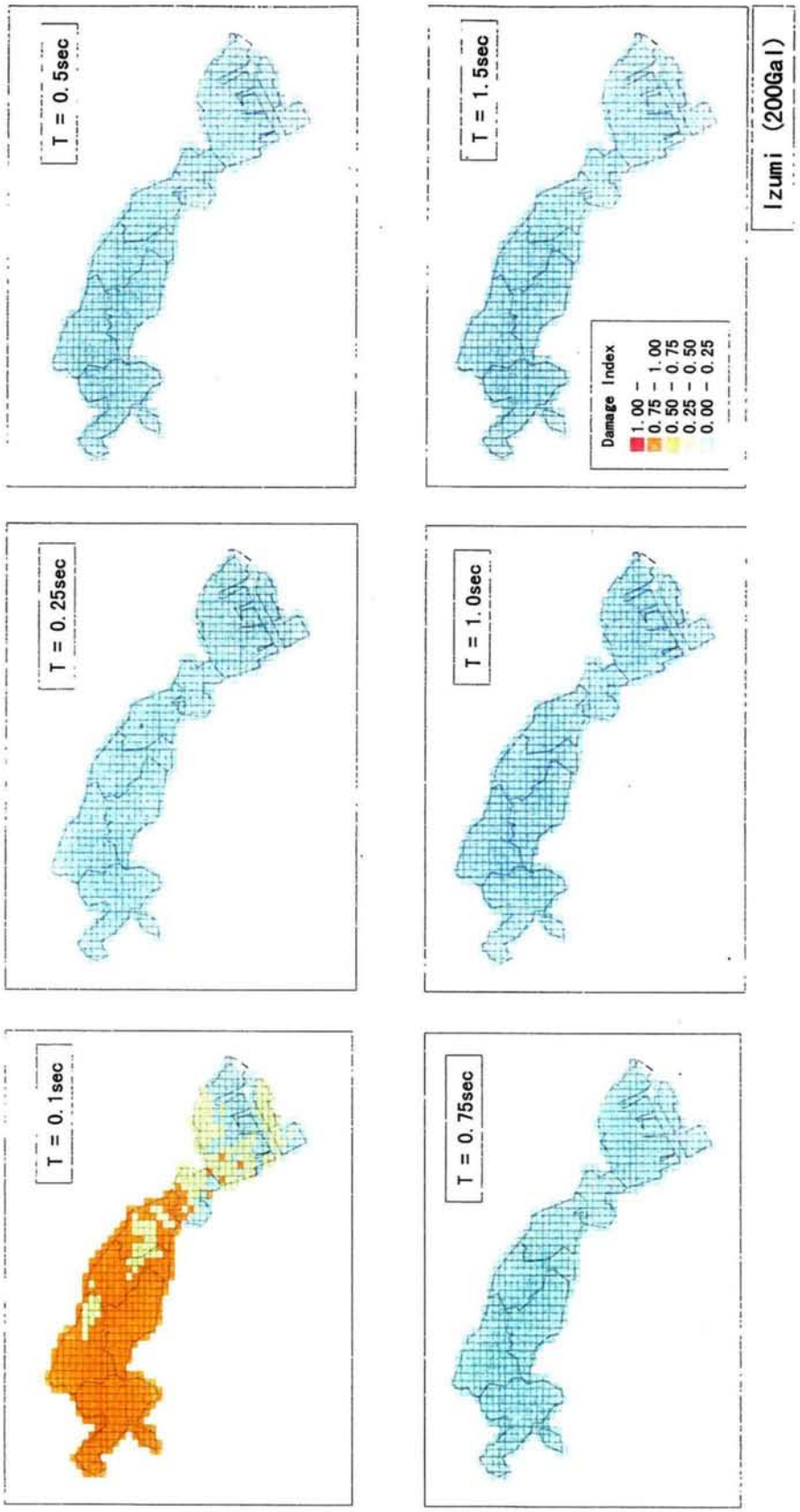

Figure 5.7(1) Distribution of damage indices at selected natural periods
(input motion: Izumi, PGA:200Gal)

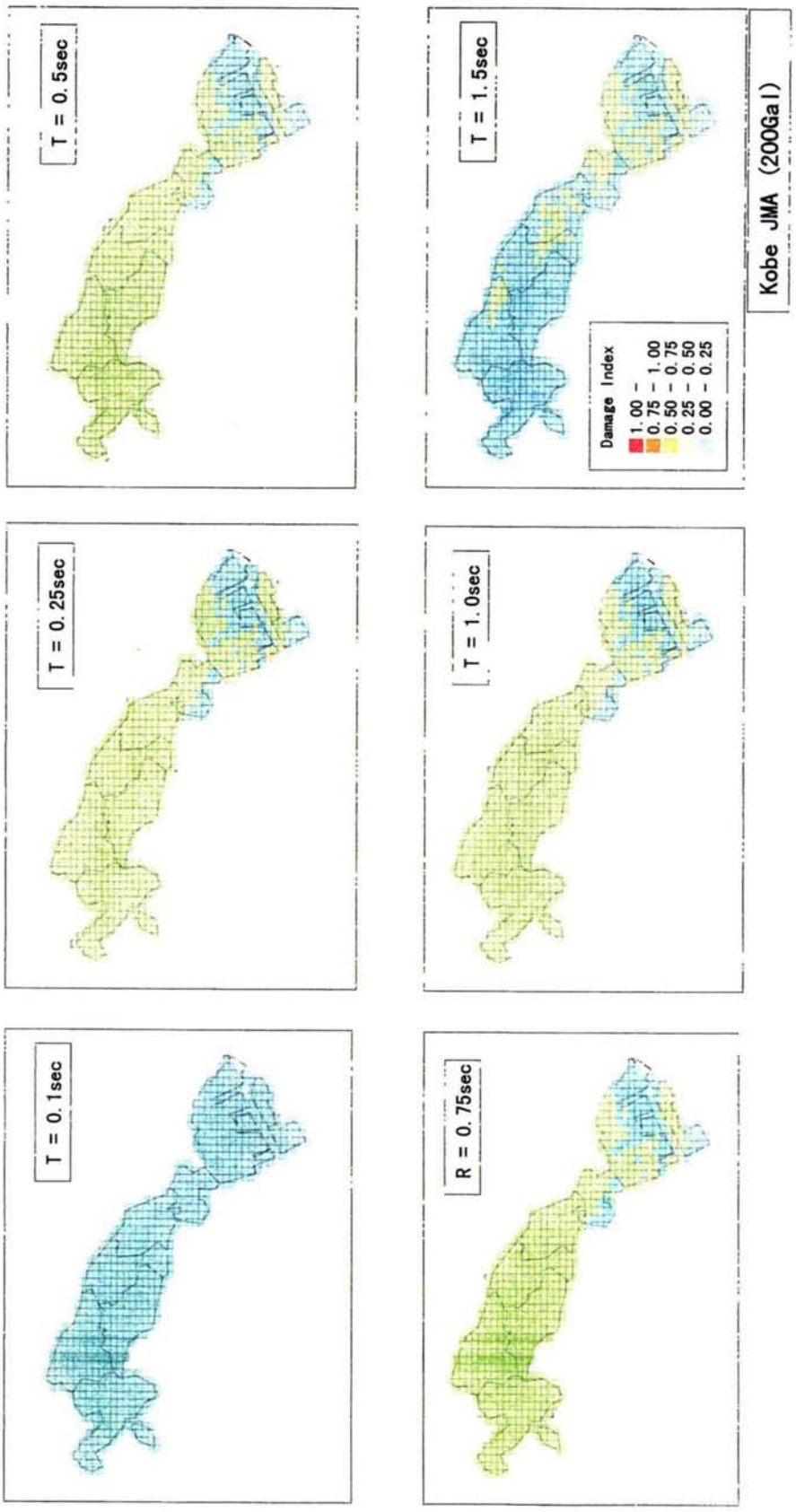

Figure 5.7(2) Distribution of damage indices at selected natural periods
(input motion: Kobe JMA, PGA:200Gal)

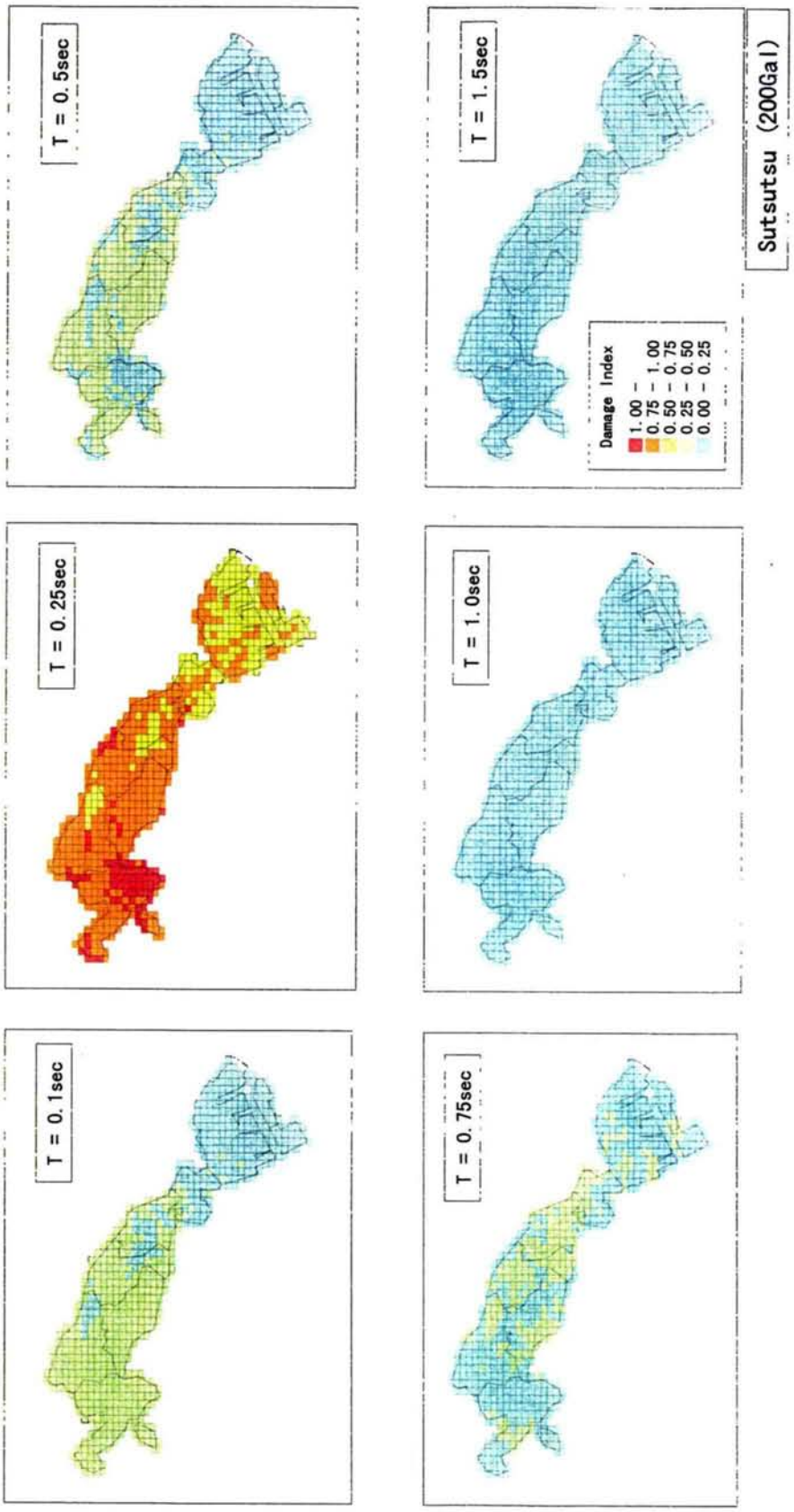

Figure 5.7(3) Distribution of damage indices at selected natural periods
(input motion: Sutsu, PGA:200Gal)

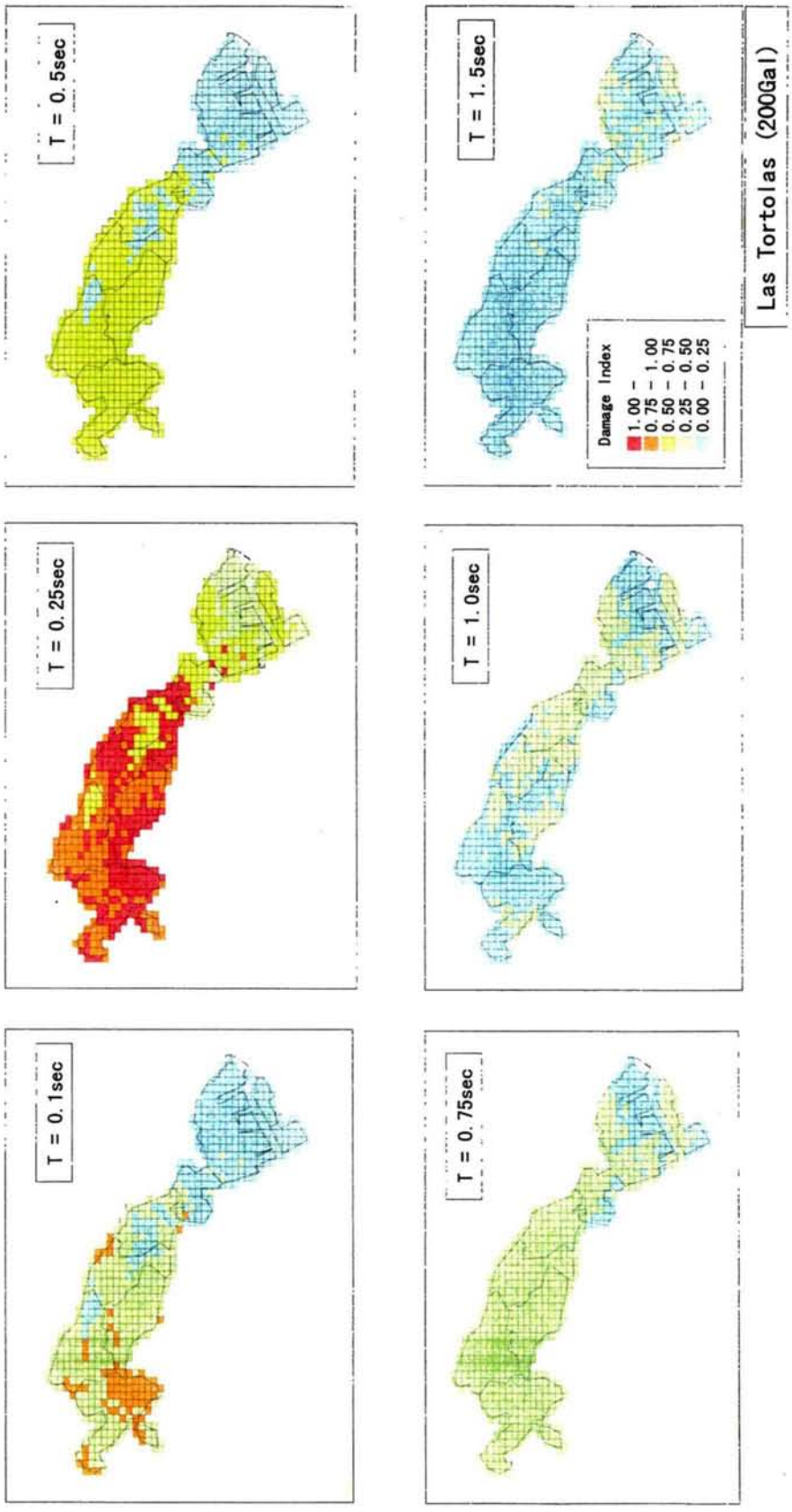

Figure 5.7(4) Distribution of damage indices at selected natural periods
(input motion: Las Tortolas, PGA:200Gal)

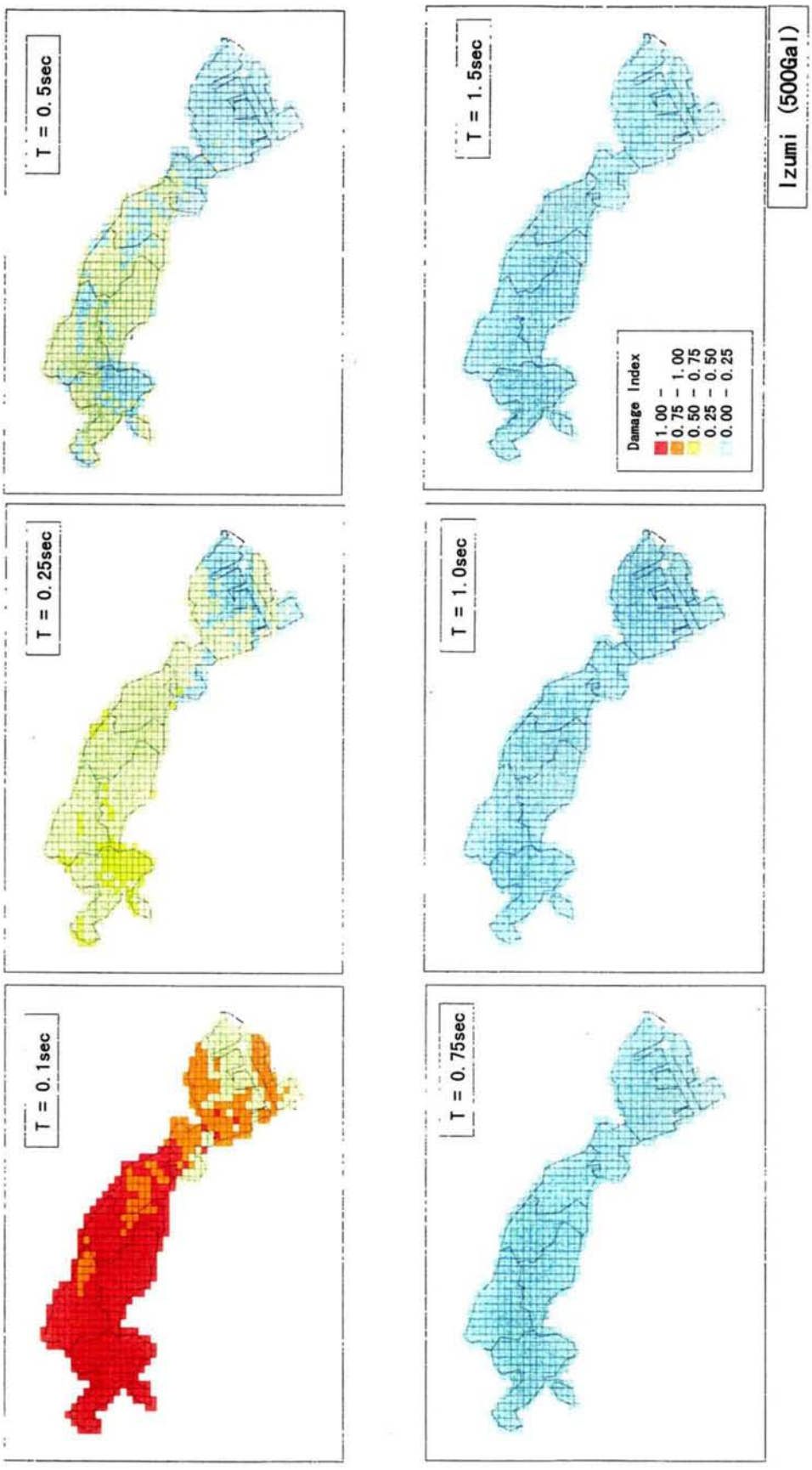

Figure 5.8(1) Distribution of damage indices at selected natural periods
(input motion: Izumi, PGA:500Gal)

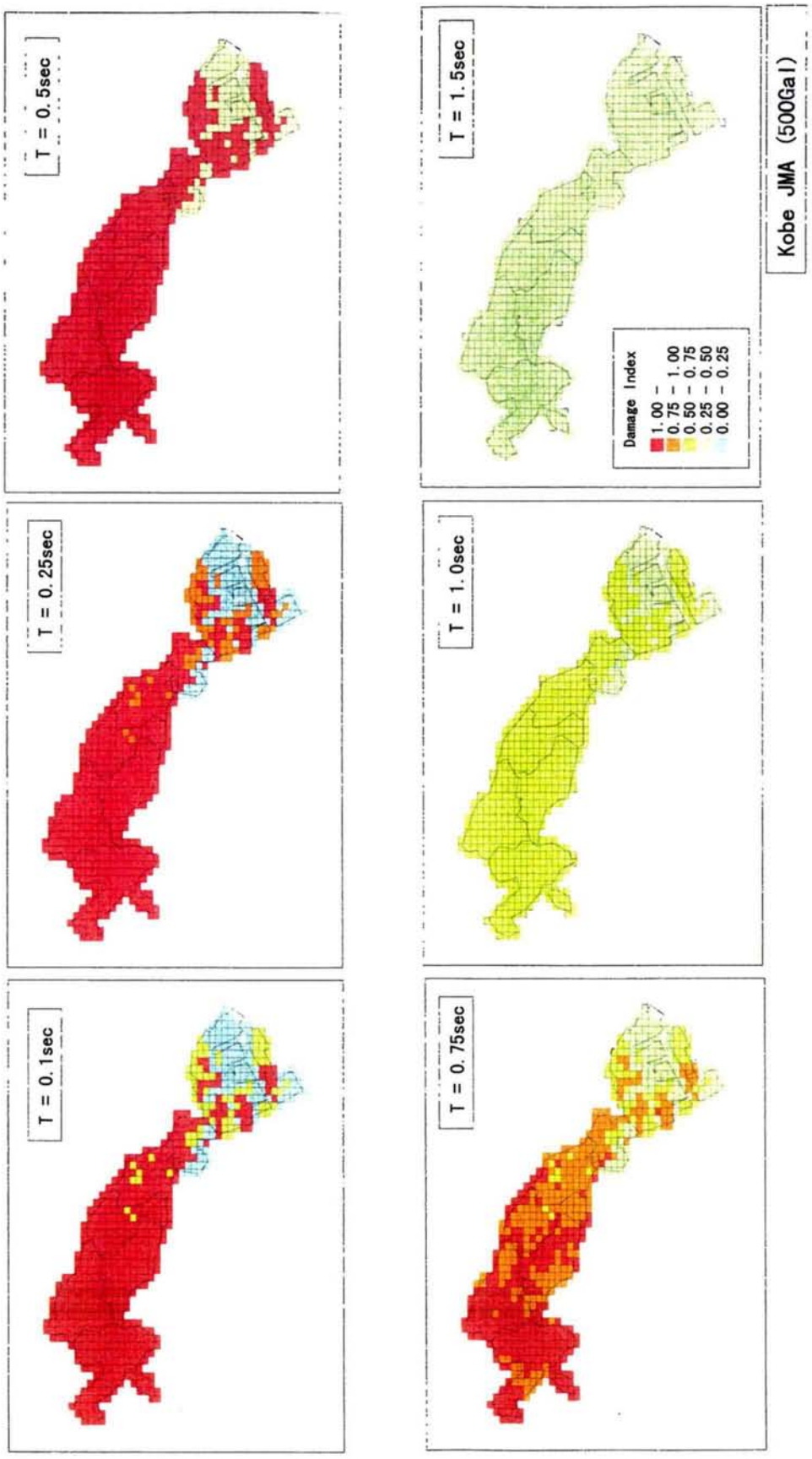

Figure 5.8(2) Distribution of damage indices at selected natural periods
(input motion: Kobe JMA, PGA:500Gal)

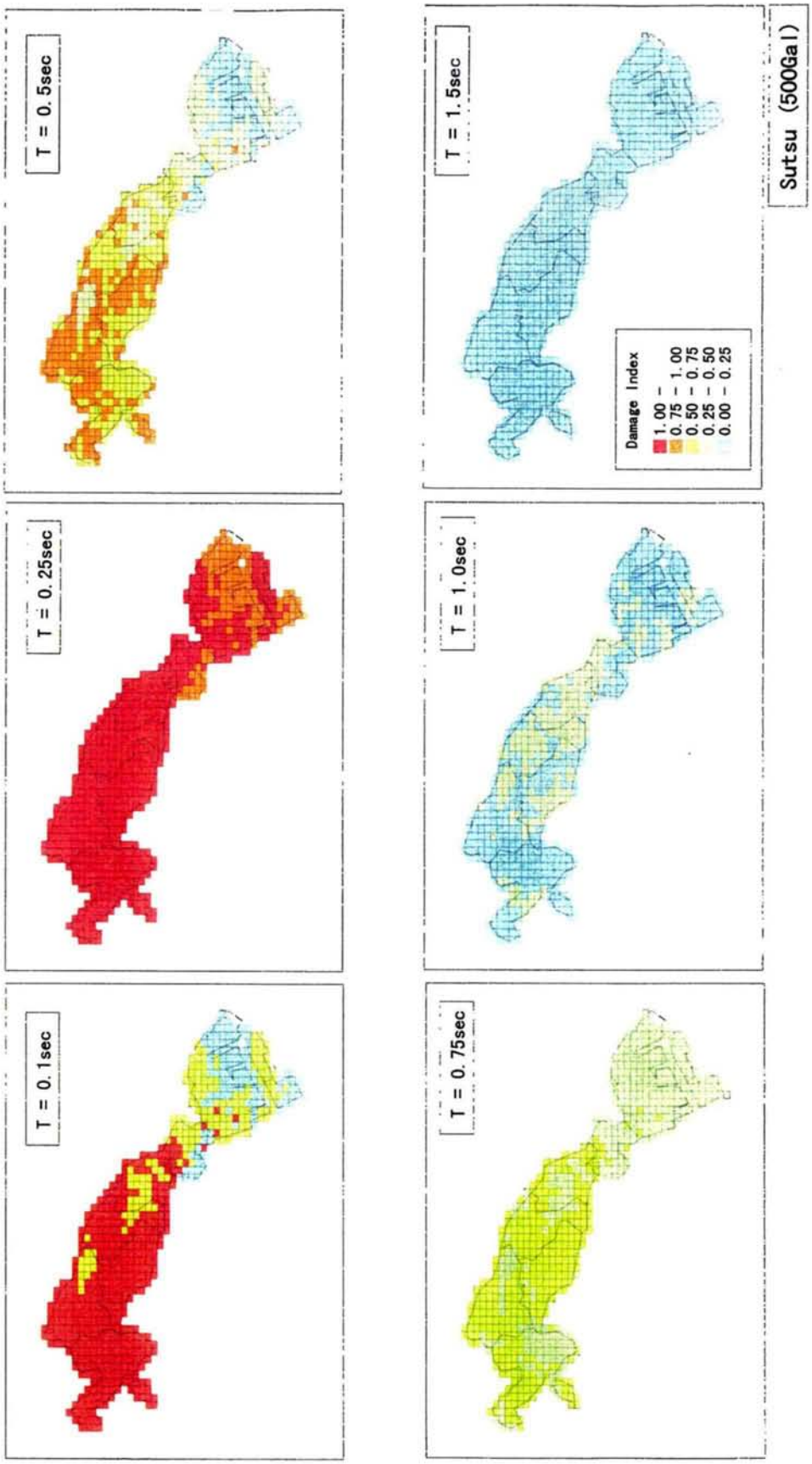

Figure 5.8(3) Distribution of damage indices at selected natural periods
(input motion: Sutsu, PGA:500Gal)

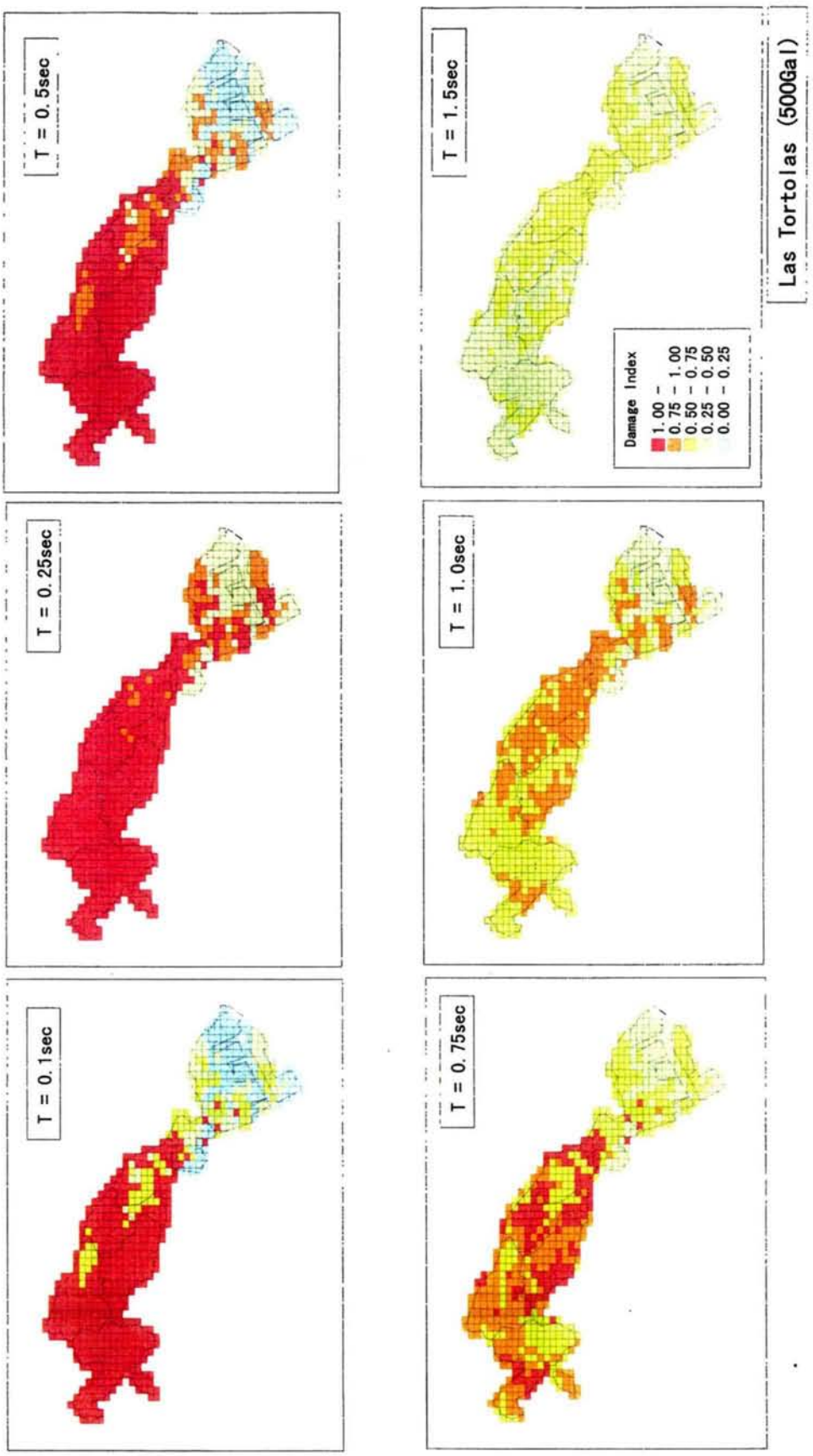

Figure 5.8(4) Distribution of damage indices at selected natural periods
(input motion: Las Tortolas, PGA:500Gal)

5.3.3 DAMAGE POTENTIAL OF GROUND MOTIONS IN KAWASAKAI CITY

In this section, damage potential of ground motions in Kawasaki City during a large scenario earthquake is evaluated. The selected input ground motion at bedrock is the hypothetical Kanto earthquake ground motion evaluated by Ohta, Shima et al. (1991) for seismic design of buildings in Tokyo bay area. The ground motion reflects the site geological conditions and characteristics of the earthquake by employing the hypothetical Kanto earthquake fault model shown in Figure 5.1. The input ground motion at bedrock and the response spectra of the ground motion are shown in Figure 5.9. The peak ground acceleration of the ground motion is 333 cm/sec^2 and the duration is about 60 sec. The acceleration spectrum normalized by PGA shows that the predominant periods of the ground motion range widely and that the acceleration responses are relatively large even at long period of 2.0 sec.

Ground motions at the soil surfaces are calculated by response analysis of the soil profile models for the selected input ground motion. Then damage spectra of the ground motions are calculated.

In order to demonstrate visually the damage potential over Kawasaki City, the damage indices for different structural periods in all cells are shown in Figure 5.10. Based on the figure, the following points on the damage potential of ground motions in Kawasaki City are emphasized:

(1) In the northwestern part with relatively stiff ground in Kawasaki City, the ground motions have high damage potential for structures with natural period lower than about 0.75 sec.
(2) In the southeastern bay area with relatively soft ground, the ground motions have higher damage potential for the structures with natural period higher than about 0.5 sec.
(3) For the structures with natural period higher than about 1.0 sec., ground motions in the middle part of Kawasaki City have high damage potential.

The method for estimating damage potential of ground motions in a large area presented in this chapter is a very efficient and effective tool that can be used in design and retrofit decisions, disaster mitigation strategies and for emergency response planning purposes. It provides a new quantitative and visual approach for measuring and displaying damage potential information. It combines key components such as input ground motions, local soil characteristics and structural information that can easily be utilized for various governments and private industry decision makers.

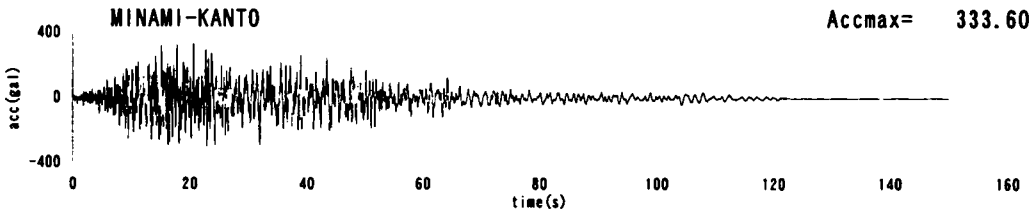

(a) Input ground motion

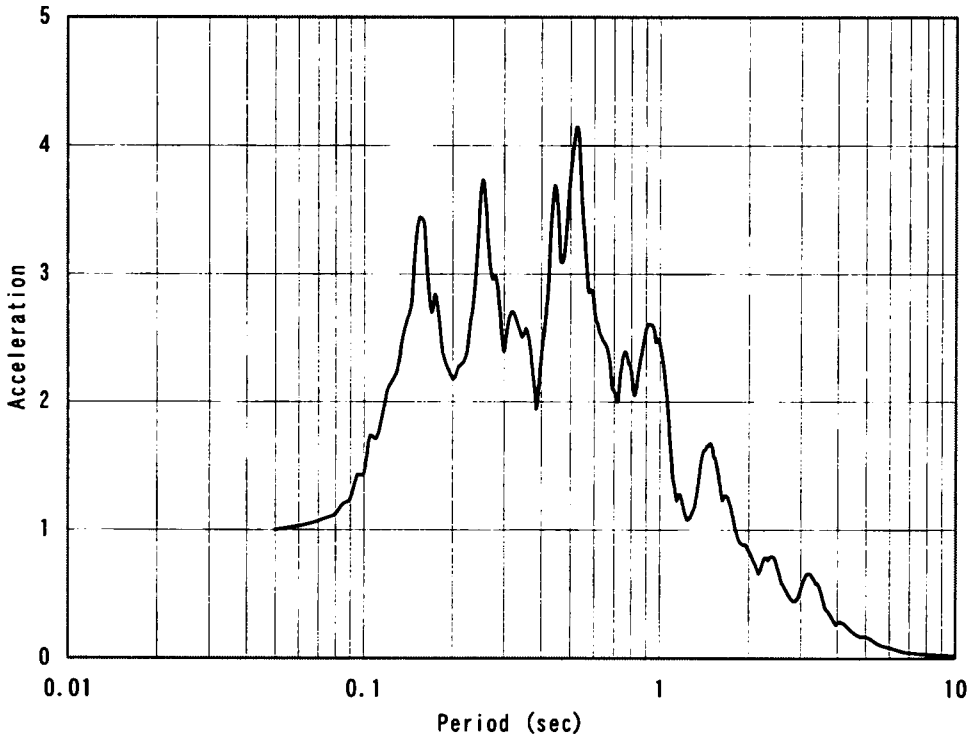

(b)Normalized acceleration response spectra

Figure 5.9 Selected input ground motion at bedrock

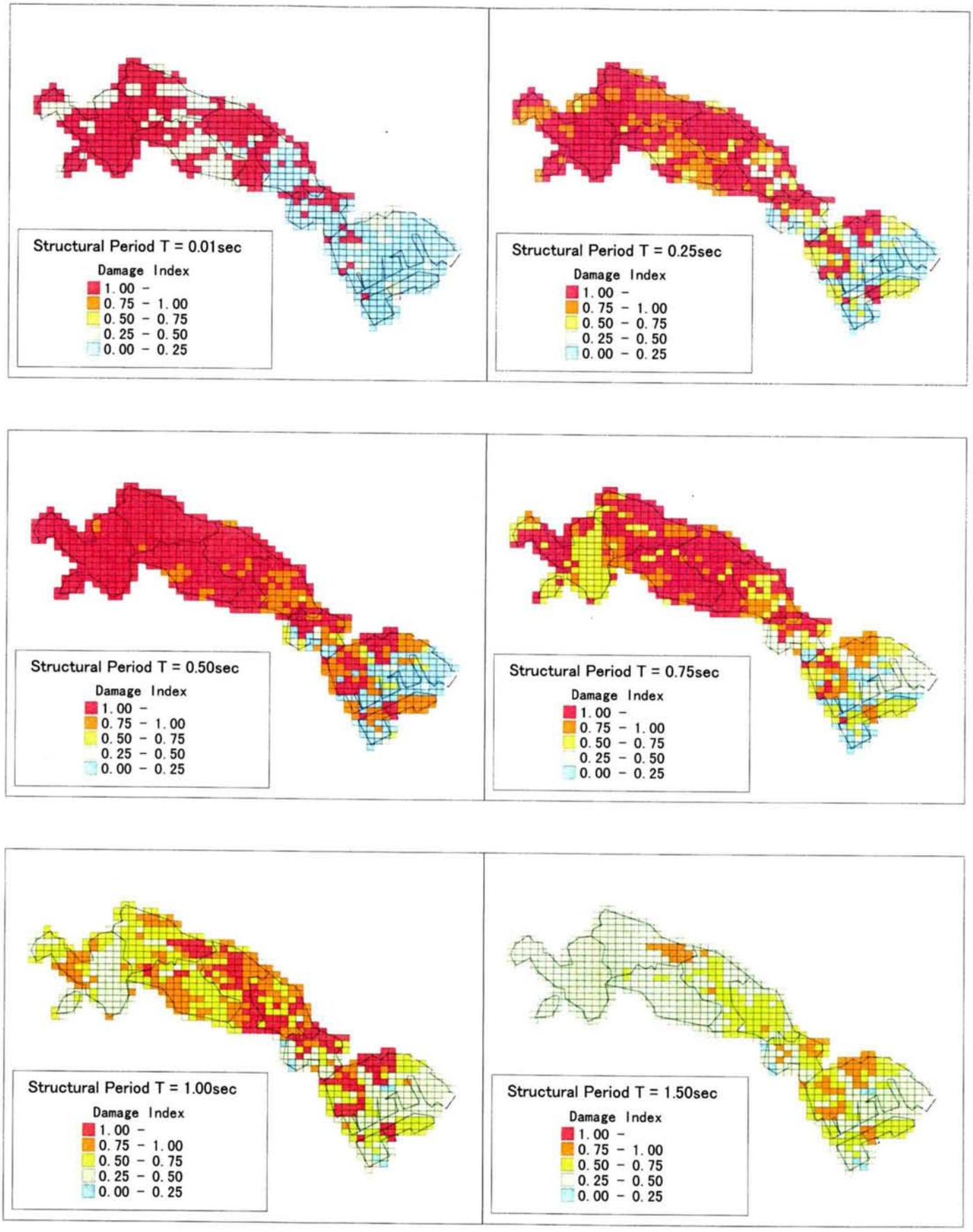

Figure 5.10 Damage potential of ground motion in Kawasaki City for different structural periods

5.4 CONCLUSIONS

In this chapter, a methodology for the evaluation of damage potential of ground motions during large earthquakes in a large area was presented. The method was applied to Kawasaki City located in the southern part of Kanto, in Japan. Some case studies were conducted, and damage potential of the hypothetical Kanto earthquake was described. The following can be concluded:

(1) In the cases of input motions with PGA of 200 cm/sec^2, the average damage spectra are smaller than 1 for almost all natural periods during near-source type earthquakes, and the average damage spectra of some surface ground groups are larger than 1 for special natural periods during inter-plate type earthquakes. On the other hand, in the cases of the input motions with PGA of 500 cm/sec^2, the average damage spectra are larger than 1 for natural periods shorter than the particular values that depend on the earthquake type and surface ground group.

(2) Damage potential in a large area greatly depends on the type of earthquake. The ground motions induced by earthquakes that might have wide frequency contents have great damage potential in a large area. The damage potential of ground motions depends on the ground conditions, too. Therefore, distribution of damage indices in a large area would be very complex according to the distribution of the ground conditions.

(3) Damage potential of ground motions in Kawasaki City during a large scenario earthquake i.e. the hypothetical Kanto earthquake was evaluated. According to the results, in the northwestern part with relatively stiff ground in Kawasaki City, the ground motions have very high damage potential for the structures with natural period lower than about 0.75 sec. In the southeastern bay area with soft ground, the ground motions have relatively high damage potential for the structures with natural period longer than about 0.5 sec. For the structures with natural period lower than about 0.75 sec., ground motions in the northwestern part have higher damage potential than those in the southern part. For the structures with natural period higher than 1.0 sec., ground motions in the middle part of Kawasaki City have high damage potential.

(4) The method for estimation of damage potential of ground motions in a large area presented in this chapter is a very efficient and effective tool that can be used in design and retrofit decisions, disaster mitigation strategies and for emergency response planning purposes. It provides a new quantitative and visual approach for measuring and displaying damage potential information. It combines key components such as input ground motions, local soil characteristics and structural information that can easily be utilized for various governments and private industry decision makers.

CHAPTER 6

STRENGTH DEMAND SPECTRA WITH UNIFORM DAMAGE LEVEL IN LIFETIME OF STRUCTURE

6.1 INTRODUCTION

Earthquakes followed by strong aftershocks have caused extensive structural damage, and induced huge loss of life and property. For example, it was reported that an aftershock of the 1987 Whittier Narrows earthquake increased the damage of the I-5/I-605 separator that had been caused by the mainshock (Priestley, 1988). The 1990 Philippine earthquake that consisted of two distinct earthquakes separated by about a minute's interval caused the severest structural damage in recent years (EQE Engineering, 1990). An aftershock of the 1999 Kocaeli Earthquake caused extensive damage to structures around Duzce in Turkey. Furthermore, an aftershock of the 1999 Chi-Chi Earthquake caused extensive damage to structures in Taiwan. It is clear that aftershocks are crucial to structural safety in the event of earthquakes.

After a strong earthquake has subsided, the normal expectation is that the serious danger is over. However, this is not a scientifically sound assumption, because it overlooks at least three well-recognized possibilities (Richter, 1958):

1) A strong and damaging shock may be a foreshock of a greater and more destructive earthquake.

2) Aftershocks of major earthquakes may be as large as ordinary locally damaging shocks. Moreover, the epicenters are likely to be distributed over a wide area; a large aftershock may originate closer to a center of population, and cause more damage there, than the main earthquake, as was the case in the 1952 Bakersfield earthquake.

3) In certain areas a strong shock has historically been followed within comparatively few hours by an equal or larger one.

In this chapter, damage spectra of ground motions during aftershocks are calculated and the damage potential is studied by using recorded ground motions. A simulation model for mainshock-aftershock sequences and a method for estimating damage spectra of site ground motions from mainshock-aftershock earthquake sequences in a desired design period are presented. Then, a method for evaluating the strength demand spectra with uniform damage level in the lifetime of a structure considering mainshock-aftershock earthquake sequences is proposed. The proposed method is applied to estimation of damage potential of ground motions and strength demand spectra in a lifetime of a structure considering mainshock-aftershock earthquake sequences in Eureka, California.

6.2 DAMAGE SPECTRA OF GROUND MOTIONS DURING AFTERSHOCKS

In order to study the damage potential of ground motions during aftershocks, relatively large ground motion record sets during both mainshock and aftershock are needed. However, such record sets are very few. Several of these are discussed in this section.

Mainshock of the Coalinga, California earthquake occurred on May 2, 1983 with magnitude 6.5. Then an aftershock with magnitude 6 occurred on July 22, 1983. At some stations, relatively large ground motions were recorded during the aftershock. The observed ground motions during the mainshock and aftershock are shown in Figure 6.1. The damage spectra of the ground motions are also shown in Figure 6.2. Damage spectra of ground motions in a sequence of mainshock-aftershock are calculated considering cumulative damage related with both the response deformation and the dissipated hysteretic energy of the SDOF during the sequence. In this example, the damage indices of ground motions recorded at PVP045 Basement and Switchyard with short natural periods due to the mainshock and the aftershock is larger than that due to the mainshock alone. On the other hand, the ground motions recorded at PVP135 Basement and Switchyard during the aftershock do not enlarge damage indices due to the mainshock.

The mainshock of the Whittier Narrows, California earthquake occurred on October 1, 1987. Then an aftershock occurred on October 4, 1987. Relatively large ground motions were recorded during the aftershock. The observed ground motion during the mainshock and aftershock are shown in Figure 6.3. The damage spectra of the ground motions during the mainshock and aftershock are also shown in Figure 6.4. In this example, it is found that the damage index due to the mainshock and the aftershock combined is larger than that due to the mainshock alone in the range of natural periods roughly between 0.2 and 0.4 sec.

An aftershock with a magnitude of 7 occurred at Bolu on November 12, 1999. Large ground motions were recorded at Bolu and Duzce. Unfortunately, the seismograph at Bolu did not work during the mainshock. The recorded ground motions and damage spectra at Duzce during the mainshock and aftershock are shown in Figure 6.5 and Figure 6.6, respectively. In this example, the damage spectra of the mainshock and the aftershock ground motions are much larger than those of the mainshock ground motions alone over almost the entire spectra.

Based on the three examples presented herein, it can be concluded that the combination of mainshock-aftershock ground motions can be more damaging to structures than the ground motions from the mainshock alone. What is interesting to observe is that structures which may have experienced relatively little damage from the mainshock has much greater damage index following the aftershock. For example, the damage index from the mainshock in the period range from 0.2 sec. to 0.4 sec. in the Whittier Narrows earthquake is about 0.2, but it increases to a maximum of 0.5 following the aftershock.

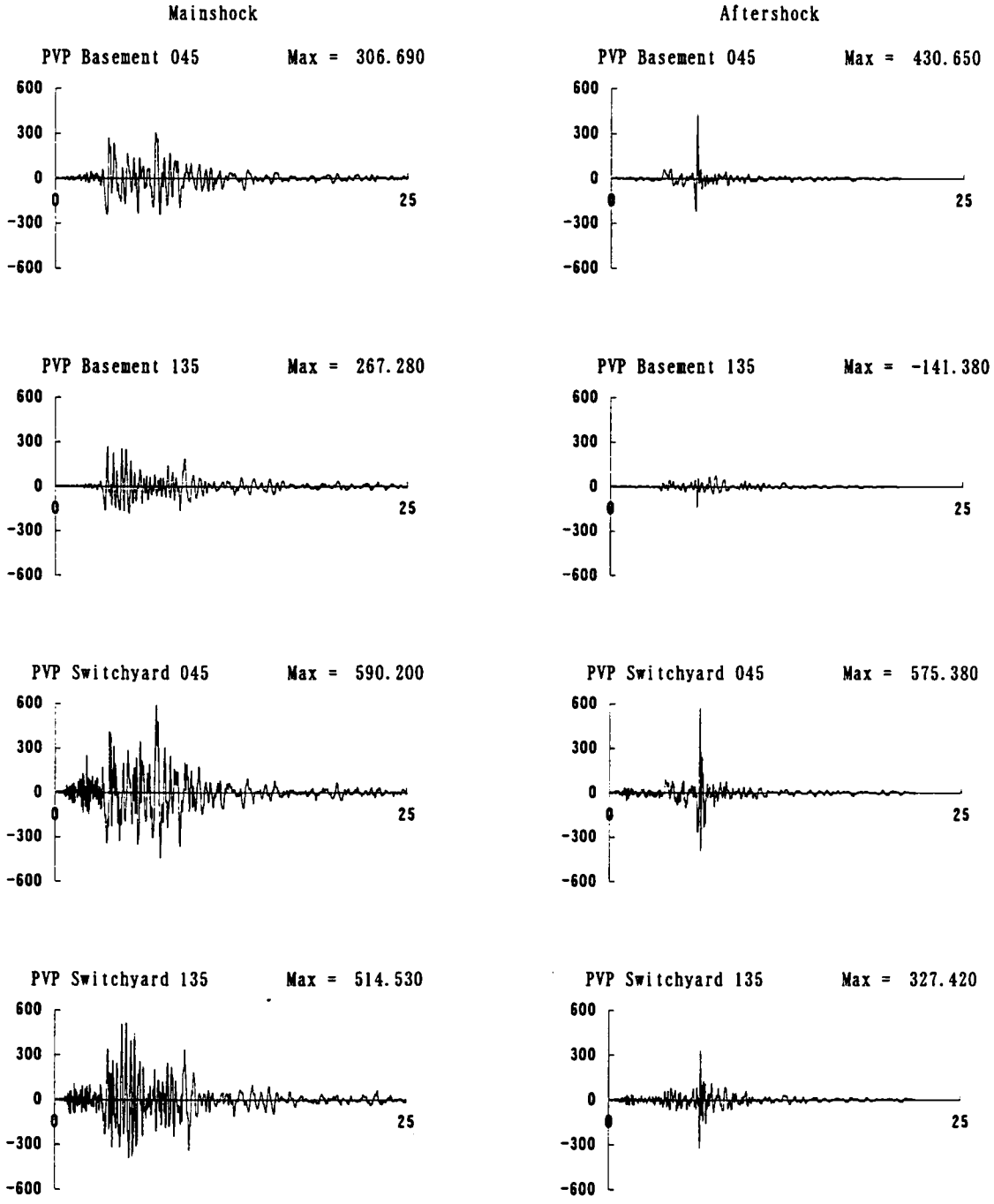

Figure 6.1 Observed ground motions during mainshock and aftershock of the 1983 Colinga earthquake, California

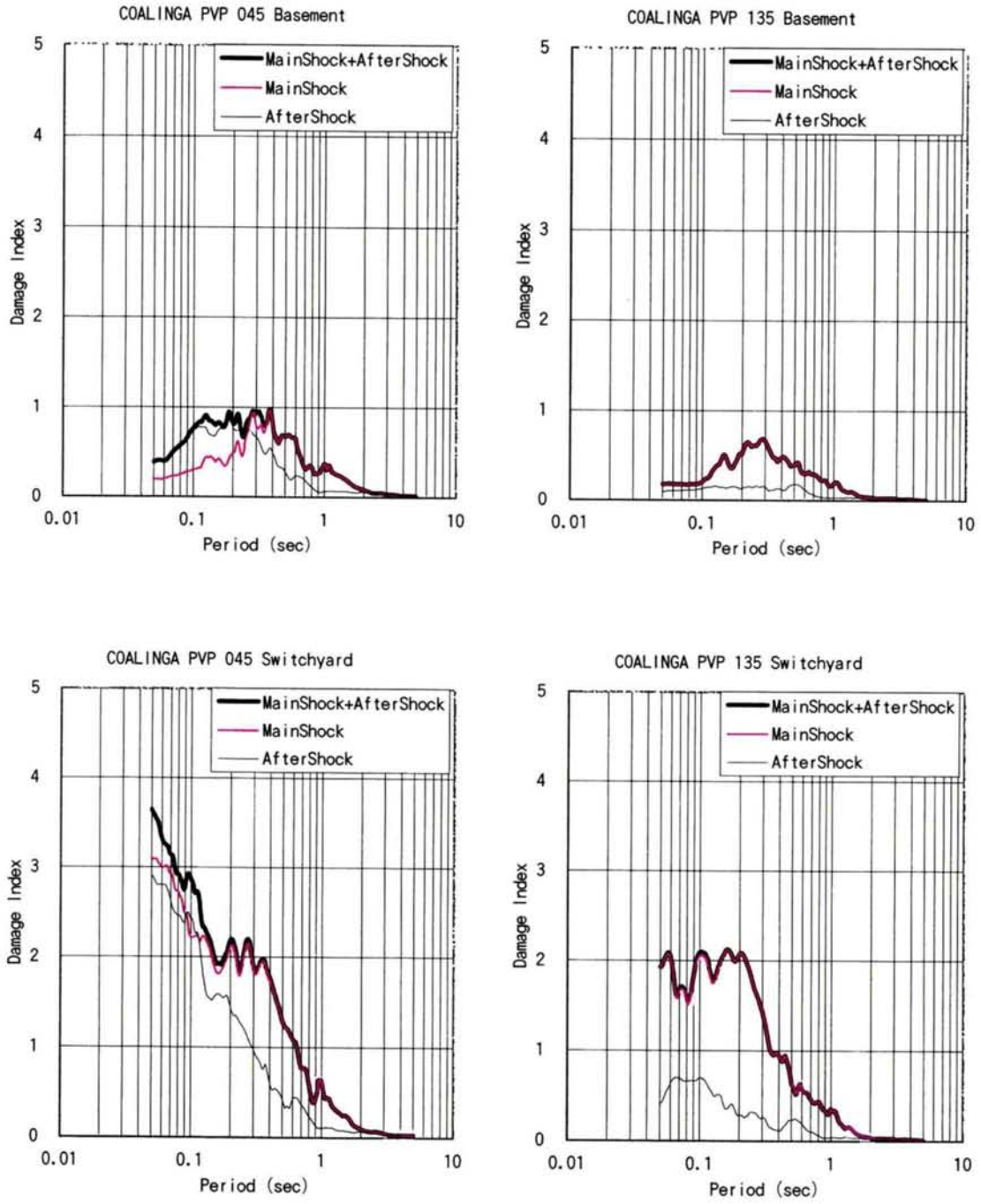

Figure 6.2 Damage spectra of ground motions during mainshock and aftershock of the 1983 Coalinga earthquake, California

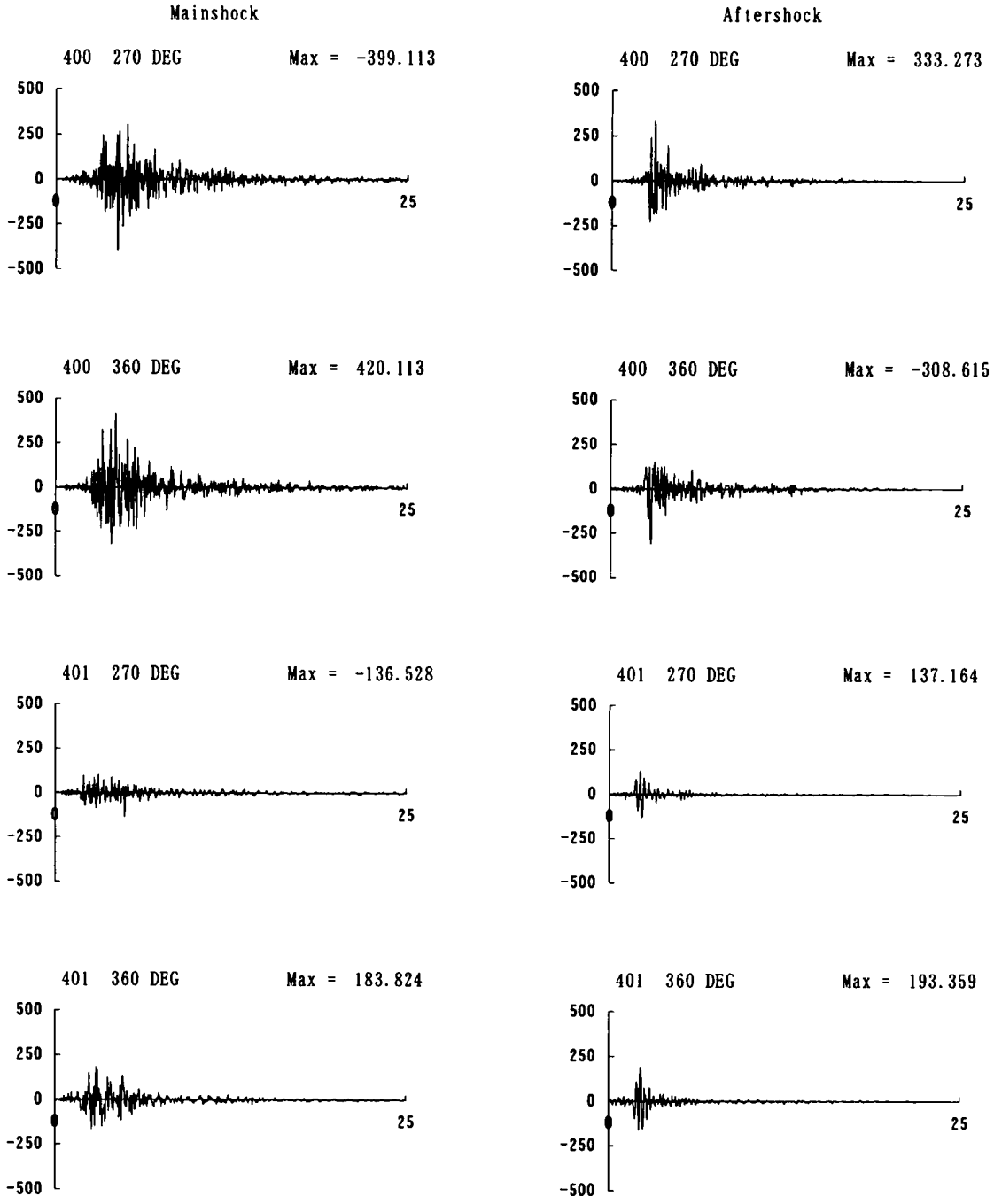

Figure 6.3 Observed ground motions during mainshock and aftershock of the 1987 Whittier Narrows earthquake, California

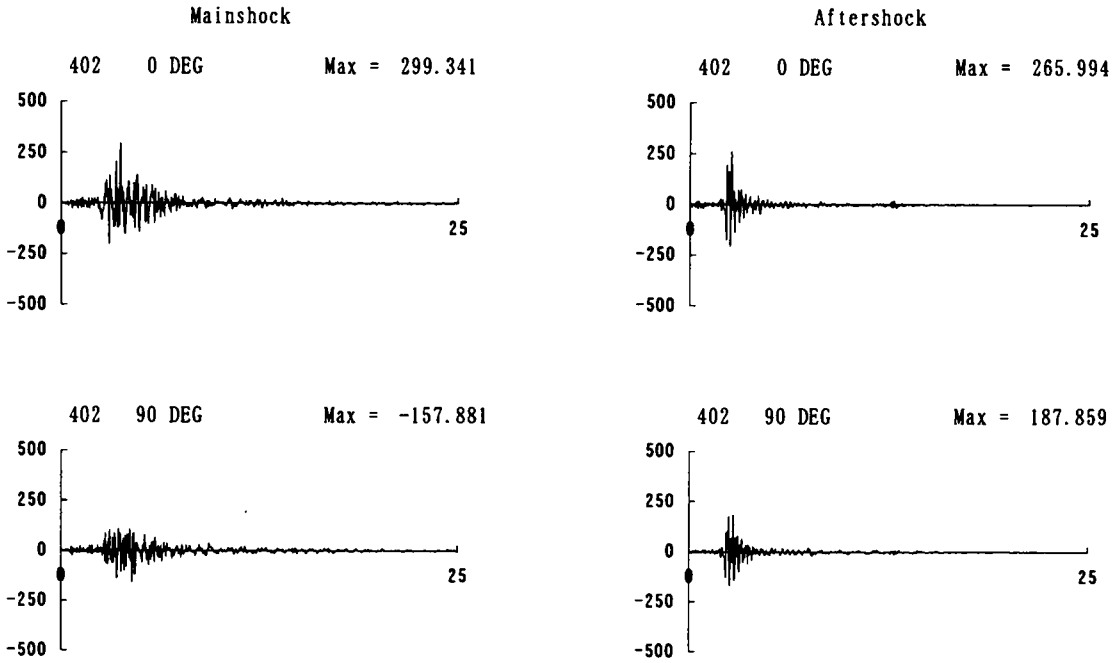

Figure 6.3 (continue)

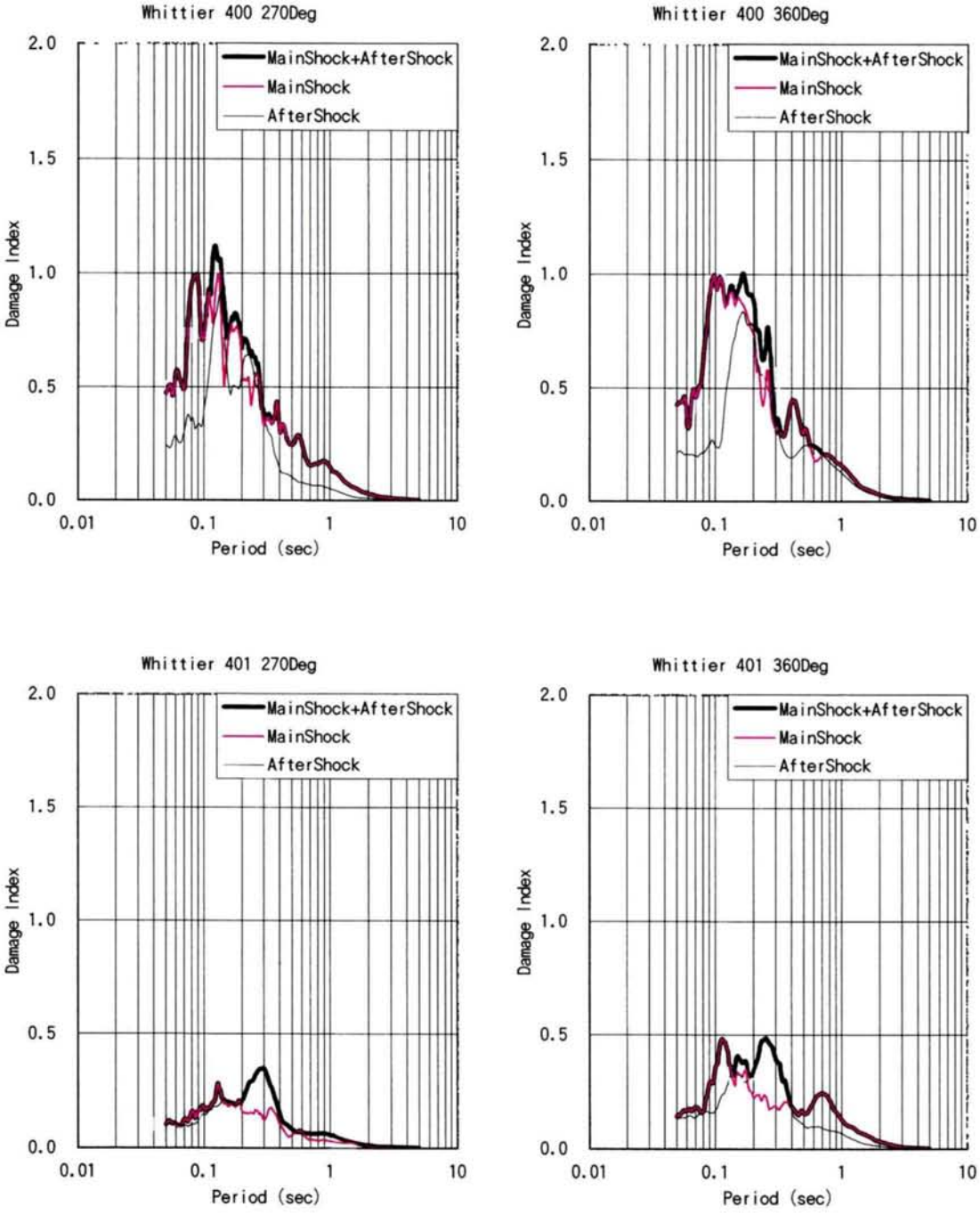

Figure 6.4 Damage spectra of ground motions during mainshock and aftershock of the 1987 Whittier Narrows earthquake

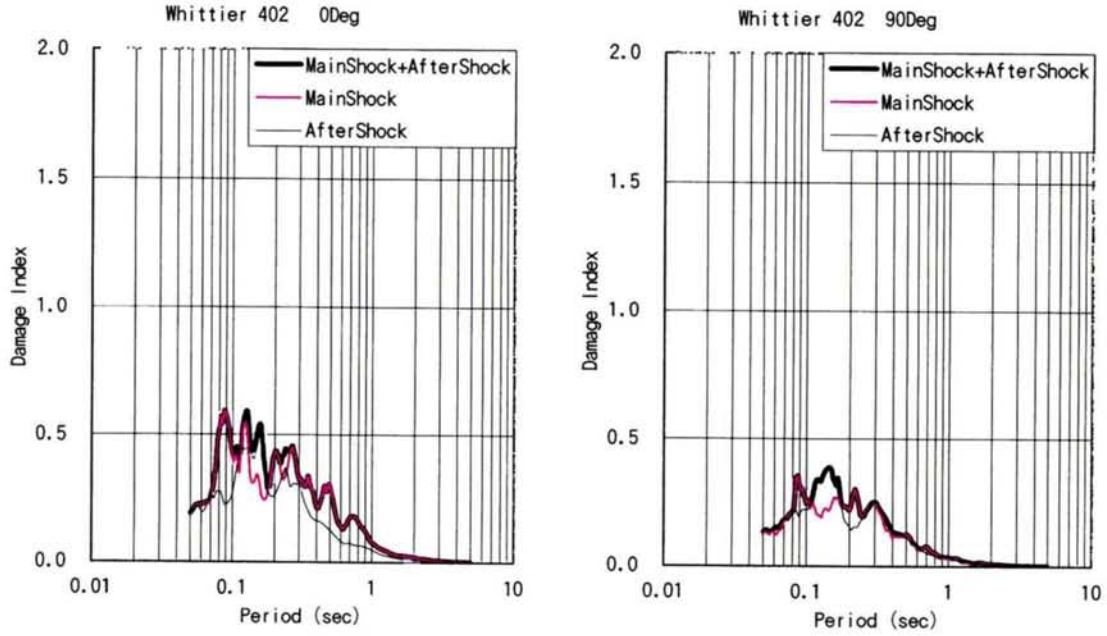

Figure 6.4 (continued)

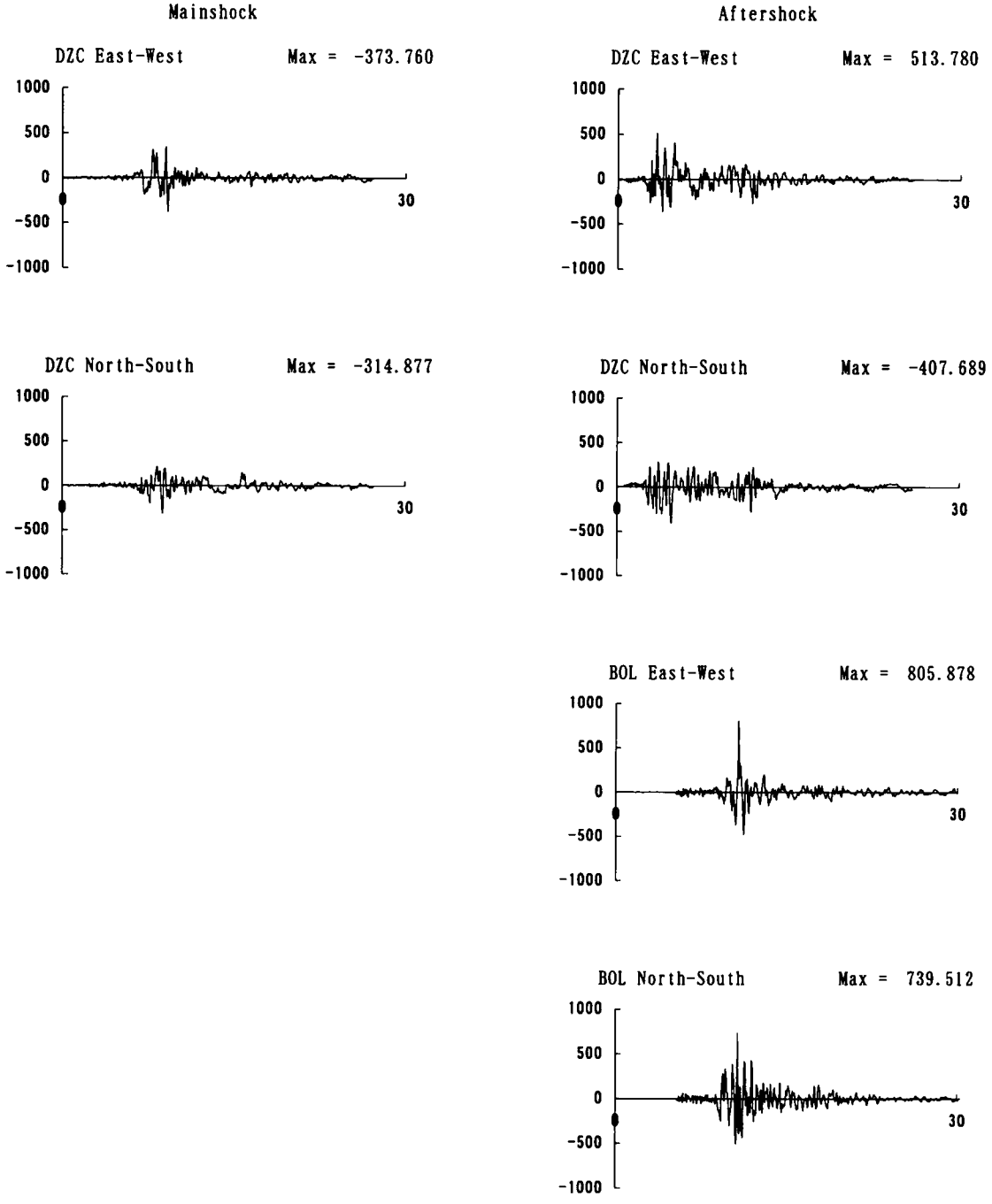

Figure 6.5 Observed ground motions during mainshock and aftershock of the 1999 Turkey earthquake

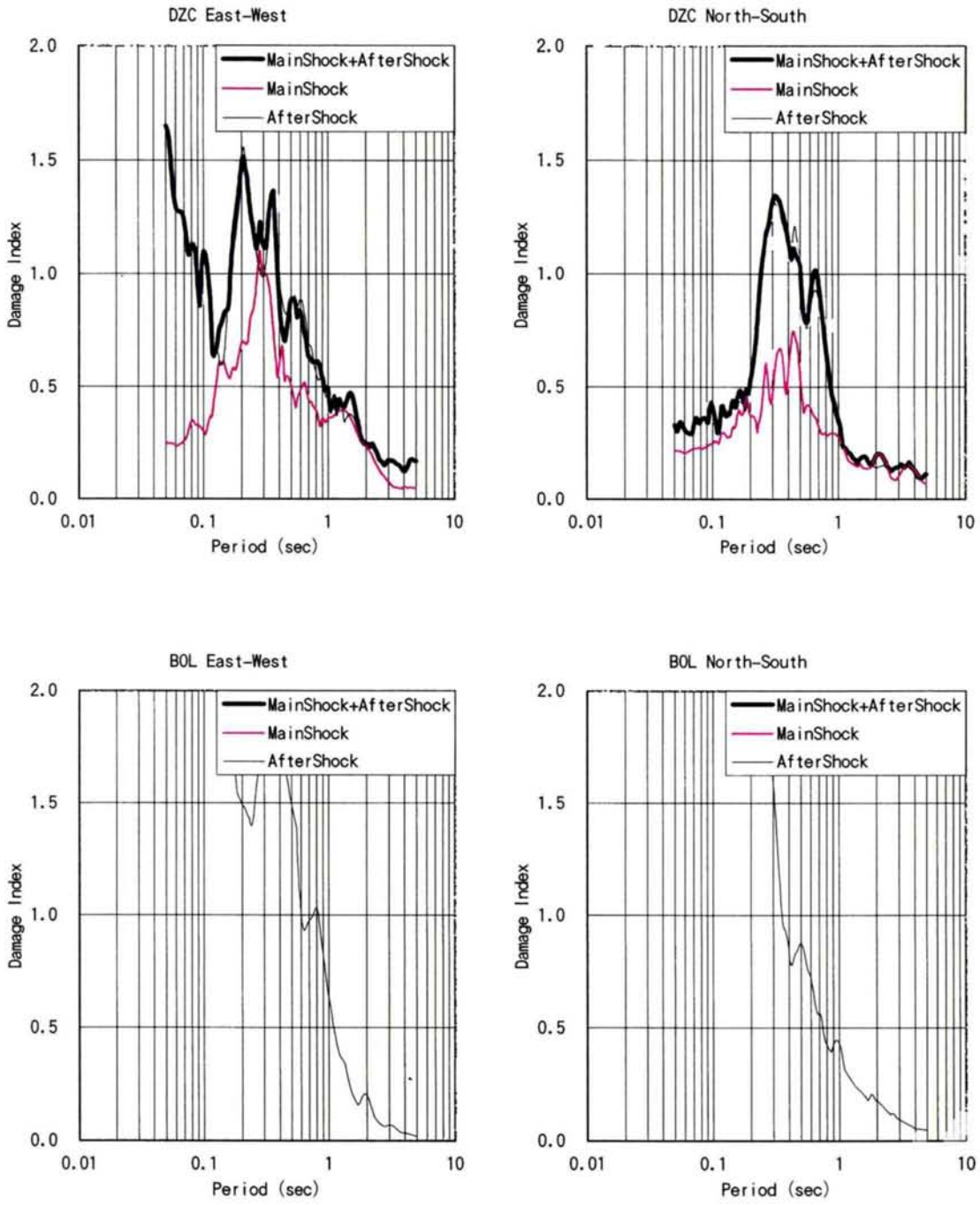

Figure 6.6 Damage spectra of ground motions during mainshock and aftershock of the 1999 Turkey earthquake

6.3 METHODOLOGY FOR STRENGTH DEMAND SPECTRA WITH UNIFORM DAMAGE LEVEL IN LIFETIME OF STRUCTURE

Earthquake events are typically composed of foreshock, mainshock and aftershock sequences. The mainshock in most cases releases the largest amount of energy and thus causes the most damage and destruction. Aftershocks, however, have also been known to cause considerable damage and are particularly detrimental to structures that have been weakened by the mainshock (Sunasaka and Shimizu, 1990). In this section, a probabilistic occurrence model of mainshock-aftershock sequences (Sunasaka and Kiremidjian, 1994a, 1994b), and a simulation methodology for damage spectra considering mainshock-aftershock earthquake sequences in desired design period of a structure are presented. Then, a method for evaluating the strength demand spectra with uniform damage level in the lifetime of a structure considering mainshock-aftershock earthquake sequences is proposed. The proposed method is applied to estimation of damage potential of ground motions and strength demand spectra in a lifetime of a structure considering mainshock-aftershock earthquake sequences in Eureka, California.

6.3.1 MODELING OF MAINSHOCKS

For structural safety, it is important to review the characteristics of earthquakes around the site and to select a probabilistic model of the earthquake occurrence. The characteristics of earthquakes and modeling of earthquakes in terms of occurrence times and magnitudes are presented.

(1) Occurrence Times

Because earthquakes are inherently rare and random in nature, they are frequently represented by stochastic models. The most commonly used model for earthquake occurrence is the Poisson model. In this model, the interarrival times are independent and exponentially distributed as

$$f_T(\tau) = \nu \exp(-\nu \tau) \quad (6.1)$$

where $f_T(\tau)$ is the probability density function of the interarrival time τ, and ν is the average occurrence rate.

The following Weibull model is applicable for the interarrival time distribution in some regions.

$$f_T(\tau) = \nu \gamma \tau^{\gamma-1} \exp(-\nu \tau^{\gamma}) \quad (6.2)$$

where ν and γ are constants. In this model, the hazard rate depends on the interarrival time. In the case of γ = 1.0, equation (6.2) becomes the exponential distribution.

Shimazaki and Nakata (1980) presented the time-predictable and slip-predictable models in which future earthquakes depend respectively on the magnitude or the time of occurrence of the last earthquake. Anagnos and Kiremidjian (1984) and Kiremidjian and Anagnos (1984) used these hypotheses to develop the stochastic time- and slip-predictable models for estimating the frequency of earthquakes based on occurrence patterns and geophysical mechanisms.

The occurrence time distribution model of mainshocks should be selected according to the earthquake data near the site. If the parameter γ of the Weibull distribution is nearly equal to 1.0, then the exponential distribution is applicable. Elsewhere, the time- or slip-predictable model can be applied to the occurrence time distribution of mainshocks.

For one sequence, the occurrence time of the n-th mainshock t_n is expressed as:

$$t_n = T_1 + \sum_{i=1}^{n} \tau_i \quad , \quad T_1 < t_n < T_2 \qquad (6.3)$$

where τ_i is the i-th interarrival time, and T_1 and T_2 are the starting time and the ending time of the sequence, respectively. In the design stage, T_2 - T_1 means the desired design period of a structure.

(2) Magnitudes

Gutenberg and Richter obtained the following expression relating earthquake magnitudes to the number of earthquakes:

$$N(M) = \alpha \exp(-\beta M) \qquad (6.4)$$

where N(M) is the number of earthquakes with magnitude greater than or equal to M, and α, β are the zone-dependent constants. The probability density function of magnitudes of mainshocks is derived from equation (6.4):

$$f_M(m) = \frac{\beta e^{-\beta m}}{e^{-\beta M_{min}} - e^{-\beta M_{max}}} \qquad (6.5)$$

where M_{min} is the minimum magnitude to be considered in the analysis, and M_{max} is the maximum magnitude around the site.

Coppersmith and Schwartz (1984) showed that for certain regions or faults, the Gutenberg and Richter formula is not applicable. It has been proposed that a fault has a characteristic earthquake

with a magnitude corresponding to its length (Wesnousky et al., 1983). This is called the maximum magnitude model.

The choice of magnitude distribution depends on whether or not the magnitude is to be bounded between a minimum and maximum value. Thus, if the magnitude is limited, then equation (6.5) is the appropriate probability distribution. In the development of the mainshock-aftershock occurrence model, the minimum and maximum magnitudes need to be considered. Therefore, equation (6.5) will be used to describe the magnitudes of mainshocks.

6.3.2 MODELING OF AFTERSHOCKS

For structural safety evaluation, it is important to take large aftershocks and a dense series of aftershocks into consideration. The duration in which large aftershocks occur is relatively short in comparison with the interarrival time of the mainshock, and has no significant effect on the occurrence of the mainshock. Thus, in order to evaluate structural safety taking the mainshock-aftershock sequences into account, we need a magnitude distribution model of aftershocks.

Occurrences of aftershocks in Japan were studied by Utsu (1961). He showed that the Gutenberg and Richter formula can apply to the distribution of magnitudes of aftershocks. The difference in magnitude between the mainshock and the largest aftershock is expressed by

$$M_0 - M_1 = 4.7 - 0.45 M_0 \qquad (6.6)$$

where M_0 is the magnitude of the mainshock and M_1 is the magnitude of the largest aftershock. However, the above equation has huge dispersion.

For aftershock sequences in Greece from 1912 to 1968, Drakopoulos (1971) expressed the total number of aftershocks with magnitudes greater than or equal to M by

$$N_a(M) = A \exp(-\beta M) \qquad (6.7)$$

$$A = \exp(3.62\beta + 1.1 M_0 - 3.46) \qquad (6.8)$$

where $N_a(M)$ is the number of aftershocks with magnitude greater than or equal to M, M_0 is the magnitude of the mainshock. Equation (6.7) is essentially the same as the Gutenberg and Richter formula. The Drakopoulos formulas represent the dependence of the number of aftershocks with magnitudes greater than or equal to M on the magnitude of mainshock and the β-value.

Characteristics of aftershocks appear to depend on their mainshocks. It is, therefore, appropriate to assume that the number of aftershocks and the β-value depend on the magnitude of the

mainshock:

$$N_a(M) = \exp(a+bM_0+(c-M)\ \beta) \quad (6.9)$$

$$\beta = \exp(d-eM_0) \quad (6.10)$$

where a, b, c, d, and e are constants. Equation (6.9) is essentially the same as equations (6.7) and (6.8).

Furthermore, it is assumed that magnitudes of aftershocks cannot exceed the magnitude of the mainshock. Substituting $M_{max} = M_0$ into equation (6.5) yields:

$$f_M(m) = \frac{\beta e^{-\beta m}}{e^{-\beta M_{min}} - e^{-\beta M_0}} \quad (6.11)$$

Therefore, equation (6.11) will be used to describe the magnitudes of mainshocks and equations (6.9) and (6.10) will be used to simulate the number of aftershocks for each mainshock of magnitude M_0.

6.3.3 ESTIMATION OF GROUND MOTION TIME HISTORIES

The structural damage under mainshock-aftershock sequences can be calculated by inelastic analysis of structural response. These analyses require that the time history of ground motion be available. Thus, it is necessary to generate ground acceleration for each event of the simulated mainshock-aftershock sequences.

A number of stochastic models have been proposed for generating the earthquake ground accelerations. Tung et al. (1992) proposed a method that generates the time histories of ground accelerations using the duration independent envelope function. This method is very useful for the simulation of time histories during the mainshock-aftershock sequences, because it requires that very few parameters be defined. The parameters needed include the response spectra, the duration of ground acceleration, and the peak ground acceleration. These parameters are discussed in the following sections.

(1) Response Spectra and Peak Ground Acceleration

The response spectra and the peak ground acceleration of ground motion can be calculated using, for example, the attenuation equation proposed by Boore, Joyner and Fumal (1997). The attenuation will be used for the purposes of the ground motion simulation. This equation is given as

follows:

$$\log(Y) = b_1+b_2(M-6)+b_3(M-6)^2+b_5 \log(r)+b_V\ln(V_S/V_A) \quad (6.12)$$

where

$$r = (r_{jb}^2+h^2)^{1/2}$$

In this equation, Y is the ground-motion parameter (peak horizontal acceleration or pseudo-acceleration response in g), M is the moment magnitude of earthquake, V_S is the average shear-wave velocity (m/sec) over 30 m in surface ground, r_{jb} is the shortest distance (km) from the site to the vertical projection of the earthquake fault rupture, and b_1, b_2, b_3, b_5, b_V, V_A and h are constants.

For attenuation equations, we need the epicentral distance as well as the magnitude of earthquake. It is appropriate to assume that epicenters of mainshocks are uniformly distributed along the active fault, and epicenters of aftershocks are uniformly distributed along the rupture length of mainshock. The rupture length of a mainshock can be related to its magnitude using the equations of Wells and Coppersmith (1994):

$$\log(L) = -2.57+0.62M \quad \text{for strike-slip fault} \quad (6.13)$$

$$\log(L) = -2.42+0.58M \quad \text{for reverse fault} \quad (6.14)$$

where L is the subsurface rupture length (km) and M is the moment magnitude of the mainshock. Only the equations for strike-slip and reverse faults are given here. Formulas for other types of faults are also given in the same reference.

(2) Duration of Ground Acceleration

The duration of ground acceleration depends on the duration of the rupture process, the magnitude of the earthquake, the epicentral distance and the soil conditions of the site. Usually larger earthquakes produce ground motions with longer duration. The following relationship has been obtained from analysis of data (Bullen and Bolt, 1985),

$$T_d = 7.5 \tanh(M-6)+7.5 \quad (6.15)$$

where T_d is the duration of ground acceleration, and M is the magnitude of earthquake. Although several other relations have been proposed for ground motion duration, equation (6.15) will be used in the calculation of ground motion duration because of its simplicity.

6.3.4 SIMULATION PROCEDURE

The simulation procedure for estimating the structural damage under mainshock-aftershock earthquake sequences in desired design period of a structure consists of the following steps:

At step (1), the interarrival time of a mainshock is simulated by equation (6.1) or (6.2).

At step (2), the occurrence time of the mainshock is calculated by equation (6.3) considering desired design period of a structure.

At step (3), the magnitude of the mainshock is simulated by equation (6.5).

At step (4), the number of aftershocks which belong to the mainshock is calculated by equations (6.9) and (6.10).

At step (5), the magnitudes of aftershocks are simulated by equation (6.11).

From step (1) to (5), a mainshock-aftershock sequence is obtained.

At step (6), the epicenters for the mainshock-aftershock sequence are simulated and the epicentral distances are calculated.

At step (7), the response spectra and the peak ground accelerations at the site for the sequence are calculated by equation (6.12).

At step (8), the duration times of ground accelerations for the sequence are calculated by equation (6.15).

At step (9), the time histories of ground accelerations for the sequence are calculated using the duration independent envelope function (Tung et al., 1992).

At step (10), the damage spectrum is calculated by equation (3.1).

Finally, steps (1) to (10) are repeated to obtain the average and the deviation of the damage spectra.

It is very useful for the design purpose to obtain a spectrum of the required yield strength ratio of ground motion with the average (or average+ σ) damage potential during the mainshock-aftershock earthquake sequences so as to satisfy a safety level with the damage index=1.0. The strength demand spectrum with uniform damage in the lifetime of a structure is defined to be the spectrum of the required yield strength ratio obtained like this. The strength demand spectrum can rationally reflect the seismic activities around the site by considering mainshock-aftershock earthquake sequences in desired design period of a structure.

6.4 APPLICATION TO EUREKA, CALIFORNIA

The proposed method is applied to estimation of damage potential of ground motions in Eureka and Rio Dell, California. The parameters for the probabilistic occurrence model of the mainshock-aftershock sequence are developed according to the earthquake data near Eureka.

The mainshock-aftershock sequence is modeled based on earthquake data near Eureka provided by the United States Geological Survey (USGS). There were 1519 earthquakes that occurred from 1940 to 1992 with magnitudes greater than or equal to 3.0, latitudes from 39.5°N to 42°N, longitude from 125°W to 123°W. Epicenters of all earthquakes are shown in Figure 6. 7.

(1) Discrimination of Aftershocks

First, it is necessary to discriminate aftershocks from the earthquake data. Then, the occurrence model of mainshocks and aftershocks can be determined.

The earthquake clustering method developed by Veneziano and Van Dyck (1984) is applied to discriminate aftershocks from earthquake data. In this method, clusters that consist of a mainshock and aftershocks are statistically tested and discriminated with a specified significance level (Shimizu and Sunasaka, 1989, Sunasaka and Shimizu, 1989).

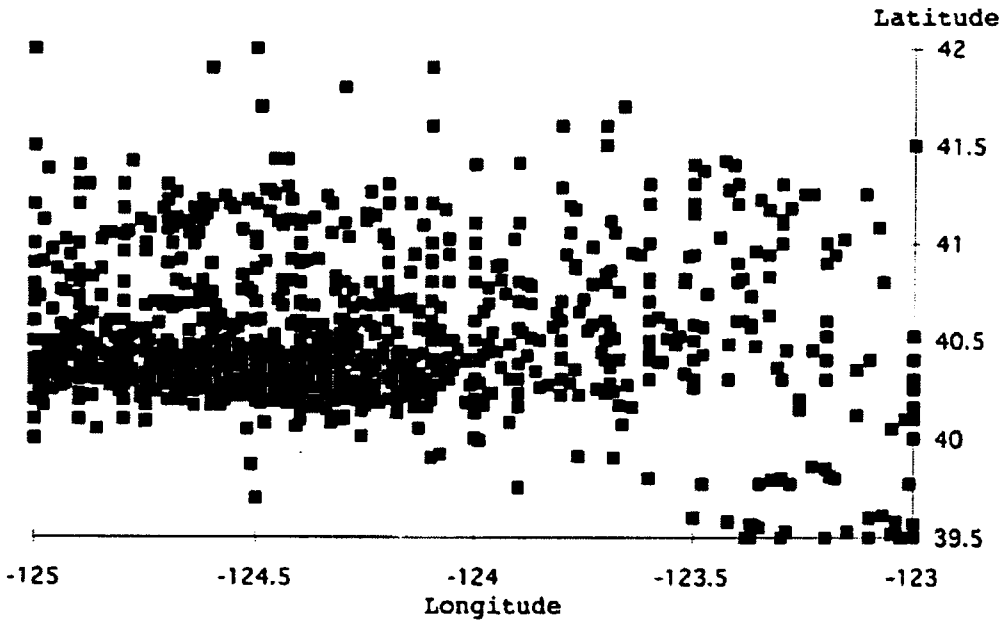

Figure 6.7 Distribution of earthquake epicenters in the vicinity of Eureka, California from 1940 to 1992 (data from USGS)

Table 6. 1 Results of clustering of the earthquake data near Eureka

Magnitude (mb)	Number of earthquakes	Number of aftershocks	Rate of aftershocks
3.0	472	267	0.57
3.25	284	176	0.62
3.5	268	150	0.56
3.75	102	58	0.57
4.0	128	61	0.48
4.25	79	38	0.48
4.5	84	35	0.42
4.75	32	9	0.28
5.0	30	12	0.40
5.25	9	4	0.44
5.5	11	2	0.18
5.75	4	1	0.25
6.0	7	3	0.43
6.25	1	0	0.00
6.5	4	3	0.75
6.75	1	1	1.00
7.0	2	0	0.00
7.25	1	0	0.00
Total	1519	820	0.54

The results of clustering of the earthquake data near Eureka are summarized in Table 6. 1. The amount of discriminated aftershocks is 54% of all the earthquakes in the database. Figure 6.8 shows epicenters of mainshocks which occurred from 1940 to 1992 with magnitudes greater than or equal to 3.0. Figure 6.9 shows sequences of mainshocks which occurred from 1940 to 1992 with magnitudes greater than or equal to 5.0.

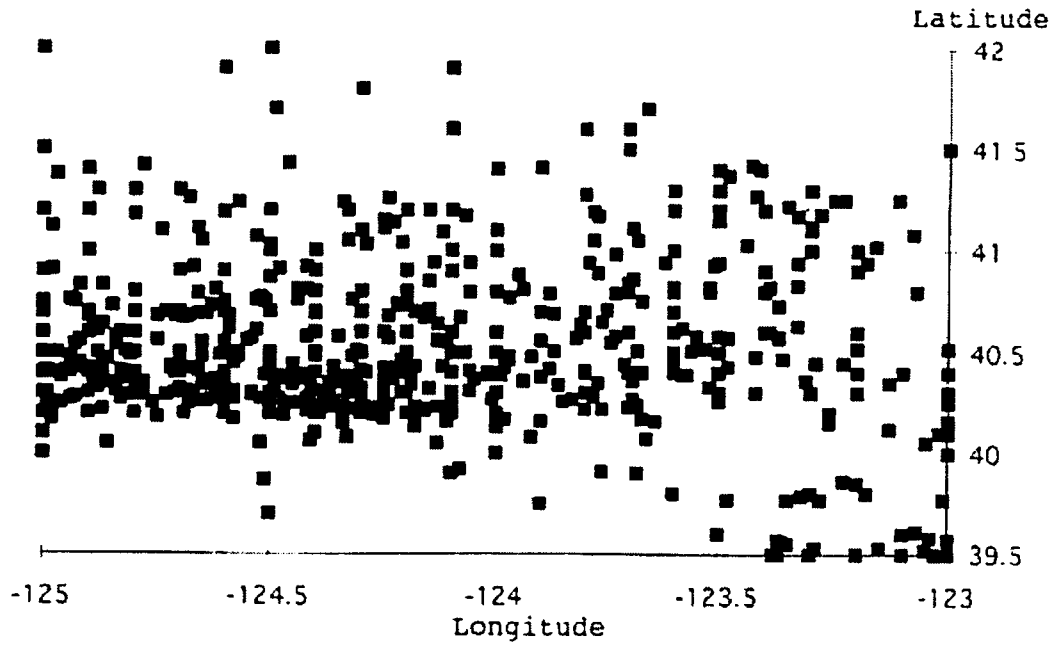

Figure 6. 8 Epicenters of mainshocks from 1940 to 1992 with magnitudes greater than or equal to 3.0

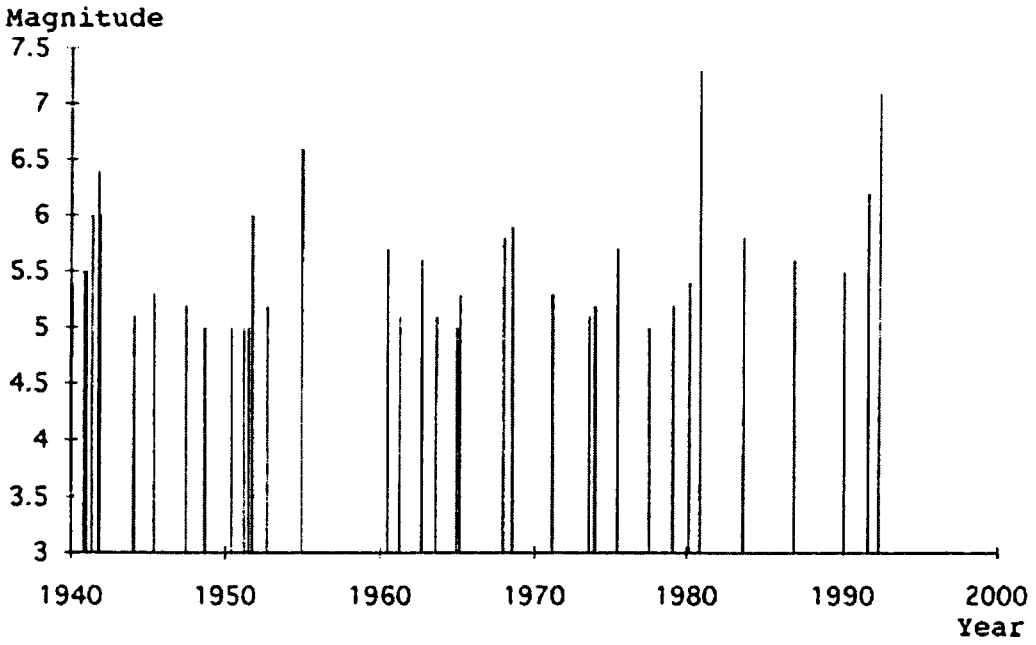

Figure 6. 9 Sequence of mainshocks from 1940 to 1992 with magnitudes greater than or equal to 5.0

(2) Occurrence Model of Mainshocks

In the following development, it is assumed that the interarrival times of mainshocks are distributed according to the Weibull distribution expressed by equation (6.2). The parameters ν and γ of the Weibull distribution are determined using following relationships:

$$m_\tau = \frac{1}{\nu}\Gamma(1+1/\gamma) \qquad (6.16)$$

$$V_\tau^2 = \frac{\Gamma(1+2/\gamma)}{\Gamma^2(1+1/\gamma)} - 1 \qquad (6.17)$$

where m_τ is the mean value of τ and V_τ is the coefficient of variation of τ. Based on the mainshock data near Eureka which occurred from 1940 to 1992 with magnitudes greater than or equal to 5.0, we have m_τ=1.197 (years), and V_τ^2=0.994. Thus, the constants ν and γ are determined to be 0.84 and 1.006, respectively. Since the constant γ is very close to 1.0, it is appropriate to assume that the interarrival times of mainshocks is exponentially distributed:

$$f_T(\tau) = 0.84 \exp(-0.84\,\tau) \qquad (6.18)$$

The Gutenberg and Richter's relationship is shown in Figure 6.10 based on the mainshock data near Eureka that occurred from 1940 to 1992 with magnitudes greater than or equal to 5.0. The value of the slope β for the mainshocks is thus found to be 1.4 (or b=1/β =0.61). The probability density function of magnitudes of mainshocks is then expressed as follows:

$$f_M(m) = \frac{1.4e^{-1.4m}}{e^{-1.4M_{min}} - e^{-1.4M_{max}}} \qquad (6.19)$$

An example of simulated mainshock sequence is shown Figure 6.11.

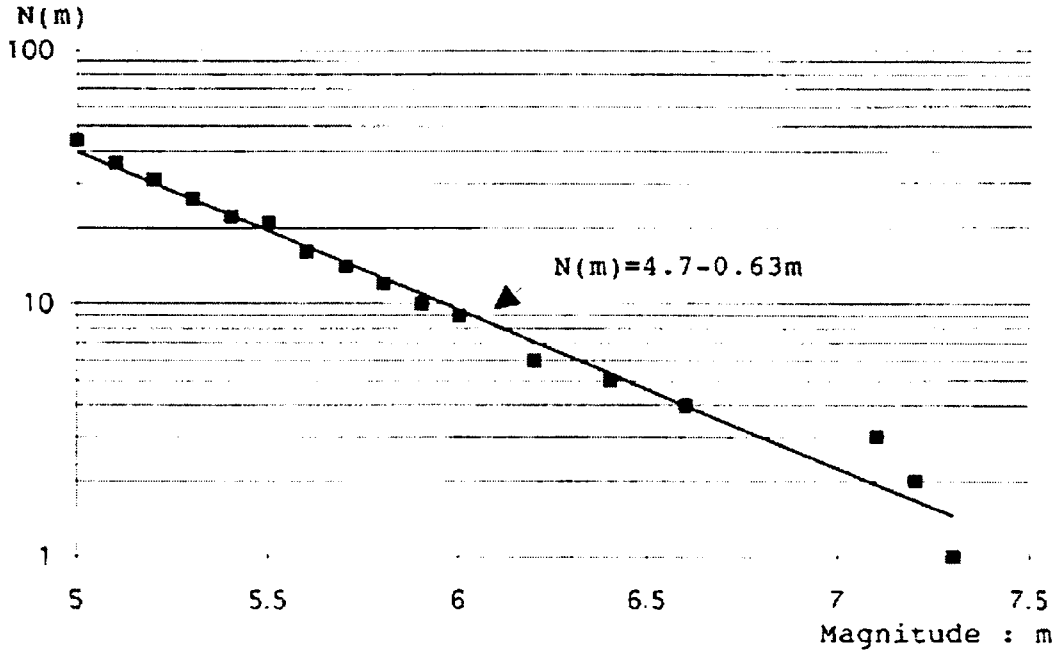

Figure 6.10 Gutenberg and Richter's relationship based on the mainshock data from 1940 to 1992 with magnitudes greater than or equal to 5.0

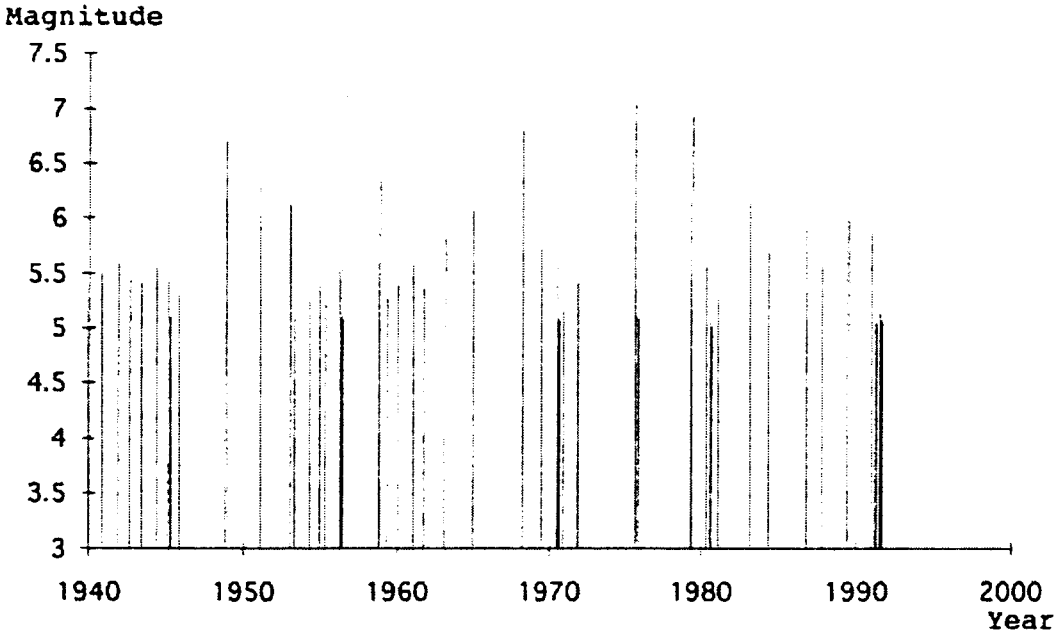

Figure 6.11 Example of simulated mainshock sequence

(3) Occurrence Model of Aftershocks

Among the 1519 earthquakes, there are 11 clusters which consist of a mainshock with magnitude greater than or equal to 5.0 and more than 10 aftershocks. Table 6.2 shows the magnitude of the mainshock, the number of aftershocks with magnitudes greater than or equal to 3.0, and the b-value for aftershocks, where b= β /2.3.

Based on the data of Table 6.2, a relationship is developed between the number of aftershocks with magnitudes greater than or equal to 3.0, $N_a(3)$, and the magnitude of mainshock, M_0. This relationship is shown in Figure 6.12. The linear regression of the logarithm of $N_a(3)$ as a function of M_0 is obtained as follows:

$$\log(N_a(3)) = -0.28+0.29M_0 \qquad (6.20)$$

The conditional standard deviation of the logarithm of $N_a(3)$ on M_0 is 0.36 and the correlation coefficient is 0.50.

Table 6.2 Statistics of clusters

Cluster number	Magnitude of mainshock	Number of aftershocks	b-value
1	6.6	10	0.29
2	5.7	14	0.42
3	5.9	51	0.66
4	5.3	30	0.52
5	5.7	15	0.49
6	7.3	156	0.55
7	5.8	15	0.41
8	5.6	86	0.81
9	5.5	22	1.12
10	6.2	38	1.16
11	7.1	96	0.55

The relationship between the b-value and the magnitude of mainshock is shown in Figure 6.13. The relationship between the logarithm of the b-value and M_0 is obtained by linear regression as follows:

$$\log(b) = 0.12\text{-}0.059M_0 \quad (6.21)$$

The conditional standard deviation of the logarithm of the b-value on M_0 is 0.19 and the correlation coefficient is 0.21.

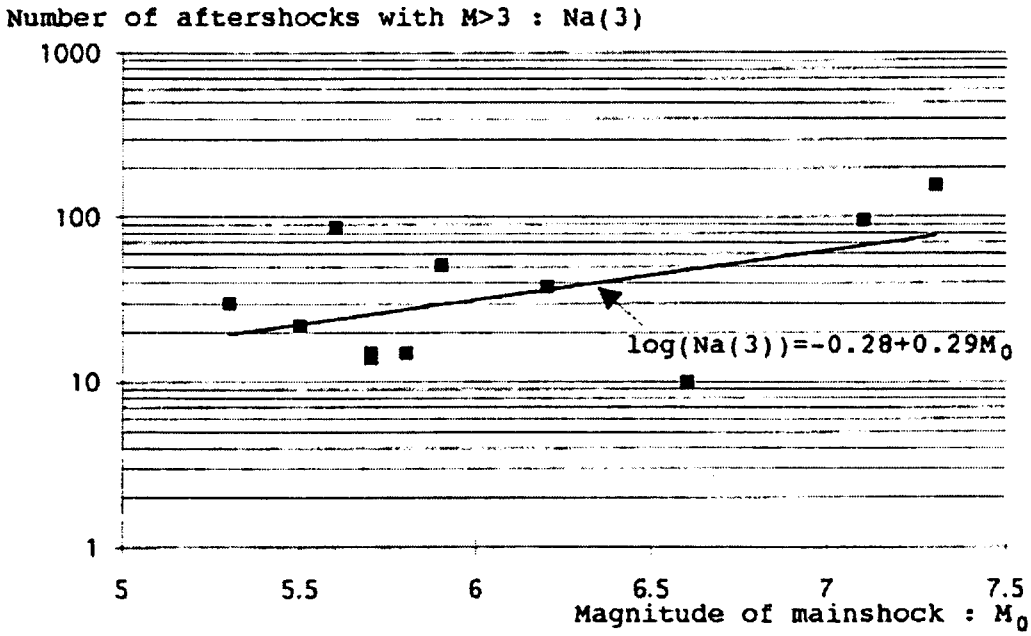

Figure 6.12 Relationship between the number of aftershocks with magnitudes greater than or equal to 3.0, $N_a(3)$, and the magnitude of mainshock, M_0

We can assume that the Gutenberg and Richter formula (6.4) can apply to the distribution of magnitudes of aftershocks:

$$N_a(M) = \alpha \exp(-\beta M) \quad (6.22)$$

In the case of M=3, we have

$$N_a(3) = \alpha \exp(-3\beta) \quad (6.23)$$

Comparing equation (6.20) with (6.22) gives

$$\alpha = \exp(-0.64+0.67M_0+3\beta) \quad (6.24)$$

Substituting equation (6.24) into (6.22) yields:

$$N_a(M) = \exp(-0.64+0.67M_0+(3-M)\beta) \quad (6.25)$$

where the β-value is expressed as follows from equation (6.21):

$$\beta = \exp(1.11-0.136M_0) \quad (6.26)$$

Figure 6.14 shows the relationship between $N_a(M)$ and M according to equations (6.25) and (6.26).

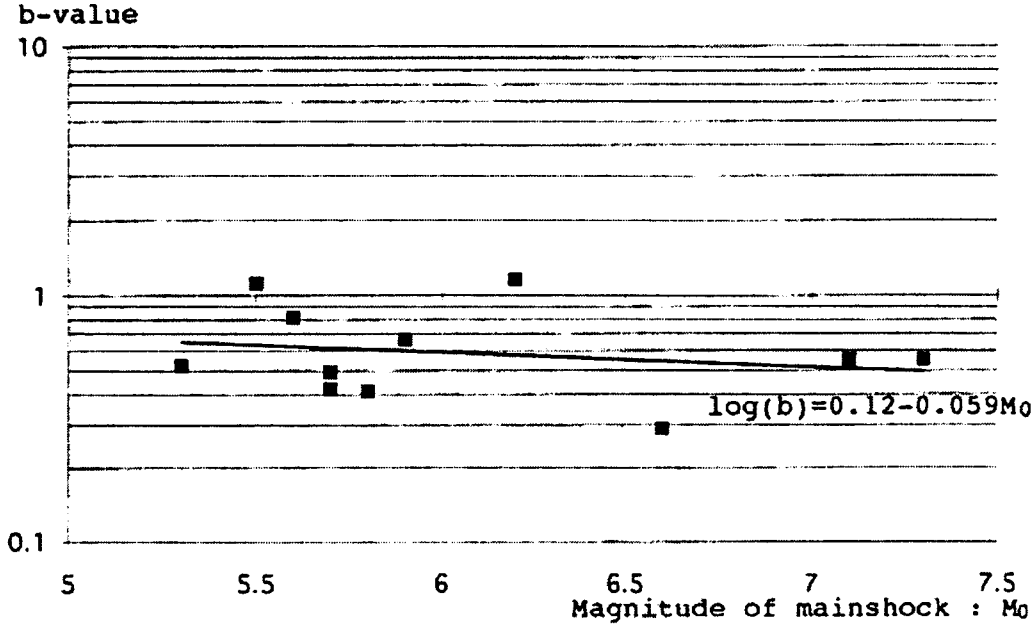

Figure 6.13 Relationship between the b-value and the magnitude of mainshock

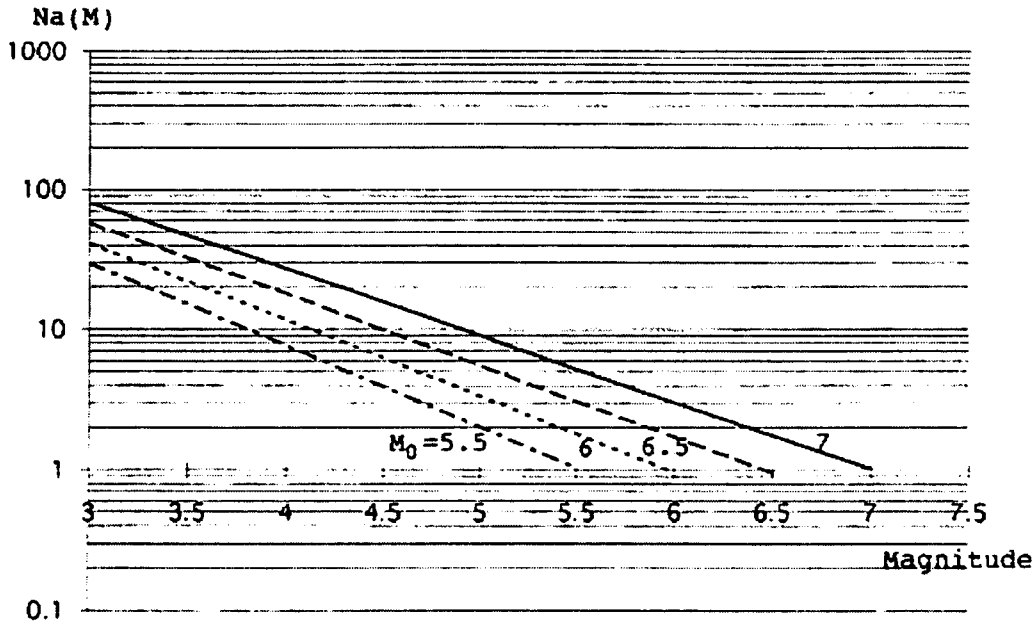

Figure 6.14 Relationship between the number of aftershocks $N_a(M)$ and aftershock magnitude M as a function of the mainshock magnitude M_0

(4) Faults Model

The generalized tectonic map of northern California by Kelsey and Carver (1988) is shown in Figure 6.15. Tectonic faults in the region are modeled according to Figure 6.15. The faults and location of Eureka and Rio Dell is shown in Figure 6.16. The geometric parameters for each of these faults are shown in Table 6.3, where the distance H is the perpendicular distance from the site and L2-L1 represents the fault length as shown in Figure 6.17.

Table 6.3 Geometric parameters of modeled faults for the site

Fault	Distance(km)	Length(km)		
	H	L1	L2	
F1 (Little Salmon Fault)	10	-5	45	For Eureka
	5	-20	30	For Rio Dell
F2 (Russ Fault)	30	-12.5	12.5	For Eureka
	13	-2.5	22.5	For Rio Dell
F3	40	2.5	22.5	For Eureka
	18	5	25	For Rio Dell
F4 (Mendocino Fault Zone)	50	20	65	For Eureka
	25	30	75	For Rio Dell

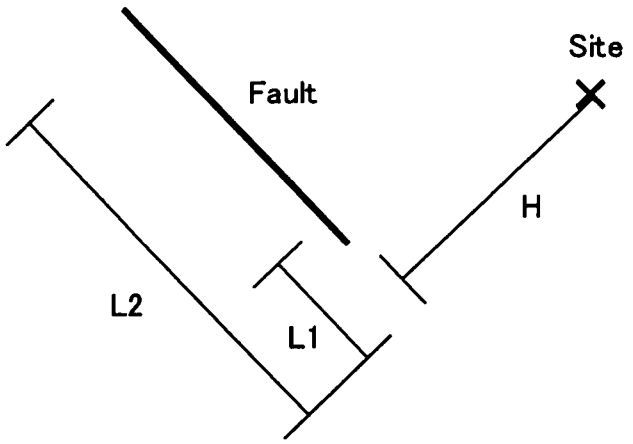

Figure 6.17 Geometric Parameters of fault

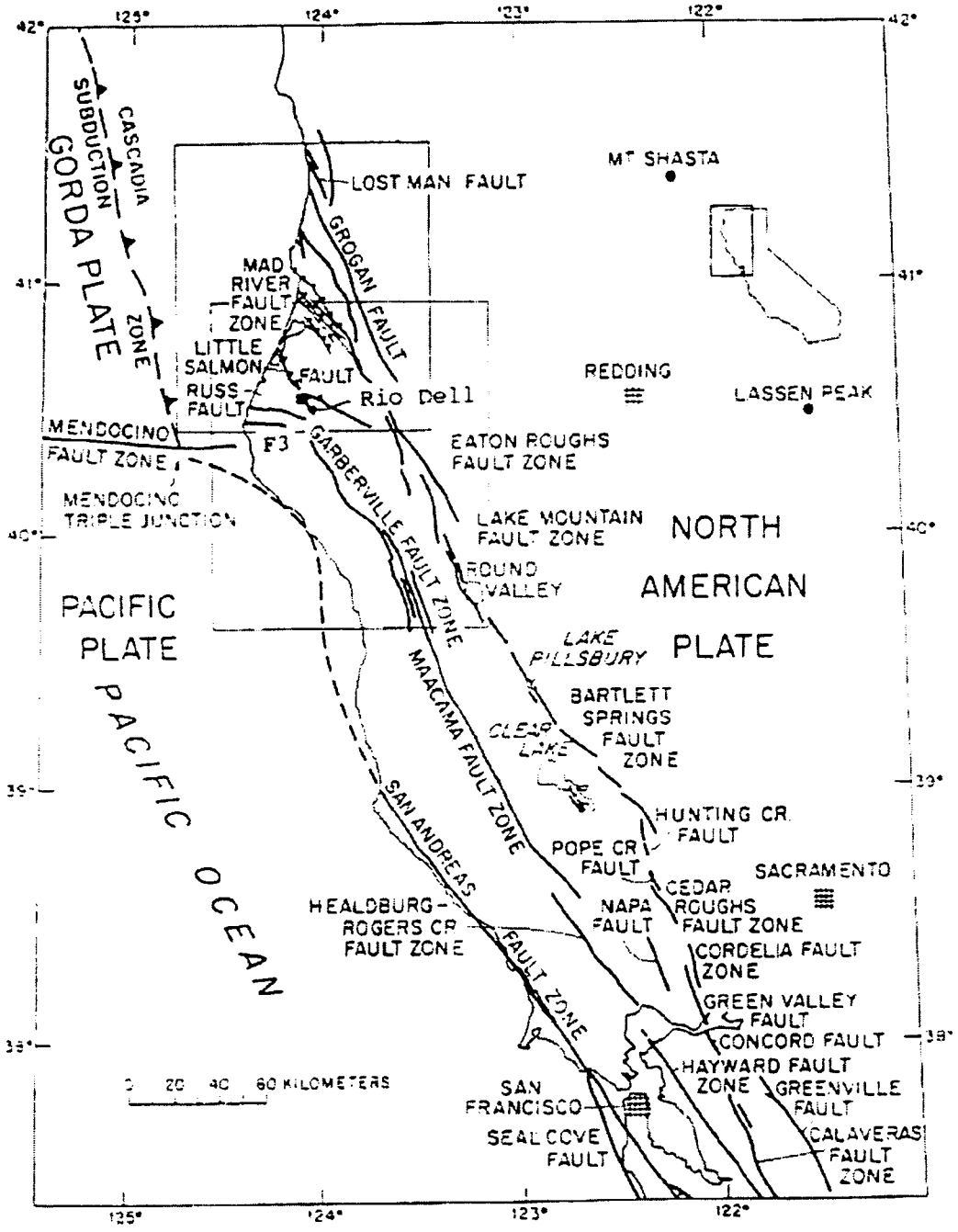

Figure 6.15 Generalized tectonic map of northern California
by Kelsey and Carver (1988)

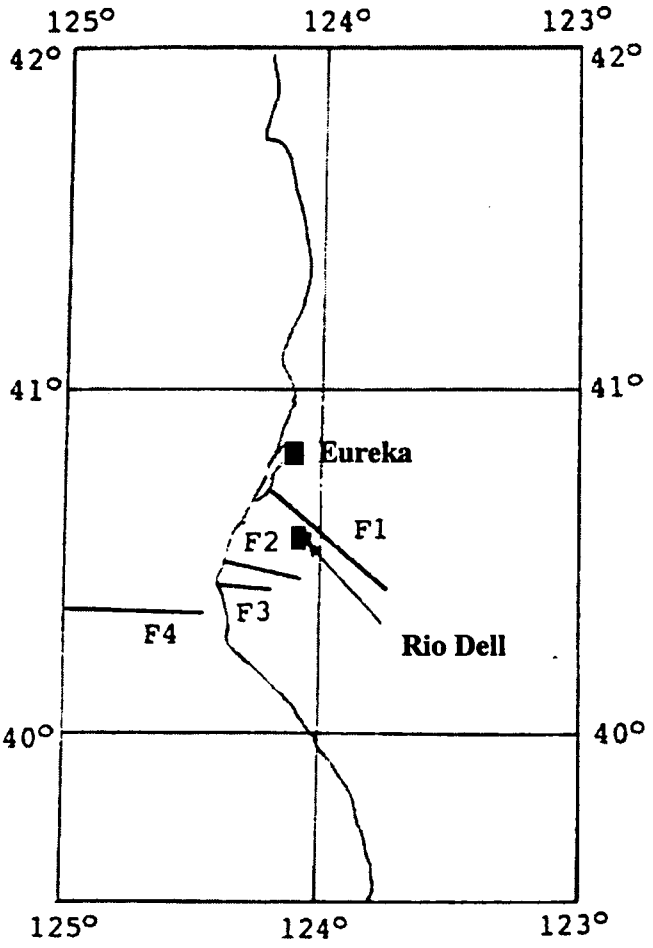

Figure 6.16 Map of faults model around Eureka and Rio Dell

(5) DAMAGE POTENTIAL AND STRENGTH DEMAND SPECTRA

Damage potential of ground motions considering mainshock-aftershock earthquake sequence at Eureka and Rio Dell, California is estimated by applying the simulation procedure described in Section 6.3. The parameters for the probabilistic occurrence model of the mainshock-aftershock sequence described above are used.

Figure 6.18 shows damage potential of ground motions of mainshock-aftershock earthquake sequences in 50 years at Eureka and Rio dell. In this figure, the upper two figures show damage potential of ground motions of simulated 50 mainshock-aftershock earthquake sequences in 50 years, the middle two figures show the average and the average plus/minus one standard deviation (σ), the bottom figure shows the average damage potential at Eureka and Rio Dell. Figure 6.19 shows damage potential of ground motions of only mainshocks in 50 years at Eureka and Rio Dell. Figure 6.20 shows comparison between average damage potential of ground motions in 50 years at Eureka and Rio dell. Based on these figures, it is found that damage potential of ground motions at Rio Dell is significantly higher than damage potential at Eureka, and that the effect of aftershocks on damage potential of ground motions is negligible in this area.

Figure 6.21 shows the strength demand spectra of ground motions with average damage potential in 50 years at Eureka and Rio Dell. The strength demand spectra of the ground motions are obtained so as to satisfy a safety level with the damage index=1.0. Figure 6.22 and Figure 6.23 show the strength demand spectra of ground motions with average and average+ σ damage spectrum in 50 years at Eureka and Rio Del, respectively. Based on these figures, it is found that the strength demand spectra at Rio Dell are significantly higher than those at Eureka. These strength demand spectra are very useful for design purpose. Based on the Figures 6.22 and 6.23, the required yield strength ratio 0.35 can be taken for design of structures with natural periods smaller than 0.6 sec. at Eureka and 0.5 at Rio Dell.

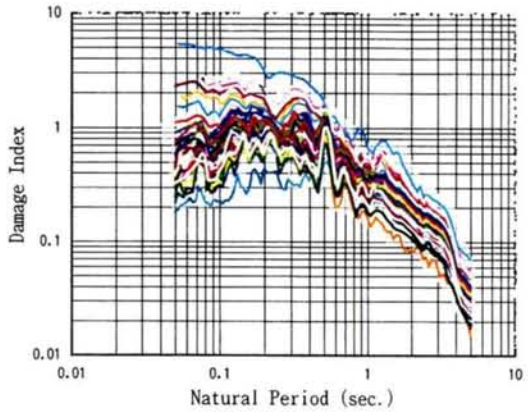

RioDell

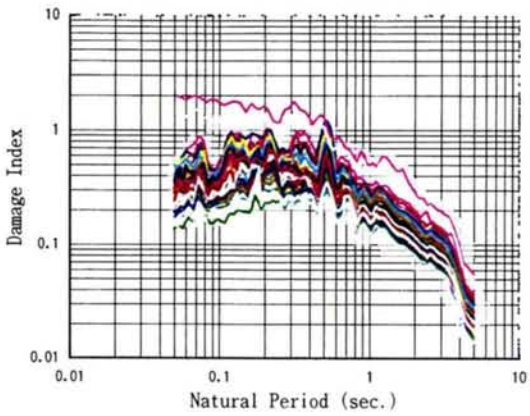

Eureka

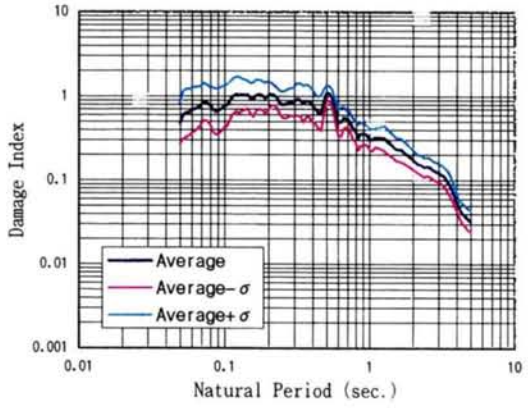

RioDell

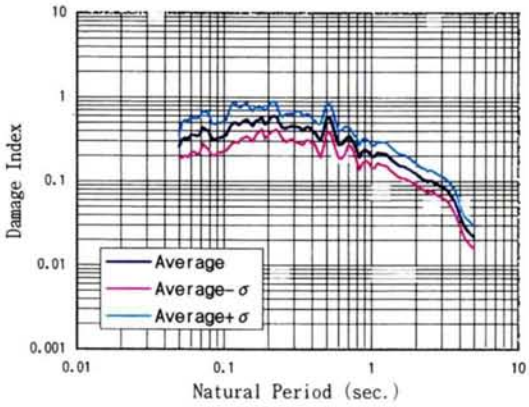

Eureka

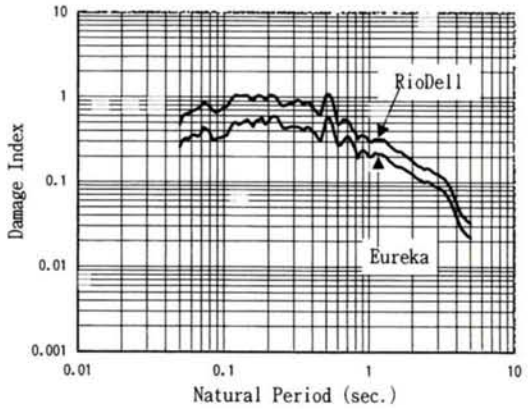

Figure 6.18 Damage potential of ground motions of mainshock-aftershock sequences in 50 years at Eureka and Rio Dell

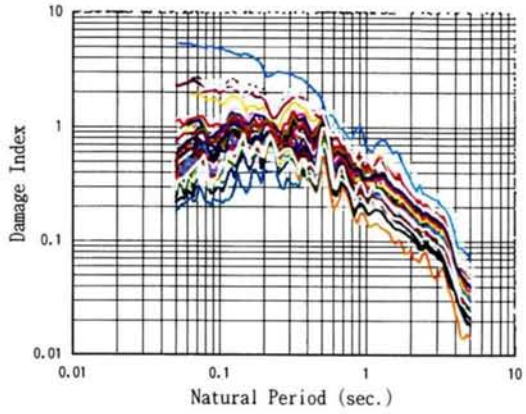

RioDell

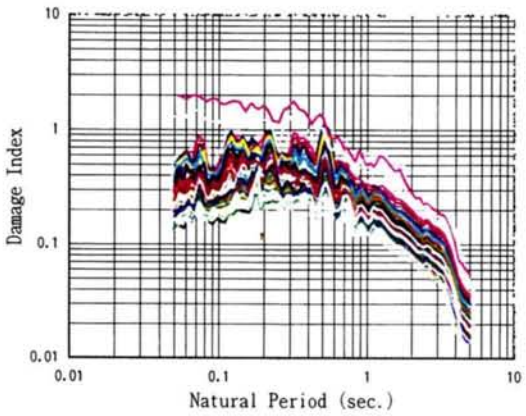

Eureka

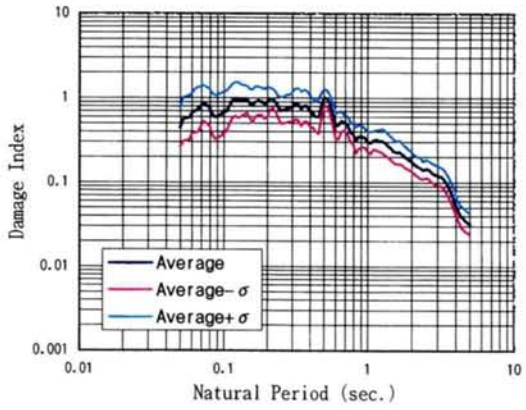

RioDell

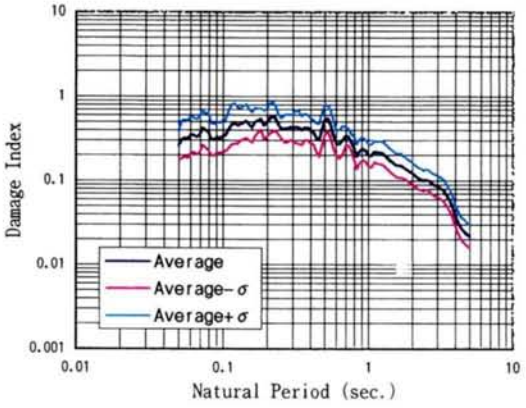

Eureka

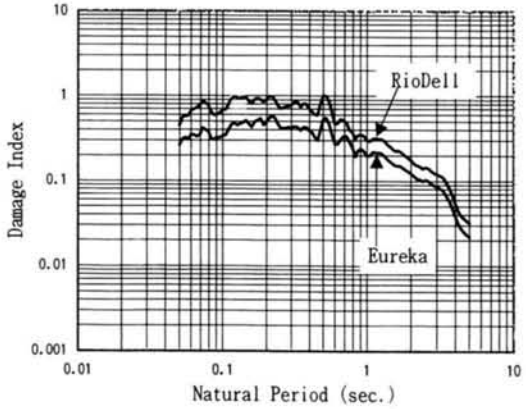

Figure 6.19 Damage potential of ground motions of mainshocks in 50 years at Eureka and Rio Dell

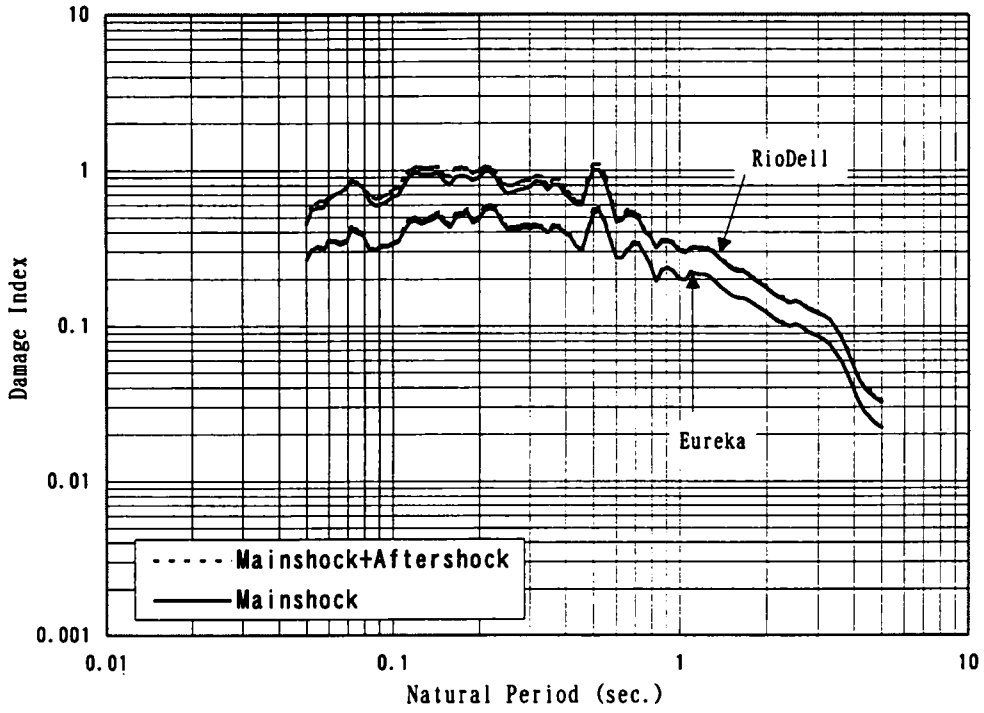

Figure 6.20 Comparison between average damage potential of ground motions in 50 years at Eureka and Rio Dell

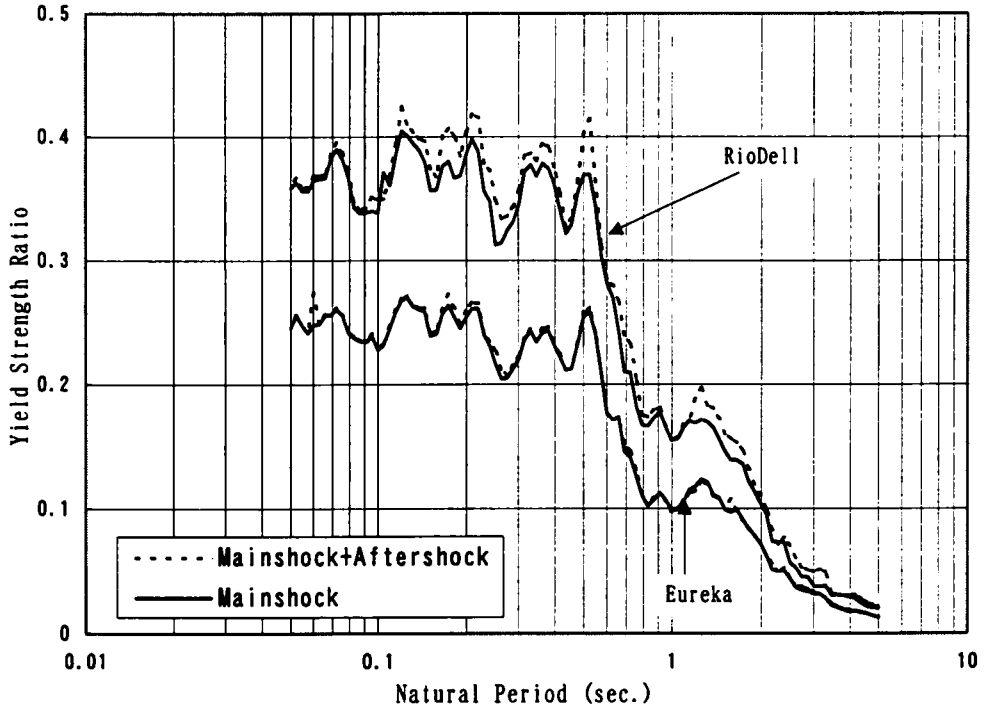

Figure 6.21 Strength demand spectra of ground motions with average damage potential in 50 years at Eureka and Rio Dell

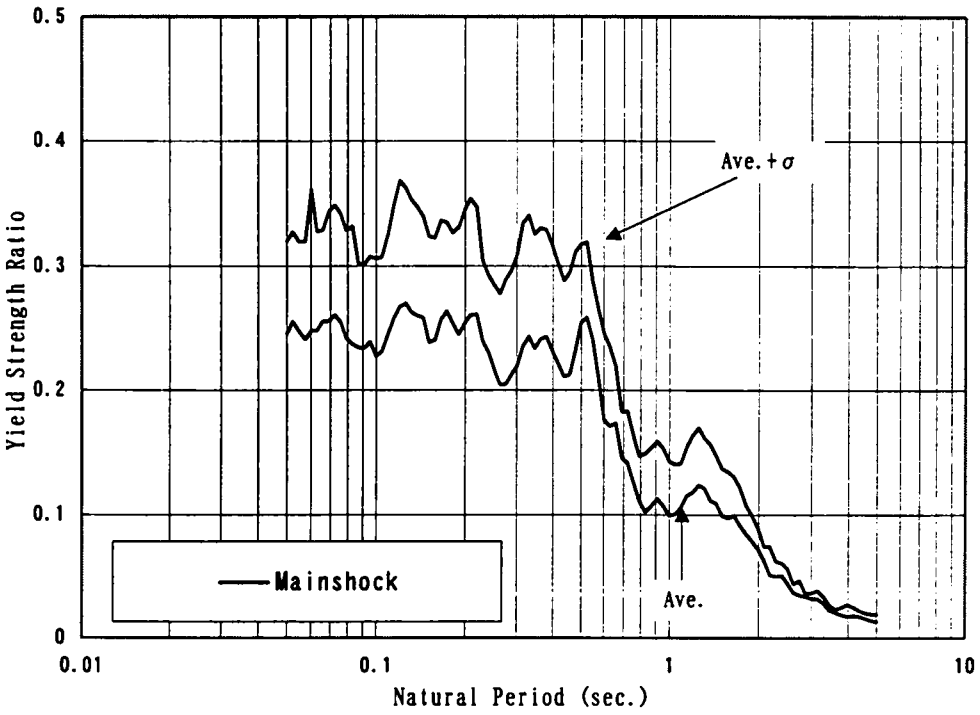

Figure 6.22 Strength demand spectra of ground motions with average and average+ σ damage potential in 50 years at Eureka

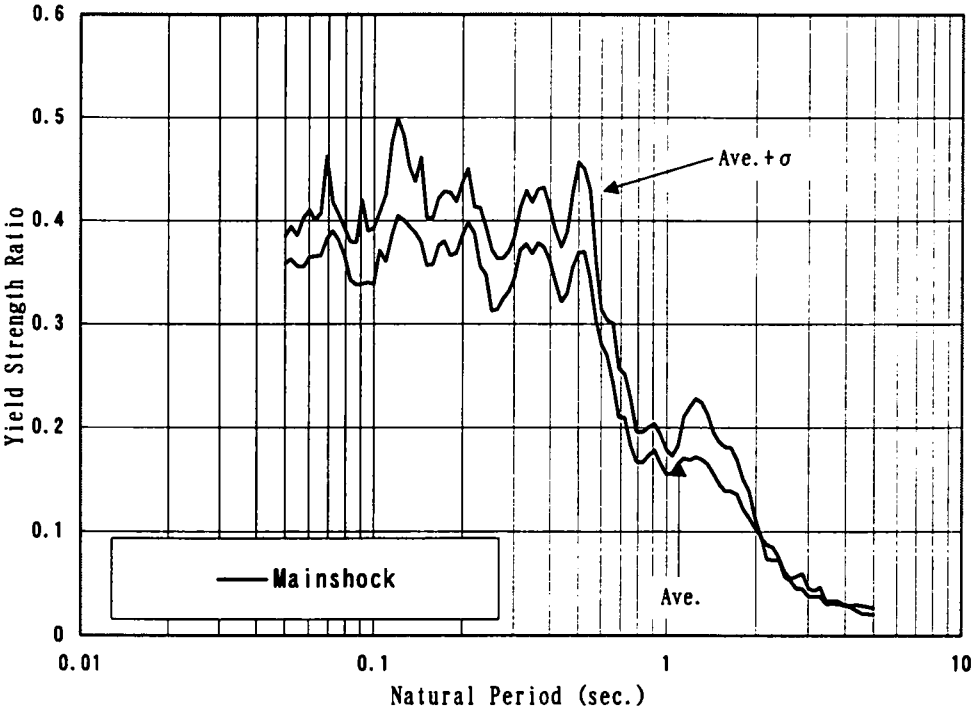

Figure 6.23 Strength demand spectra of ground motions with average and average+ σ damage potential in 50 years at RioDell

6.5 CONCLUSIONS

The damage spectra of ground motions during large aftershocks of past earthquakes including the 1983 Coalinga earthquake, the 1987 Whittier Narrows earthquake in California, and the 1999 Kocaeli earthquake in Turkey were studied. Based on the three examples, it can be concluded that the combination of mainshock-aftershock ground motions can be more damaging to structures than the ground motions from the mainshock alone. What is interesting to observe is that structures that may have experienced relatively little damage from the mainshock have a much greater damage index following the aftershock. For example, the damage index from the mainshock in the period range from 0.2 sec. to 0.4 sec. in the Whittier Narrows earthquake is about 0.2, but it increases to a maximum of 0.5 following the aftershock.

A simulation methodology for damage spectra considering mainshock-aftershock earthquake sequences in desired design period of a structure were presented. The simulation procedure consists of the following steps: (1) simulation of the interarrival time of a mainshock, (2) simulation of the magnitude of the mainshock, (3) calculation of the number of aftershocks which belong to the mainshock, (4) simulation of the magnitudes of aftershocks, (5) simulation of the epicenters for the mainshock-aftershock sequence, (6) calculation of the response spectra and the peak ground accelerations at the site for the sequence, (7) calculation of the duration times of ground accelerations, (8) calculation of the time histories of ground accelerations, (9) calculation of the damage spectra of the ground motions for the sequence. Finally, steps (1) to (9) are repeated to obtain the average and the deviation of the damage spectra.

The strength demand spectrum with uniform damage level in the lifetime of a structure is defined to be the spectrum of the required yield strength ratio of ground motions with the average (or average+σ) damage spectrum during the mainshock-aftershock earthquake sequences so as to satisfy a safety level with the damage index=1.0. The strength demand spectrum is very useful for the design and can rationally reflect the seismic activities around the site by considering mainshock-aftershock earthquake sequences in desired design period of a structure.

The proposed method was applied to estimation of damage potential of ground motions considering mainshock-aftershock earthquake sequences in Eureka and Rio Dell, California. The parameters for the probabilistic occurrence model of the mainshock-aftershock sequences were modeled based on earthquake data near Eureka provided by the United States Geological Survey (USGS). Damage spectra of the simulated ground motions considering mainshock-aftershock earthquake sequence at Eureka and Rio Dell in 50 years were calculated. Based on the results, it is found that damage potential of ground motions at Rio Dell is significantly higher than damage potential at Eureka, and that the effect of aftershocks on damage potential of ground motions is negligible in this area. Also, it is found that strength demand spectra at Rio Dell are significantly

higher those at Eureka. The required yield strength ratio 0.35 can be taken for design of structures with natural periods smaller than 0.6 sec. at Eureka and 0.5 at Rio Dell. The strength demand spectra obtained like this can rationally reflect the seismic activities around the site by considering mainshock-aftershock earthquake sequences in desired design period of a structure.

CHAPTER 7

CONCLUSIONS

In this dissertation, the damage spectrum of ground motion during an earthquake was used to estimate the damage potential of an earthquake at a site. The damage spectrum is defined as damage indices of SDOF systems with natural period ranging 0.05 to 5.0 sec. The damage index D proposed by Park and Ang (1985) and bilinear load-deformation model are used to calculate the damage spectrum. $D \geqq 1$ indicates total damage or collapse. $0<D<0.7$ indicates the slight damage, and $0.7<D<1.0$ indicates severe damage (Park and Ang, 1985). Damage potential of recorded ground motions during recent great earthquakes and earthquake ground motions that have been used for design purpose was studied. A method of evaluating damage potential of ground motions in large areas was described. The damage potential of ground motions during aftershocks was studied, and a method of evaluating damage potential of ground motions considering mainshock-aftershock earthquake sequences in a design period was proposed. Then, a method for evaluating the strength demand spectra with uniform damage level in the lifetime of a structure considering mainshock-aftershock earthquake sequences is proposed. The proposed method is applied to estimation of damage potential of ground motions and strength demand spectra in a lifetime of a structure considering mainshock-aftershock earthquake sequences in Eureka, California. Main conclusions are as follows:

(1) Structural damage in Kobe during the 1995 Hyogoken-Nanbu earthquake was concentrated in a belt 0.7 to 1.2 km wide stretching from southwest to northeast along the foot of the Rokko Mountains. The damage spectrum of the ground motion recorded in the heavily damaged zone is the largest of the recorded ground motions in almost all natural periods. The damage indices of the ground motion recorded in and around the heavily damaged zone are larger than 1.0 at natural periods smaller than about 1.0 sec. However, the damage spectra of ground motions recorded outside of the heavily damaged zone are smaller than 1.0 for all natural periods.

(2) The damage spectra of the ground motions that were simulated by Motosaka and Nagano (1996) to estimate the amplification characteristics of ground motions in the heavily damaged zone in the city of Kobe during the Hyogoken-Nanmu earthquake were calculated and studied. The damage spectra of the simulated ground motions at ground surface points in the heavily damaged zone are relatively large. Among them, the largest is the damage spectra of the ground motion at a point located between JR and the Hanshin Railway Line. The damage indices of the ground motions at the point are larger than 1.0 at natural periods smaller than about 1.5 sec. The intensity of the damage spectra of ground accelerations decreases with distance from the center of the heavily damaged zone. These results demonstrate that the damage spectra well correlate with the structural damage, and that

the concentration of structural damage in the shallow zone stretching from southwest to northeast along the foot of the Rokko Mountains is mainly explained by the geological deep ground conditions of Kobe.

(3) Damage spectra of the recorded ground motions at Duzce (DZC), Gebze (GBZ), Izmit (IZT) and Sakarya (SKR) during the 1999 Kocaeli earthquake in Turkey were studied. Damage indices of ground motions at GBZ and IZM are much smaller than 1.0 for all periods. Damage indices of ground motions at DZC and SKR are larger than 1.0 for a narrow period range around 0.1 sec. In spite of relatively small damage spectra of the observed ground motions during the earthquake, structural damage was very severe. This is thought to imply poor earthquake-resistant capacity of the structures in Turkey.

(4) Damage spectra of the recorded ground motions at the stations very close to the Chelongpu Fault during the 1999 Chi-Chi earthquake in Taiwan were studied. Station TCU068 is located in the northern part and eastern side of the fault where rupture arrived. The ground motion observed at that station has relatively low PGA, low dominant frequency, and then high damage potential for relatively long natural periods around 1.0 sec. Station CHY028 is located in the southern part and western side of the fault where rupture arrived. The ground motion observed at the station has a large maximum acceleration and very short duration, and its damage potential is very large for natural periods less than 0.9 sec. Station TCU065 and TCU129 are located at the middle of the fault. In spite of the large maximum acceleration and long duration of the ground motion observed at the stations, their damage potential is high only for the short natural periods less than 0.6 sec. The tendency that the ground motions observed on eastern side of the fault have larger damage spectra, peak ground velocities (PGV), and peak ground displacements (PGD) than those on western side of the fault can be observed.

(5) The damage potential of ground motions in Kawasaki City located in the southern part of Kanto in Japan during the hypothetical Kanto earthquake was studied. In the northwestern part with relatively stiff ground in Kawasaki City, the ground motions have high damage potential for structures with natural period lower than about 0.75 sec. In the southeastern bay area with relatively soft ground, the ground motions have higher damage potential for structures with natural period higher than about 0.5 sec. For structures with natural period lower than about 0.75 sec., ground motions in the northwestern part have higher damage potential than in the southeastern part. For structures with natural period higher than about 1.0 sec., ground motions in the middle part of Kawasaki City have high damage potential. The method for ground motion damage evaluation presented in this paper is a very efficient and effective tool that can be used in design and retrofit decisions, disaster mitigation strategies and for emergency response planning purposes. It provides a new quantitative and visual approach for measuring and displaying damage potential information. It combines key components such as input ground motions, local soil characteristics and structural

information that can easily be utilized for various governments and private industry decision makers.

(6) The damage spectra of ground motion during large aftershocks of past earthquakes including the 1983 Coalinga earthquake, the 1987 Whittier Narrows earthquake in California, and the 1999 Kocaeli earthquake in Turkey were studied. Based on the three examples, it can be concluded that the combination of mainshock-aftershock ground motions can be damaging to structures than the ground motions from the mainshock alone.

(7) A simulation methodology for damage spectra considering mainshock-aftershock earthquake sequences in desired design period of a structure were presented. The simulation procedure consists of the following steps: (i) simulation of the interarrival time of a mainshock, (ii) simulation of the magnitude of the mainshock, (iii) calculation of the number of aftershocks which belong to the mainshock, (iv) simulation of the magnitudes of aftershocks, (v) simulation of the epicenters for the mainshock-aftershock sequence, (vi) calculation of the response spectra and the peak ground accelerations at the site for the sequence, (vii) calculation of the duration times of ground accelerations, (viii) calculation of the time histories of ground accelerations, (ix) calculation of the damage spectra of the ground motions for the sequence. Finally, steps (i) to (ix) are repeated to obtain the average and the deviation of the damage spectra. The strength demand spectrum with uniform damage level in the lifetime of a structure is defined to be the spectrum of the required yield strength ratio of ground motions with the average (or average+ σ) damage spectrum during the mainshock-aftershock earthquake sequences so as to satisfy a safety level with the damage index=1.0. The strength demand spectrum is very useful for the design and can rationally reflect the seismic activities around the site by considering mainshock-aftershock earthquake sequences in desired design period of a structure.

(8) The proposed method was applied to estimation of damage potential of ground motions considering mainshock-aftershock earthquake sequences in Eureka and Rio Dell, California. The parameters for the probabilistic occurrence model of the mainshock-aftershock sequences were modeled based on earthquake data near Eureka provided by the United States Geological Survey (USGS). Damage spectra of the simulated ground motions considering mainshock-aftershock earthquake sequence at Eureka and Rio Dell in 50 years were calculated. Based on the results, it is found that damage potential of ground motions at Rio Dell is significantly higher than damage potential at Eureka, and that the effect of aftershocks on damage potential of ground motions is negligible in this area. Also, it is found that strength demand spectra at Rio Dell are significantly higher than those at Eureka. The required yield strength ratio 0.35 can be taken for design of structures with natural periods smaller than 0.6 sec. at Eureka and 0.5 at Rio Dell. The strength demand spectra obtained like this can rationally reflect the seismic activities around the site by considering mainshock-aftershock earthquake sequences in desired design period of a structure.

ACKNOWLEDGMENTS

I would like to express my sincere gratitude to my advisor, Professor Kenzo Toki of Kyoto University, for his guidance, encouragement, and valuable advice. My sincere thanks are extended to Professor Anne S. Kremidjian of Stanford University for her helpful advice and support. Also, I would like to express my sincere gratitude to Professor Hirokazu Iemura and Professor Tadanobu Sato of Kyoto University, who reviewed this dissertation and gave me valuable advices.

The financial support from Kajima Corporation is gratefully acknowledged. I would like to express my special thanks to former general manager Mr. Susumu Ukai and Mr. Kenji Yanagiya, general manager Dr. Masaaki Yamamoto of the Civil Engineering Design Division, and manager Mr. Yasuaki Simizu of the Engineering Development Department in Kajima Corporation. The technical support from many colleagues in Kajima Corporation is also acknowledged. Particularly, I would like to thank Dr. Tomonori Ikeura of Kajima Technical Research Institute, Dr. Masayuki Nagano of Kobori Research Complex, and Mr. Akira Ishii, Mr. Nobuhisa Shiozaki, and Mr. Yoshihiro Sasaki of the Civil Engineering Design Division. I would like to express my special thanks to Mr. Keiichi Kimura of Wise Corporation, Ms. Hisako Hiratsuka, and Ms. Maho Miyazaki of Kajima Corporation for their assistance in drawing figures and tables.

Finally, I would like to extend my sincere thanks to my wife, Hiroko, for her continued love and support.

REFERENCES

Abe, S., Y. Fujino, and M. Abe (1999). An analysis of damage to Hanshin Elevated Expressway during 1995 Hyogoken Nanbu Earthquake, Jour. of JSCE, No.612/I-46, 181-199.

Anagnos, T. and A.S. Kiremidjian (1984). Stochastic time-predictable model for earthquake occurrences, Bull. of Seism. Soc. of Ame., Vol.74, 2593-2611.

Basu, B. and V.K. Gupta(1995). A probabilistic assessment of seismic damage in ductile structures, Earthq. Eng. Struct. Dyn. 24 (10), 1333-1342.

Blume, J.A. and A.S. Kiremidjian (1977). Probabilistic procedures for peak ground motions, J. Struc. Div., ASCE, Vol.105, 2293-2311.

Boore, D.M., W.B. Joyner and T.E. Fumal (1997). Equations for estimating horizontal response spectra and peak acceleration from Western North American earthquakes: A summary of recent work, Seismological Research Letters, Vol.68, No.1, January/February, 128-151.

Bullen, K.E. and A.B. Bolt (1985). An introduction to the theory of seismology, Cambridge University Press.

Coppersmith, J.K. and D.P. Schwartz (1984). Introduction to the special section on fault behavior and earthquake generation process, J. Geophys. Res., Vol.89, No.B7, 5669-5673.

Cornell, C.A. (1968). Engineering seismic risk analysis, Bull. of Seism. Soc. of Ame., Vol.58, 1583-1606.

CWB(1999), Free-field strong-motion data from the 921 Chi-Chi earthquake: Volume1. Digital acceleration files on CD-ROM

Der Kiureghian and A.H.-S. Ang (1977). A fault rupture model for seismic risk analysis, Bull. of Seism. Soc. of Ame., Vol.67, 1173-1194.

Department of Civil Engineering, Faculty of Engineering, Kobe University (1995). Emergency study report on the damage due to the Great Hanshin Earthquake.

Drakopoulos (1971). A statistical model on the occurrence of aftershocks in the area of Greece, Bull. Int. Inst. Seismol. Earthq. Eng., Vol.8, 17-39.

Editorial Committee for the Report on the Hanshin-Awaji Earthquake Disaster (1998a). Report on the Hanshin-Awaji Earthquake Disaster, General Issues Volume 2, 172.

Editorial Committee for the Report on the Hanshin-Awaji Earthquake Disaster (1998b). Report on the Hanshin-Awaji Earthquake Disaster, General Issues Volume 1, 45.

EQE Engineering (1990). The July 16, 1990 Philippines earthquake, a quick look report.

Fajfar, P. (1992). Equivalent ductility factors, taking into account low-cycle fatigue, Earthq. Eng. Struct. Dyn., 21, 837- 848.

Housner, G. W. (1952). Spectrum intensities of strong-motion earthquakes, Proc. of the Symposium on Earthquakes and Blast Effects on Structures, Earthquake Engineering Research Institute.

Iemura, H., A. Igarashi and Y. Takahashi (1998). Ductility and strength demand for near field

earthquake ground motion: comparative study on the Hyogo-ken Nanbu and the Northridge earthquakes, Structural Safety and Reliability, Rotterdam,1705-1708.

Iemura, H., Y. Takahashi and T. Hirate (1998). Estimation of earthquake intensity from the damage of RC piers of viaducts, The 10th Japan Earthquake Engineering Symposium, 83-86.

Ishii, A., N. Shiozaki, S. Nagata and N. Ohbo (1999). Study on soil amplification characteristics in estimation of ground motions among observation sites during earthquakes, The 54th annual conference of Japan Society of Civil Engineers, 178-179.

Japan Road Association (1990), (1996). Design specifications of highway bridges.

Japan Society of Civil Engineers (1995). Preliminary report on the great Hanshin earthquake.

Japan Society of Civil Engineers (1996a). Study of earthquake resistance and damage by earthquake disaster of reinforced concrete rigid frame bridge, Jour. JSCE, Vol.81, No.3, 68-71.

Japan Society of Civil Engineers (1996b). Proposal on earthquake resistance for civil engineering structures.

Japan Society of Civil Engineers (1999). Reconnaissance report of the 1999 Kocaeli Earthquake, Turkey -Investigation into damage to Civil Engineering structures.

Jeon, G.D. and W.D. Iwan (1988). The effect of earthquake duration on the damage of structures, Earthq. Eng. Struct. Dyn., 16, 1201-1211.

Kawasaki City (1988). Damage prediction survey report in Kawasaki City, Kawaskai City.

Kelsey, H.M. and G.A. Carver (1988). Late neogene and quaternary tectonics associated with northward growth of the San Andreas transform fault, northern California, J. Geophys. Res., Vol.93, No.B5, 4797-4819.

Kiremidjian, A.S. and T. Anagnos (1984). Stochastic slip predictable model for earthquake occurrences, Bull. of Seism. Soc. of Ame., Vol.74, 739-755.

Krawinkler, H. et al. (1983). Recommendations for experimental studies on the seismic behavior of steel components and materials, The John A. Blume Earthquake Engineering Center Report No.61, Dept. Civil Engineering, Stanford University, Stanford, Ca.

Motosaka, M. and M. Nagano (1996), Analysis on amplification characteristics of ground motions in Kobe City taking account of deep irregular underground structure - Interpretation of heavily damaged belt zone during the 1995 Hyogoken Nanbu Earthquake-, Jour. of Structural and Construction Engineering, AIJ, No.488, 39-48.

Nagata, K., E. Watanabe and K. Sugiura (1996). Non-linear dynamic interaction of foundation-structure system, Jour. of Structural Engineering, JSCE, Vol.42A, 593-602.

Park, Y.J. and Ang A.H.-S., Wen Y.K. (1985). Seismic damage analysis of reinforced concrete buildings , Jour. of Structural Engineering, ASCE, Vol.111, No.4, 722-739.

Park, Y.J. and A.H.-S. Ang (1985). A mechanistic seismic damage model for reinforced concrete, Jour. of Structural Engineering, ASCE, Vol.111, No.4, 740-754.

Paulay, T. and M.J.N. Priestley (1992). Seismic design of reinforced concrete and masonry buildings, John Wiley & Sons, New York.

Priestley, M.J.N. (1988). The Whittier Narrows, California earthquake of October 1, 1987 - damage to the I-5/I-605 separator, Earthq. Spectra, Vol.4, No.2, 389-405.

Richter, C.F. (1958). Elementary Seismology, W.H. Freeman and Company, San Francisco.

Sasada, S., K. Hirao, Y. Nariyuki, T. Sawada and T. Mikami (1996). A study on damage estimation of a structure subjected to severe earthquake motions, Jour. of Structural Engineering, JSCE, Vol.42A, 661-668.

Sasada, S., K. Hirao, Y. Nariyuki, T. Sawada and T. Mikami (1996). Influence of soil-structure interaction on required yield strength ratio of RC pier under strong earthquake motions, Jour. of Structural Engineering, JSCE Vol.42A, 615-626.

Shakai, A. et al. (1992). CSMIP strong-motion records from the Petrolia, California earthquakes of April 25-26, 1992, California Strong Motion Instrumentation Program, Report No. OSMS 92-05.

Shimazaki, K. and T. Nakata (1980). Time predictable recurrence for large earthquakes, Geophys. Res. Letters, Vol.7, 279-282.

Simizu Y. and Y. Sunasaka (1989). Seisimic intensity and hazard in the Kanto district based on earthquake clustering method, Proc. of the 44th Annual Conference of Japan Society of Civil Engineers, Vol. 1, 974-975.

Sunasaka, Y. (1996). Study on damage spectrum of ground acceleration at JMA Kobe (1995), Proc. of the 51st Annual Conference of Japan Society of Civil Engineers, Vol. 1-B, 468-469.

Sunasaka, Y. (1997). Damage spectra of ground accelerations during the 1995 Hyogoken-Nanbu earthquake, Proc. of the 52nd Annual Conference of Japan Society of Civil Engineers, Vol. 1-B, 650-651.

Sunasaka, Y. (1998). Damage spectra of ground accelerations during earthquakes, Proc. ICOSSAR'97, Vol.3, 1699-1702.

Sunasaka, Y. and A. S. Kiremidjian (1994a). A method for cumulative damage estimation from mainshock-aftershock earthquake sequences, Proc. of the Fifth U.S. National Conference on Earthquake Engineering, Vol. I, 481-490.

Sunasaka, Y. and A. S. Kiremidjian (1994b). Probabilistic occurrence model of mainshock-aftershock earthquake sequences, Proc. of the 49th Annual Conference of Japan Society of Civil Engineers, Vol. 1-B, 1460-1461.

Sunasaka, Y., A. S. Kiremidjian and K. Toki (2002). Strength demand spectra with uniform damage level in lifetime of structure, Journal of Structural Engineering, JSCE (on application).

Sunasaka, Y. and Y. Simizu (1989). Earthquake clustering in the Kanto district, Proc. ICOSSAR'89, Vol.1, 597-604.

Sunasaka, Y. and Y. Simizu (1994). A method of estimating aftershock effects on seismic damage of structures, Proc. of the Eighth Japan Earthquake Engineering Symposium-1990, Vol. 2, 2039-2042.

Sunasaka, Y., T. Toki and A. S. Kiremidjian (2001). Evaluation of damage potential of ground motions during great earthquakes, Earthquake Spectra (on application).

Toki, K., J. Kiyono, H. Ishizaki and Y. Ono (1998). Strength demand spectrum taking into account soil-structure interaction, Proc. of the 10th Earthquake Engineering Symposium, Vol.2, 1861-1866.

Tung, A.T.Y., J.N. Wang, A.S. Kiremidjian and E. Kavazanjian (1992). Statistical parameters of AM and PSD functions for generation of site-specific strong ground motions, Proc. of Tenth World Conference on Earthq. Engineering, Madrid, Spain, July, 867-872.

Utsu, T. (1961). A statistical study on the occurrence of aftershocks, Geophys. Magazine, Vol.30, No.1, 521-616.

Veneziano, D. and J. Van Dyke (1984). Statistical discrimination of aftershocks and their contribution to seismic hazard, Consulting Report to Dames & Moore, Golden, Colorado.

Wells D.L. and K.J. Coppersmith (1994). New empirical relationships among magnitude, rapture length, rapture width, rapture area, and surface displacement, Bull. of Seism. Soc. of Ame., Vol.84, No.4, 974-1002.

Wesnousky, S.G., C.H. Scholz, K. Shimazaki and T. Matsuda (1983). Earthquake frequency distribution and the mechanics of faulting, Jour. Geophys. Res., Vol.88, No.B11 9331-9340.